UNIVERSITY of the
WESTERN CAPE

Constraining the stratigraphy and paleotectonic development of the Cango Caves and Kansa Groups (Western Cape, South Africa) using detrital zircon and whole-rock geochemistry

by

Keanan Alan Woolf

Thesis submitted in fulfilment of the requirements for the degree of Master of Science in the Faculty of Natural Sciences at the University of the Western Cape

Supervisor: Prof. Dirk Frei

Department of Earth Sciences

November 2022

DECLARATION

I declare that "*Constraining the stratigraphy and paleotectonic development of the Cango Caves and Kansa Groups (Western Cape, South Africa) using detrital zircon and whole-rock geochemistry"* is my own work, that it has not been submitted for any degree or examination in any other university, and that all the sources I have used or quoted have been indicated and acknowledged by complete references.

Name: Keanan Alan Woolf Date: 21/11/2022

Signed: ……………………………………

KEY WORDS

Basin evolution

Cango Caves Group

Geochronology

Groenefontein Formation

Huis Rivier Formation

Kango Inlier

Matjies River Formation

Nooitgedagt Member

Paleotectonic development

Provenance

Saldania Belt

ABSTRACT

The Saldania Belt is a Neoproterozoic to early Paleozoic low-grade orogenic belt that borders the southern and southwestern margins of the Kalahari Carton. It forms part of the Neoproterozoic Pan-African and Brasiliano tectonic belts in southern Africa and southeastern South America, related to the assembly of southwestern Gondwana. The Saldania Belt is composed of several inliers, one of which is the Kango Inlier. The Kango Inlier is an east-west orientated foreland basin consisting of several groups and formations. The Cango Caves Group forms the basal unit within the Kango Inlier, comprising of the Matjies River, Groenefontein and Huis Rivier formations. Using a combined study incorporating petrographic, geochemical, isotopic and U-Pb geochronological data, the Cango Caves Group is investigated to aid in deciphering the crustal evolution of the Kango Inlier.

The sampled rocks from the Cango Caves Groups have been gathered from the middle Nooitgedagt Member of the Matjies River Formation, the lower and middle Nelsrivier Member of the Groenefontein Formation, and the Huis Rivier Formation. These rocks have been classified as either wacke or litharenite. Based on the petrographic and geochemical analyses, the Cango Caves Group was deposited in a deepening basin, initially caused by rapid deposition from nearby sources followed by increased transportation times as the basin deepened. These rocks have undergone moderate degrees of weathering with a gradual decrease from the lower Matjies River Formation to the upper Huis Rivier Formation.

Provenance-indicating discrimination diagrams show sources from mixed tectonic settings for the Cango Caves Group. A Continental Island Arc source was determined for the Cango Caves Group, with the Groenefontein and Huis Rivier formations also showing Active Continental Margin and Passive Margin provenance sources, respectively.

The isotope geochemistry results indicate that a less-fractionated (mafic to intermediate) source appears to be the main source component for the Cango Caves Group. There is a change from a granitic source for the Nooitgedagt Member (lower stratigraphical unit) to a mixture between granitic and granodioritic sources for the Groenefontein and Huis Rivier formations. This is supported by the geochronological results.

The Nooitgedagt Member of the Matjies River Formation produced Mesoproterozoic zircon ages between 1000 and 1150 Ma, with a Concordia $^{206}Pb/^{238}U$ age of 1077 ± 3 Ma. The Groenefontein and Huis Rivier Formations produced both Mesoproterozoic and Neoproterozoic ages. The Groenefontein Formation produced Concordia ages of ~1003 - 1047 Ma and the Huis Rivier formation produced Concordia ages of ~847 - 872 Ma. Furthermore, the Groenefontein and Huis Rivier formations produced younger detrital ages of ~540 - 552 Ma and ~550 - 558 Ma respectively, which more closely reflect the depositional ages of these formations.

The zircon ages indicate that during the deposition of the Matjies River Formation, prior to the Groenefontein Unconformity, supply of sediments only occurred from a northern and eastern source area, namely from the Mesoproterozoic Namaqua-Natal Mobile Belt. These sediments were deposited in a shallow-marine to marine-shelf environment. The deposition of the Matjies River Formation was followed by the Groenefontein Unconformity, tectonic extension and the deepening of the basin, into which the Groenefontein Formation and Huis Rivier turbidites were deposited. This introduced a new source area which started to supply sediments of Neoproterozoic age. This source area presumably represents the Terra Australis Orogen located to the south of the Kango Inlier and played an increasingly important role during the deposition of the Cango Caves Group.

ACKNOWLEDGEMENTS

First and foremost, I would like to thank my parents, Wendy and Terence Woolf, for their constant support and the many sacrifices they have made throughout my academic career. I dedicate this work to you.

Furthermore, I would like to thank the National Research Fund (NRF), for funding this Master’s research project.

Thank you to my supervisor, Professor Dirk Frei, for his input and guidance through the completion of this thesis and for fulfilling the CL imagining analysis during Covid lockdown. Additionally, I would like to thank Dr Gerard Germs for his academic insight which assisted with the refinement of the analyses of this thesis.

I would like to thank Richard Harrison and Janine Botha, of the Department of Earth Sciences at the University of the Western Cape, for their assistance in the preparation of thin sections and sample preparation for geochemistry and geochronology analyses, as well as Mareli Grobbelaar, of Stellenbosch University’s Central Analytical Facilities, for her assistance with geochronology sample preparation and training.

A big thank you to my fellow students, Aidan Leetz and Musa Mhlanga, for providing direction with queries regarding data analysis and interpretation, and to Taryn Dick, for her support and the countless hours spent helping with proofreading and editing this work.

Last, but not least, I would like to thank my family, friends and work colleagues for your words of encouragement, unwavering faith and consistent motivation throughout the duration of this thesis.

TABLE OF CONTENTS

List of Figures

List of Tables

1. INTRODUCTION

There is a lack of provenance information and absolute age dating of Neoproterozoic to Early Paleozoic sedimentary basins flanking the southern margin of the Kalahari craton. Due to the uncertainty of the relationships between cratons at this stage, the construction of a definitive paleogeographic model is hindered. Paleogeographic models are further hindered by vague evidence of individual craton evolution and timing of significant tectonic or sedimentary events (Naidoo, 2013).

The Saldania Belt is a Neoproterozoic to early Paleozoic low-grade orogenic belt that borders the southern and southwest margins of the Kalahari Craton. It is composed of several inliers unroofed in mega-anticlinal hinges of the Permo-Triassic Cape Fold Belt along the southern margin of Africa, one of which is the Kango Inlier (Rozendaal et al., 1999) (**Figure 1-1** a and b). The east-west orientated Kango Inlier consists of a lower carbonate-rich Cango Caves Group which is overlain discordantly by the carbonate-deficient Kansa Group and the siliciclastic Schoemanspoort Formation, which has in turn been unconformably overlain by the Peninsula Formation of the Table Mountain Group. (Naidoo et al., 2013).

The Neoproterozoic Cango Caves Group was previously named the Goegamma Subgroup of the Kansa Group (Le Roux and Gresse, 1983). The Matjies Rivier Formation is the lower formation of the Cango Caves Group and is comprised of the basal Nooitgedagt Member and the upper Kombuis Member (**Figure 1-1**) (Germs et al., 2009). C and Sr isotope chemostratigraphy was conducted by Fölling and Frimmel (2002) and determined a pre-Ediacaran age (>630 Ma) for the Nooitgedagt Member and an Ediacaran age (<630 Ma) for the rest of the Cango Caves Group, thus indicating the existence of an unconformity between the two members.

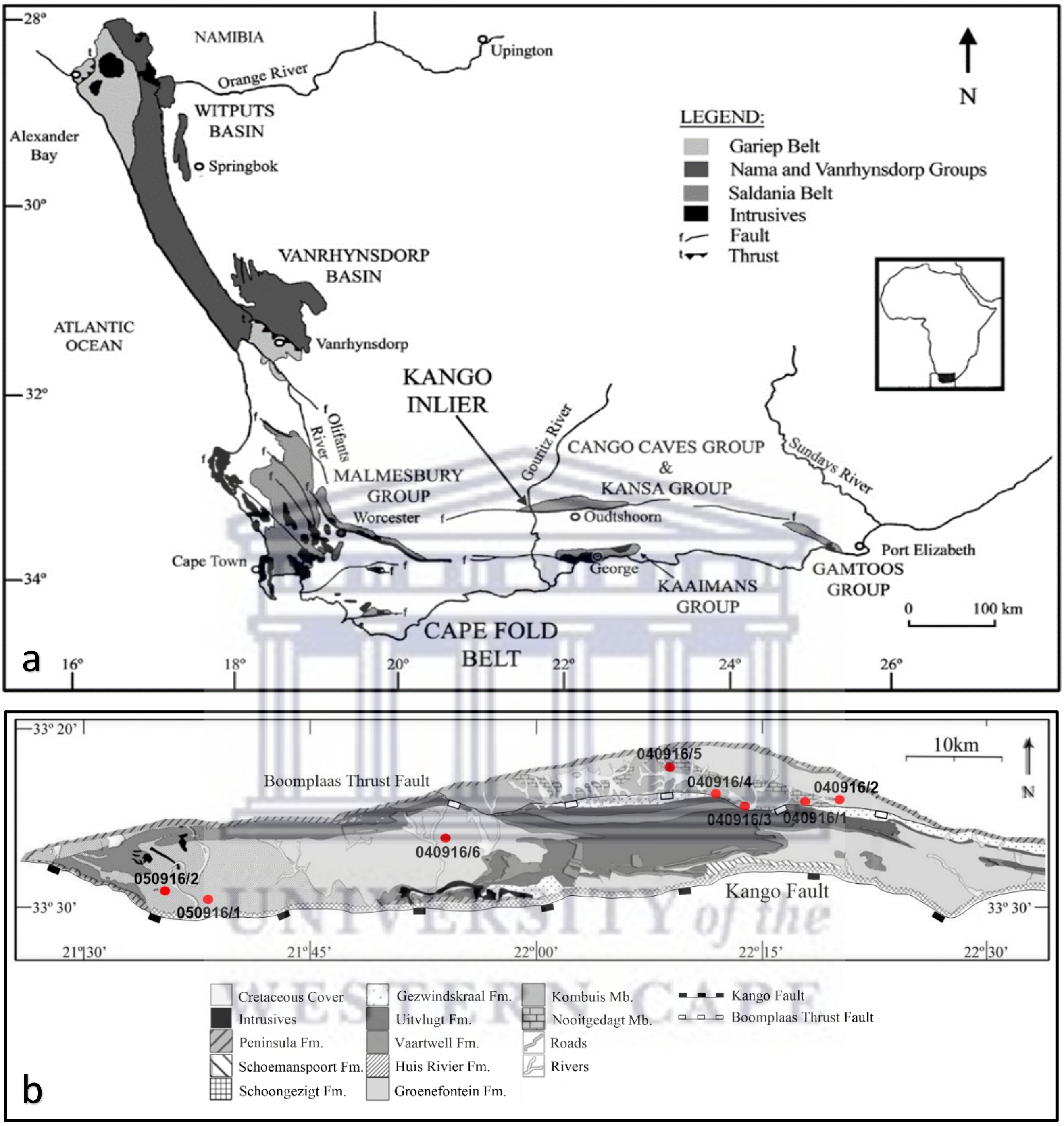

Figure 1-1: a – Map showing the mobile belts of southern African and the location of the Kango Inlier. b – Enlarged map of the Kango Inlier showing the different formations and sample locations. Modified after Van Staden et al. (2006).

The lower Matjies Rivier Formation is separated by an unconformity with the overlying Groenefontein Formation. The change in depositional environment from the Kombuis carbonate platform to the clastic turbiditic Groenefontein Formation reflects the deepening of the Kango Inlier basin (Rozendaal et al., 1999). A proposed marine condensed section in the Groenefontein Formation signifies a change from transgression to regression and deposition of the upward-coarsening turbiditic Huis Rivier Formation (Gresse et al., 1996). The Huis Rivier Formation only occurs in the western part of the Kango Inlier and was most likely eroded prior to the deposition of the Kansa Group in the eastern part of the inlier (Germs et al., 2009). U-Pb ages for the Huis Rivier Formation indicated that the formation is younger than 571 Ma (Naidoo, 2008).

U/Pb isotope dating of detrital zircons from Barnett et al. (1997) indicates that the gneisses of the Mesoproterozoic Namaqua-Natal Mobile Belt (1100 Ma) are the probable sediment source terrain for the Cango Caves Group. This has been supported by later work done by Naidoo (2008) and Naidoo et al. (2013).

This thesis aims to conduct a provenance study on the basal Kango Inlier, the Cango Caves Group. The provenance study aims to quantify the mineralogical, geochemical, isotopic and geochronological composition of rocks of the Cango Caves Group, to aid in deciphering the crustal evolution of the Group.

2. REGIONAL GEOLOGY

2.1 Saldania Belt

The Saldania Belt is a low-grade orogenic belt which forms part of the Neoproterozoic Pan-African and Brasilliano tectonic belts in southern Africa and southeastern South America, related to the construction of southwestern Gondwana (Gaucher and Germs, 2006).

The Saldania Belt is subdivided into the northwest-southeast trending western branch and the east-west trending southern branch (Frimmel, 2009). The oblique collision between the Kalahari and the Rio de la Plata Cratons is the probable cause of the formation of the western branch (Grunow et al., 1996). The Malmesbury Group is the main exposure of the western branch. The southern branch has been divided into three tectonic domains/terranes (Hartnady et al., 1974; Von Veh, 1983), namely the Boland, Swartland and Tygerberg terranes. It is not, however, clear whether these represent true allochthonous terranes (Germs et al., 2009).

The southern branch is composed of three east-west trending inliers, unroofed in mega-anticlinal hinges of the Permo-Triassic Cape Fold Belt along the southern margin of Africa (**Figure 1-1** a). The southern branch contains the Kango Inlier (Oudtshoorn area), where the study area is located, the Kaaimans Inlier (George area) and the Gamtoos Inlier (Gqeberha area) (**Figure 1-1** a). Previous work within the Kango Inlier was conducted notably by Le Roux (1977), Barnett et al. (1997), Gaucher and Germs (2006), Naidoo (2008), Naidoo et al. (2013) and Nel et al. (2018). These are summarised in **Figure 2-1** by Nel et al. (2018).

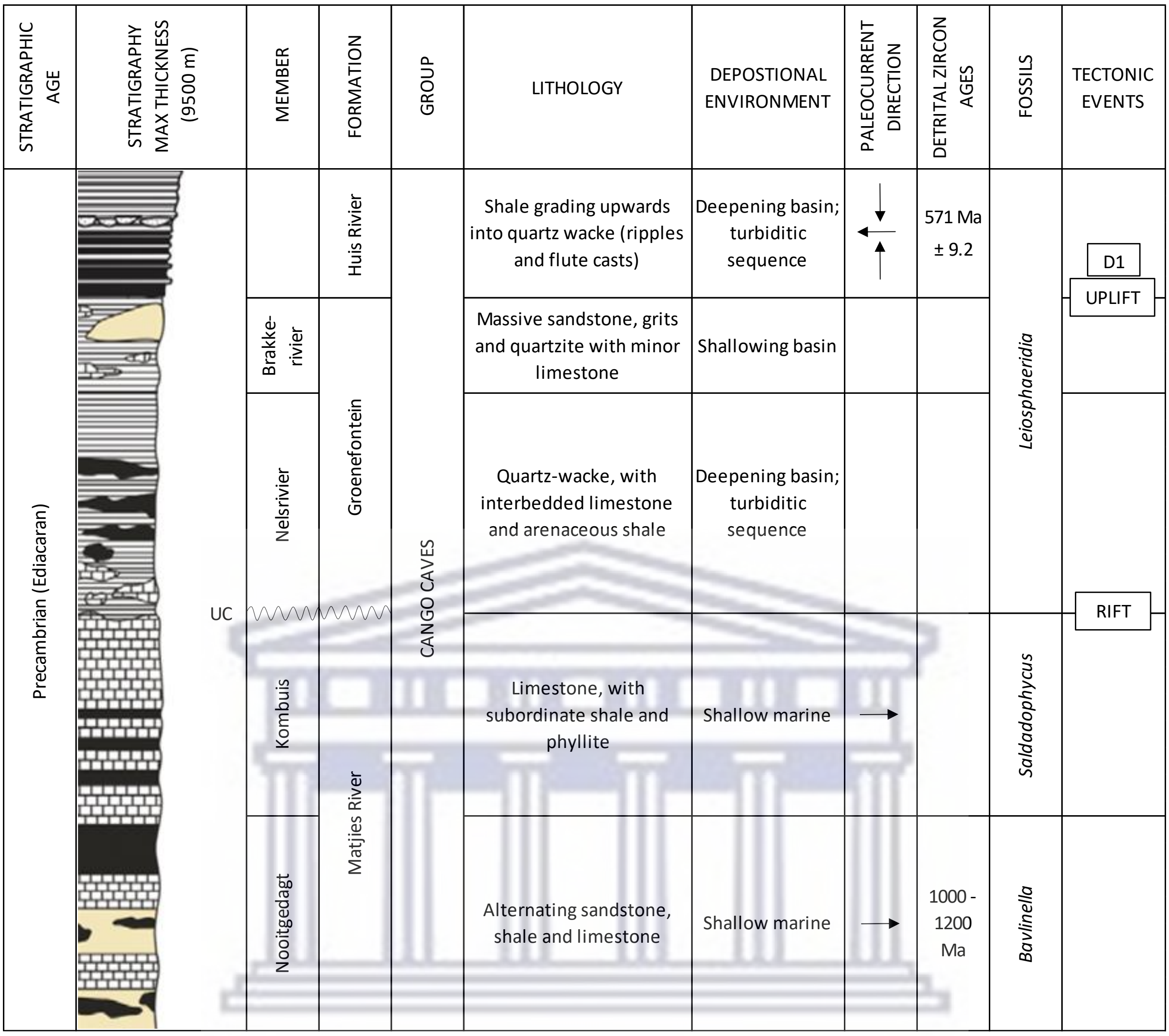

STRATIGRAPHIC AGE	STRATIGRAPHY MAX THICKNESS (9500 m)	MEMBER	FORMATION	GROUP	LITHOLOGY	DEPOSTIONAL ENVIRONMENT	PALEOCURRENT DIRECTION	DETRITAL ZIRCON AGES	FOSSILS	TECTONIC EVENTS
Precambrian (Ediacaran)			Huis Rivier	CANGO CAVES	Shale grading upwards into quartz wacke (ripples and flute casts)	Deepening basin; turbiditic sequence	↓ ← ↑	571 Ma ± 9.2	*Leiosphaeridia*	D1 UPLIFT
		Brakke-rivier	Groenefontein		Massive sandstone, grits and quartzite with minor limestone	Shallowing basin				
		Nelsrivier			Quartz-wacke, with interbedded limestone and arenaceous shale	Deepening basin; turbiditic sequence				RIFT
	UC	Kombuis	Matjies River		Limestone, with subordinate shale and phyllite	Shallow marine	→		*Saldadophycus*	
		Nooitgedagt			Alternating sandstone, shale and limestone	Shallow marine	→	1000 - 1200 Ma	*Bavlinella*	

Figure 2-1: Stratigraphy of the lithological units of the Cango Caves Group within the Kango Inlier showing the depositional environments, paleocurrent directions and zircon ages of the different geological units. Additionally showing the tectonic events which have affected the different units. Modified after Nel et al. (2018), compiled from Le Roux (1997), Barnett et al. (1997), Gaucher and Germs (2006), Naidoo (2008) and Naidoo et al. (2013).

The Kango Inlier can be described as an east-west elongated, northward-overturned anticlinorium with a strike of 140 km and a width of 14 km (Barnett et al., 1997). The rocks of the Kango Inlier possibly overlie the granitic gneiss of the Namaqua-Natal Mobile Belt (Naidoo et al., 2013). The Kango Inlier consists of a lower, carbonate-rich Cango Caves group, which is overlain discordantly by the carbonate-deficient Kansa Group and the siliciclastic Schoemanspoort Formation above (Naidoo et al., 2013). It is flanked to the north, east and the west by quartzites belonging to the Ordovician Peninsula Formation of the Table Mountain Group. To the south, across the regionally extensive normal Kango fault, the Kango Inlier is bordered by conglomerates and sandstones of the Jurassic-Cretaceous Enon formation of the Uitenhage Group (Barnett et al., 1997). The Kango Inlier comprises the lower, carbonate-rich Cango Caves Group, which is overlain discordantly by the carbonate-deficient Kansa Group and the siliciclastic Schoemanspoort Formation (Naidoo et al., 2013) (**Figure 2-1**).

2.2 Cango Caves Group

The Cango Caves Group was previously named the Goegamma Subgroup of the Kansa Group (Le Roux and Gresse, 1983). The group is predominantly a carbonate-clastic turbidite succession (Germs et al., 2009). Chemostratigraphy and organic-walled microfossils indicate that the Cango Caves Group is Neoproterozoic in age (Germs et al., 2009). The Cango Caves Group is comprised of the lowermost Matjies River Formation, the Groenefontein Formation and the uppermost Huis Rivier Formation. An unconformity separates the upper two formations from the lower Matjies River Formation, known as the Groenefontein Unconformity (Praekelt et al., 2008) (**Figure 2-1**).

The analyses of paleocurrents in sedimentary successions of the Cango Caves Group suggest that the lower Matjies River Formation had its main source area to the east, and the upper Groenefontein and Huis Rivier formations had a source to the north and south (Le Roux, 1977). Furthermore, Nel et al. (2018) determined that a northern and/or southern source provided sediment for the deposition of the Matjies Rivier Formation.

2.2.1 Matjies River Formation

The Matjies Rivers Formation is comprised of the Nooitgedagt and Kombuis members. The Nooitgedagt Member is the basal unit of the Matjies River Formation, and is comprised of shale, greywacke and limestone. C and Sr isotope chemostratigraphy by Fölling and Frimmel (2002) determined a pre-Ediacaran age (>630 Ma) for the Nooitgedagt Member, and an Ediacaran age (<630 Ma) for the rest of the Cango Caves Group. These ages, coupled with a difference of 100°C in thermal overprint, indicate the existence of an unconformity between the two members (Germs et al., 2009).

The Nooitgedagt Member was dated by Barnett et al. (1997) and recorded ages of 1200 Ma and 1050 Ma, typical for the Mesoproterozoic Namaqua-Natal Mobile Belt. The sediments of the Nooitgedagt Member were deposited as coarsening upward-deltaic sediments and shallow marine deposits (Germs et al., 2009). Furthermore, the Nooitgedagt Member contains conglomerates which comprise clasts that are derived from granites, gneisses and quartzites (Naidoo, 2013). Geological mapping by Nel et al. (2018) has identified at least three main unconformities in the Nooitgedagt Member which are associated with chert and/or ferruginous horizons.

The Kombuis Member is comprised mainly of carbonates, but shale, siltstone and dolomites are also present within the Member. The rocks within the Kombuis Member primarily accumulated on a shelf (Germs et al., 2009).

2.2.2 Groenefontein Unconformity

An unconformity, with deep karstic features, separates the carbonate-containing Kombuis Member from the overlying turbiditic sedimentary rocks of the Groenefontein Formation (Praekelt et al., 2008). This is known as the Groenefontein Unconformity. According to Praekelt et al. (2008), the Groenefontein Unconformity was presumably formed as a result of lowered sea levels caused by a circa 547 Ma minor glaciation during the late Ediacaran. The Groenefontein Unconformity comprises paleokarst topography with sinkholes and/or paleovalleys up to 400 m wide and 150 m deep. The nature of conglomerates in a fine-grained matrix, which occur in the sink holes, infers glaciofluvial deposits on a karstic surface; therefore, the Groenefontein Unconformity was determined to be sub-aerially formed (Praekelt et al., 2008).

2.2.3 Groenefontein Formation

The Groenefontein Unconformity at the base of the turbiditic Groenefontein Formation, points to deposition in a deepening basin. The Groenefontein Formation was mainly deposited as turbidites on a continental slope and/or foredeep environment (Le Roux, 1997). Fine-grained, quartz-rich wacke, above the carbonate rich Kombuis Member, marks the base of the Groenefontein Formation. The Groenefontein Formation consists mainly of sandstone and shale with minor limestone lenses (Rozendaal et al., 1999). It is subdivided into the shale-containing Nelsrivier Member and the overlying, sandy Brakkerivier Member (Praekelt et al., 2008). The Nelsrivier Member contains limestone lenses interbedded with mudrocks (Naidoo, 2008). The Brakkerivier Member is comprised of medium- to coarse-grained sandstone and limestone. There is a lack of carbonate lenses in the westernmost part of the Kango Inlier, whereas carbonate lenses to the east have been metamorphosed to marble (Naidoo, 2008).

According to Naidoo (2008), due to the structural complexity of the Kango Inlier, the Groenefontein Formation forms an upper contact with several formations. To the west of the Kango Inlier, it forms a conformable and gradational contact with the overlying Huis Rivier Formation. Within the central area, it exhibits a sharp boundary with the conglomerates of the Vaartwell Formation. Eastward, it is overlain by the Uitvlugt Formation, whereas further east within the Kango Inlier, the Groenefontein Formations is overlain by the Schoongezigt Formation. To the north of the Kango Inlier, the Groenefontein Formation is unconformably overlain by the Table Mountain Group, whereas southward, it is unconformably overlain by the Schoemanspoort Formation.

2.2.4 Huis Rivier Formation

The Huis Rivier Formation forms a gradational contact with the Groenefontein Formation. The Formation is mainly classified as a thick turbidite succession deposited in a deepening basin. It is comprised of medium- to fine-grained wacke and very fine-grained fissile mudstones (Naidoo et al., 2013). According to Le Roux and Gresse (1983), the Huis Rivier Formation was deposited on a continental slope or basal plain environment, with sediment supply from the southwestern and possibly north-western sources. Naidoo (2008) assigned an Ediacaran age for the Huis Rivier Formation. Geochemical data suggests that the Groenefontein and Huis Rivier formations were deposited on an active continental margin (Van Staden et al., 2006; Naidoo, 2008).

2.2.5 Organic-walled microfossils

Various Ediacaran organic-walled microfossils occur in the Cango Caves Group (Gaucher and Germs, 2006) (**Figure 2-1**). The Nooitgedagt Member and the Kombuis Member of the Matjies River Formation are dominated by *Bavlinella* and *Soldadophycus* respectively. The Groenefontein and Huis Rivier Formations are *Leiosphaerid* dominated (Gaucher and Germs, 2006). Only one possible Ediacaran body fossil (*Ernietta*-like) has been found in the basal Groenefontein Formation of the Cango Caves Group (Praekelt et al., 2008). Microflora assemblages within the Cango Caves Group can be correlated to those of southwestern

Gondwana, namely in the Gamtoos Group, Nama Group, Port Nolloth Group, Arroyo del Soldado Group (Uruguay) and the Corumba Group (Brazil) (Gaucher and Germs, 2006).

2.3 Structural Geology/ Deformation

According to Le Roux (1977), the rocks of the Kango Inlier have undergone four stages of deformation. The first deformational event (D1) only affected the Cango Caves Group and is associated with uplift and folding in a north-westerly direction. The secondary deformational event (D2), which involved the Cango Caves Group, was a compressional event and resulted in east-west trending folds verging north. Furthermore, D2 resulted in the formation of major thrust sheets (Naidoo et al., 2013). D2 was followed by thermal relaxation and the intrusion of dykes and sills. The third deformational event (D3) is related to the Permian Cape Orogeny (300 Ma). The final deformational event (D4) is related to crustal extension associated with the breakup of Gondwana. Rifting of Gondwana continued until the Late Mesozoic Era. D4 resulted in regional strike faults and cross folds with a south-trending axis within the Kango Inlier (Naidoo et al., 2013). The D3 and D4 deformational events affected the entire Kango Inlier, as well as the rocks of the Cape Supergroup.

2.4 Metamorphism

The Saldania Belt has generally undergone low-grade metamorphism. Poor outcrop exposure and similar low-grade metamorphic overprint during the 290-220 Ma Cape orogeny has prevented an accurate reconstruction of the Neoproterozoic to Cambrian metamorphic evolution of the belt. The peak of metamorphism (middle greenschist facies) was reached during the Pan-African orogeny 545 ± 2 Ma (Frimmel et al., 2001).

The metamorphic grade within the Kango Inlier was examined by Frimmel et al. (2001). It was determined that the lowermost unit of the Cango Caves Group, the Nooitgedagt Member, had undergone middle greenschist facies metamorphism. A temperature of ~390 °C was recorded for the Nooitgedagt Member. The Kombuis Member recorded lower temperatures of ~290 °C. Therefore, the Nooitgedagt Member reflects Pan-African Metamorphism, whereas the rest of the Kango Inlier reflect low-grade metamorphism related to the Cape Orogeny.

3. METHODOLOGY

3.1 Sampling

A total of eight outcrops of metasedimentary rocks representing different geological units of the Cango Caves Group were sampled from the Kango Inlier (**Figure 1-1** b).

The samples were prepared at the Department of Earth Sciences, University of the Western Cape (UWC) for petrography, whole-rock major and trace element geochemical analyses, as well as geochronology analysis. A total of eight thin sections were made for petrographic analysis.

For whole-rock major and trace element geochemical preparation, the samples were crushed in a jaw crusher and milled to a fine mesh in a swing mill equipped with Cr-steel rings for approximately 10 seconds. A strict cleaning regime ensued after every sample run to avoid cross-contamination (i.e., quartz run and cleaning of surfaces with acetone).

After preparation, both major and trace element analyses were done at the Central Analytical Facilities (CAF), Stellenbosch University (SUN).

3.2 Whole-rock major and trace element geochemistry analyses

Major element analysis was determined by X-ray fluorescence (XRF) spectrometry on a PANalytical Axios Wavelength Dispersive. The instrument was fitted with a Rh tube, a gas–flow proportional counter and a scintillation detector with analysing crystals including LIF200, LIF220, LIF420, PE and PX1. The gas flow's proportional counter uses a 90% Argon and 10% methane gas mixture.

The control standards used in the calibration for the major element analysis were BE-N (basalt reference values), JB-1 (basalt (depleted) reference values), BHVO-1 (basalt reference values), JG-1 (granodiorite reference values) and WITS-G (granite reference values). Loss on ignition (LOI) was calculated by weight difference after ignition at 1000 °C.

A resonetics 193 nm Exicimer laser connected to an Agilent 7500 Inductively Coupled Plasma Mass Spectrometer (ICP-MS) was used in the trace element analysis of bulk rock samples. Ablation is performed in helium gas at a flow rate of 0.35 l/min, and then mixed with argon

(0.9 l/min) and nitrogen (0.004 l/min) just before introduction into the ICP plasma. For traces in fusion, two spots of 100 µm were ablated on each sample using a frequency of 10 Hz and 8 J/cm^2 energy.

Trace elements were quantified using NIST 610 for calibration and the weight percent (wt%) SiO^2 from XRF measurements as an internal standard, using standard sample bracketing. Two replicate measurements were made on each sample, with the average reported as the measured concentration. The calibration standard was run every 15 – 20 samples. A quality control standard was run at the beginning of the sequence as well as with the calibration standards throughout (BHVO and BCR). The data was processed using Mass Hunter v4.01 software.

3.3 Rb-Sr and Sm-Nd isotopic analyses

Chemical preparation of whole-rock Sr and Nd isotope analysis was performed in PicoTrace clean lab facilities, and isotope ratios were measured with a Nu Instruments thermal ionisation mass spectrometer (Nu-TIMS) at Department de Geología, Centro de Investigación Científica y de Educación Superior de Ensenada (CICESE) in the state of Baja California (Mexico), equipped with 12 fixed Faraday cups and the Nu Instruments zoom optics for perfect alignment of all masses of interest into the Faraday cups.

Element separation was achieved in two steps. The first step constitutes using quartz glass columns filled with DOWEX AG 50W-X8 resin to separate Sr and REE, and the second step by Ln-Spec® resin to separate Nd. Samples were loaded on Re filaments using the double filament technique with H_3PO_4 for Nd and the single filament technique together with a TaF_4 activator for Sr. Both Sr and Nd isotope ratios were measured in static mode (eight blocks of 10×16 s integrations). Correction for mass bias for Sr and Nd was achieved by normalising to $^{86}Sr/^{88}Sr = 0.1194$ and $^{146}Nd/^{144}Nd = 0.7219$, respectively.

3.4 Zircon U-Pb geochronology

A total of six samples (040916/2, 040916/3, 040916/5, 040916/6, 050916/1 and 050916/2B) were selected for U-Pb zircon age dating. Prior to U-Pb dating analysis, the following sequential steps were followed: crushing, milling and sieving of samples at the Department of Earth Science, UWC; hand washing, to remove material finer than 40 µm, followed by gravity separation using a super panner, at the Mineral Separation Laboratory, SUN; magnetic separation using a Frantz Isodynamic separator Model L-1 at the Mineral Separation Laboratory, SUN; and heavy liquid separation (tetrabromoethane – $Br_2CHCHBr_2$) at the Mineral Separation Laboratory, SUN.

After the separation process, zircon grains for analyses were picked by hand using a needle, with the aid of a binocular microscope, and mounted in epoxy discs. The discs were polished, carbon coated and imaged by cathodoluminescence imaging using a Leo© 1450VP scanning electron microscope (SEM) at the CAF.

In-situ U-Pb age dating of zircons were performed at the CAF. All U–Pb age data obtained at the CAF were acquired by laser ablation - single collector - magnetic sectorfield - inductively coupled plasma - mass spectrometry (LA-SF-ICP-MS) employing a Thermo Finnegan Element2 mass spectrometer coupled to an ASI Resolution SE S155 Excimer laser ablation system. The internal textures of the zircons were studied by CL imaging obtained at the CAF.

All U-Pb age data presented was obtained by single spot analysis with a spot diameter of 30 µm and a crater depth of approximately 10-15 µm. The methods employed for analysis and data processing are described in detail by Frei and Gerdes (2009) and Cornell et al. (2016). The calculation of Concordia ages and plotting of Concordia diagrams were performed using Isoplot/Ex 3.0 (Ludwig, 2003).

4. RESULTS

4.1 Petrography

The eight samples of the Cango Caves Group were allocated for petrographic analysis. These samples represent the lowermost, middle and upper formations of the Cango Caves Group. Samples 040916/3 and 040916/4 are from the of the Nooitgedagt Member of the Matjies River Formation. The Nooitgedagt Member marks the lowermost formation of the Cango Caves Group. Samples 040916/2, 040916/5 and 040916/6 are from the Groenefontein Formation. Samples 050916/1, 050916/2A and 050916/B were collected from the Huis Rivier Formation, the upper most formation of the Cango Caves Group.

4.1.1 Nooitgedagt Member

Two wacke samples of the Nooitgedagt Member were collected, 040916/3 and 040916/4. They are light grey in colour and poorly sorted (**Figure 4-1**). They comprise subrounded clasts in a fine-grained matrix. The clasts are mainly quartz, but in sample 040916/4, feldspar clasts are also present. The clasts can reach sizes of >2 cm. 040916/3 exhibits evidence of iron oxide which gives the orange staining to the grey rock (**Figure 4-1**).

Figure 4-1: Wacke of the Nooitgedagt Member.

Petrographically, the wackes are comprised of 40% quartz and 30% orthoclase. Plagioclase comprises 5% of the wacke and exhibits polysynthetic twinning. The mineral grains are predominantly very-fine grained, but large quartz and orthoclase clasts can be found. The large quartz grains can reach 1 cm, whereas orthoclase can reach up to 0.5 mm. Monocrystalline quartz is predominately found and exhibits undulose extinction. Although less common, polycrystalline quartz can also be found (**Figure 4-2** a and b). Orthoclase exhibits perthitic exsolution texture, breaking down to albite (**Figure 4-2** c). Plagioclase also rarely displays myrmekitic texture (**Figure 4-2** d). Furthermore, there is evidence of seritisation of feldspar (**Figure 4-2** e). Accessory minerals include elongated muscovite, microcline, zircon and calcite. Microcline exhibits cross-hatched twinning (**Figure 4-2** f). Calcite is dominantly found as secondary calcite, but primary calcite can be seen to exhibit cross-hatched twinning. The quartz-feldspar matrix makes up 30 - 45%. The matrix is also made up of calcite and muscovite.

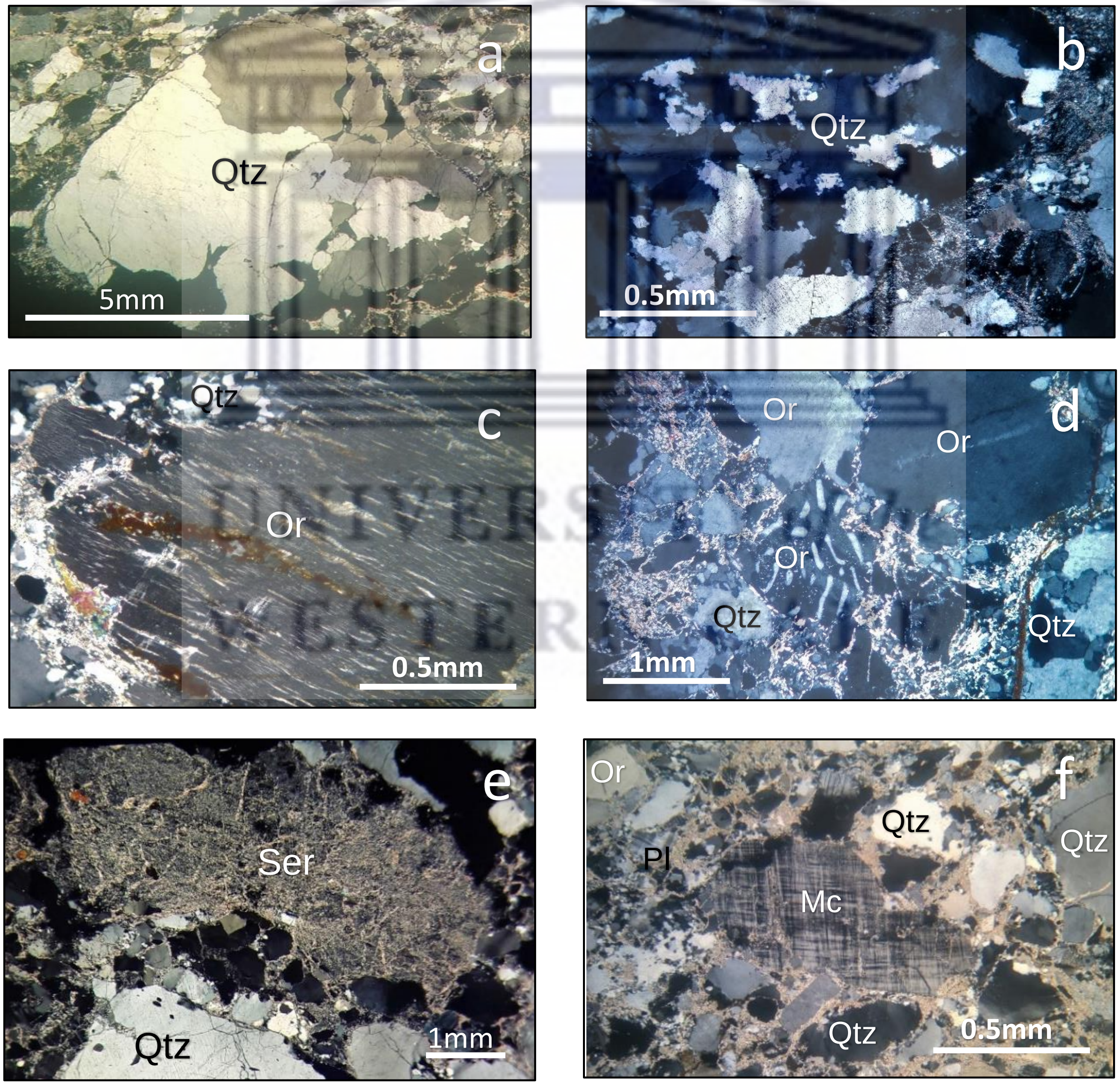

Figure 4-2: Petrographic micrographs of wacke samples of Nooitgedagt Member (all in cross-polarised light (xpl)). a – Large polycrystalline quartz (Qtz). b – Polycrystalline quartz exhibiting undulose extinction. c – Orthoclase (Or) exhibiting perthitic

exsolution. d – Plagioclase (Pl) grain exhibiting myrmekitic texture. e – Large serisitised feldspar grain. f – Large microcline (Mc) grain exhibiting cross-hatched twinning texture.

4.1.2 Groenefontein Formation

The Groenefontein Formation is characterised by quartz-wacke with interbedded limestone and arenaceous shale. The very-fine grained, quartz rich wacke of the Groenefontein Formation has been sampled. Samples 0409162 and 040916/5 were collected from the lower Nelsrivier Member of the Groenefontein Formation and 040916/6 was collected from the middle Nelsrivier Member. The samples are light brown in colour and exhibit oxidation (**Figure 4-3**). The grains are more moderately sorted and are subangular to subrounded at the base, and subrounded higher up within the unit. The wacke at the base of the Member is fine grained with the grain size being very-fine in the middle.

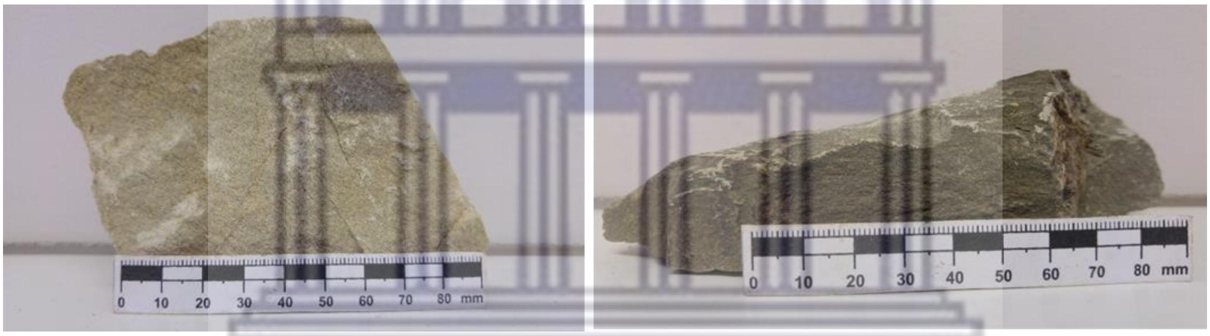

Figure 4-3: Wacke of the Groenefontein Formation.

Petrographically, the Groenefontein Formation is characterised by mineral assemblages of quartz, orthoclase and plagioclase. The general textures of the wacke samples are seen below **Figure 4-4** a, b, c and d. Quartz is seen to exhibit undulose extinction. Narrow quartz veins are also common (**Figure 4-4** e and f). There is a significant increase in the quartz composition in 040916/2 (55%) as opposed the other samples (40%). There is a lower concentration of opaque minerals within 040916/2 (3%) as opposed to the other samples which have higher concentrations (5 - 6%).

Accessory minerals include muscovite, zircon, chlorite and tourmaline. Within samples 040916/5 and 040916/6 there appears to be a red-brown staining of the matrix, which seems to be from the weathering of the opaque minerals (**Figure 4-4** g and h). The matrix staining is present in sample 040916/2, but is not as prominent as it is within the other two samples.

The rocks have been highly altered, evident by the sericitic alteration. White mica is common as there is a significant amount of seritisation. The matrix component of the Groenefontein Formation makes up 30 - 40% and comprises of quartz, feldspar, chlorite, calcite and muscovite. Furthermore, there is an alignment of elongated muscovite (**Figure 4-4** i).

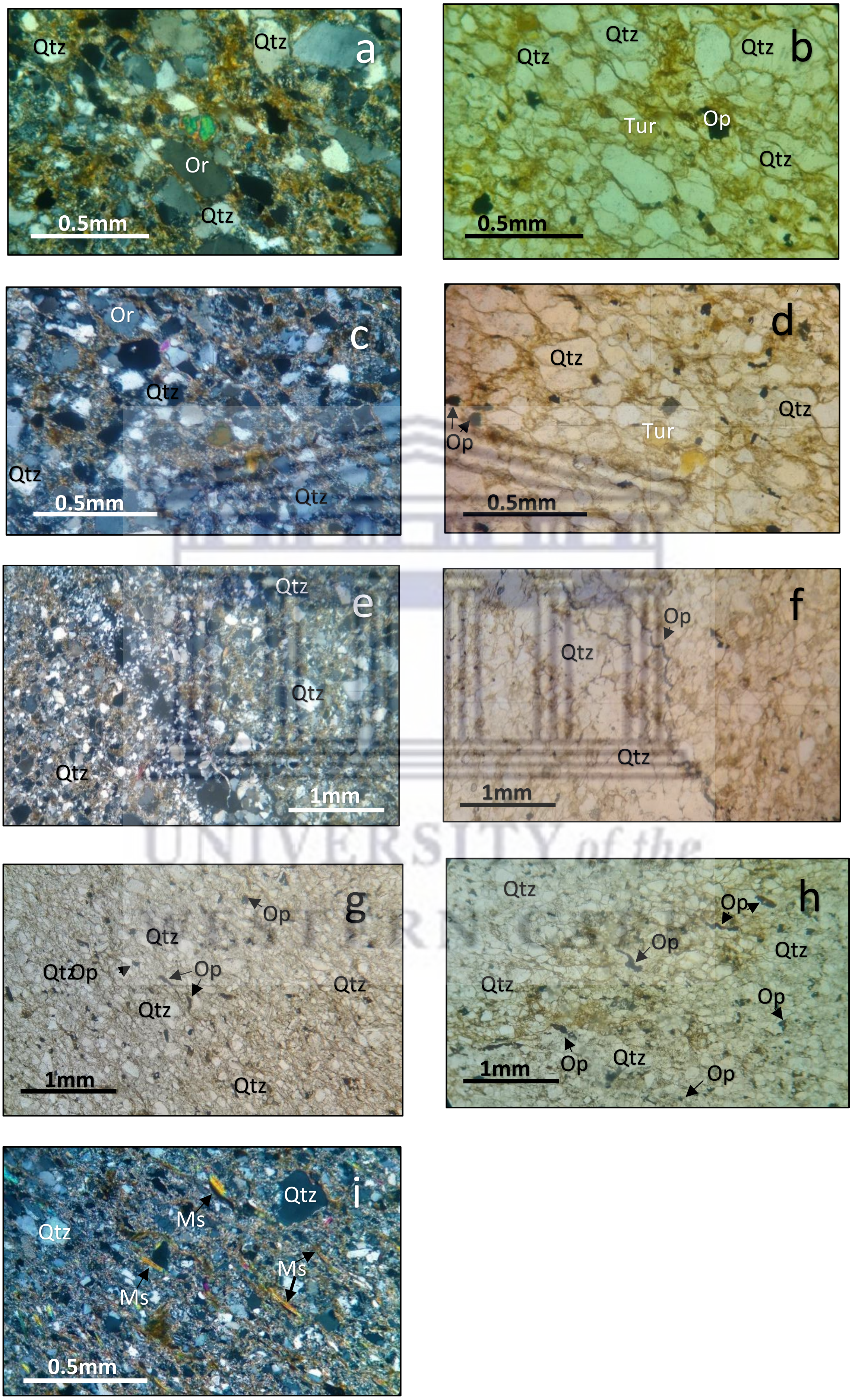
a
Qtz
Qtz
Or
Qtz
0.5mm
b
Qtz
Qtz
Qtz
Tur
Op
Qtz
0.5mm
c
Or
Qtz
Qtz
Qtz
0.5mm
d
Qtz
Qtz
Op
Tur
0.5mm
e
Qtz
Qtz
Qtz
1mm
f
Op
Qtz
Qtz
1mm
g
Op
Qtz
Qtz
Op
Op
Qtz
Qtz
Qtz
1mm
h
Qtz
Op
Op
Qtz
Qtz
Op
Op
Qtz
Op
1mm
i
Qtz
Ms
Qtz
Ms
Ms
0.5mm

Figure 4-4 : Petrographic micrographs of the Groenefontein Formation wacke samples. a, b, c, d – displaying the general texture. a and b are petrographic micrographs of the same portion of thin section, a – xpl light; b – ppl. c and d – Rare angular tourmaline (Tur) grain. c and d are petrographic micrographs of the same portion of thin section, c – xpl light; d – ppl. Note pseudomatrix of chlorite-sericite defining the framework quartz grain boundaries. e and f – Quartz (Qtz) vein and narrow vein of opaque (Op) minerals (e – xpl; f – ppl). g and h – Staining of the matrix around opaque minerals (ppl), black minerals are the opaques. i – Elongated muscovite (Ms) defining an alignment (xpl). Other mineral abbreviation not mentioned in the description: Or – Orthoclase.

4.1.3 Huis Rivier Formation

The Huis Rivier Formation is comprised of shales which grade upwards to quartz wacke. Fine-grained, greywacke and shale of the Huis Rivier Formation have been sampled. The wacke samples have undergone a petrographic analysis.

The greywackes are dark grey in colour, poorly sorted and contain turbidites. They are fine to very-fine grained. There are visible 1 mm rounded chlorite grains within the wacke (**Figure 4-5**).

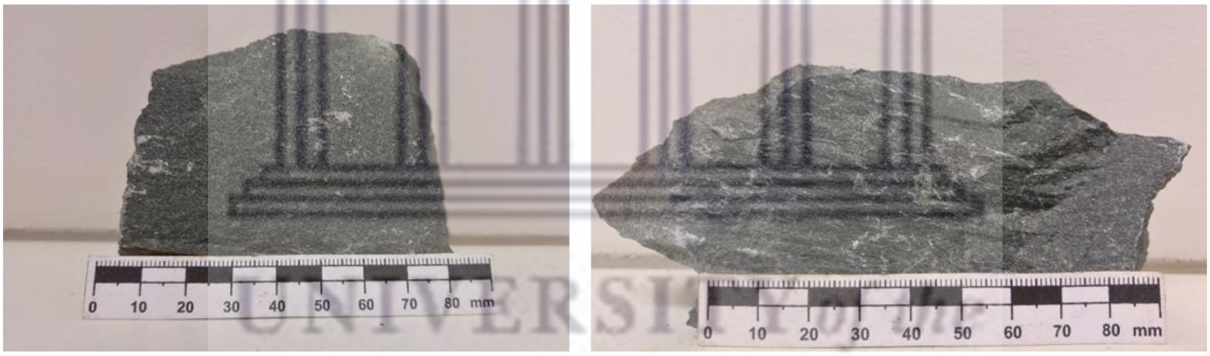

Figure 4-5: Fine-grained wacke of the Huis Rivier Formation.

Petrographically, the samples are characterised by mineral assemblages of quartz (30%), orthoclase (15%) and plagioclase (15%). Accessory minerals include anhedral calcite, elongated muscovite, angular epidote, elongated and rounded zircon, rounded chlorite and anhedral opaque minerals (**Figure 4-6** a and b). Euhedral epidote is also an accessory mineral (**Figure 4-6** c and d). Calcite mineral percentages fluctuate among samples.

The mineral grains are very-fine to fine grained and are also subrounded. Moreover, the mineral grains are moderately sorted. There is a high degree of alteration within the rocks, evident by chloritisation and seritisation. There is weathering of opaque minerals (**Figure 4-6** e and f), but not as prominent as within the Nelsrivier Member, as there are also significantly fewer opaque minerals. Primary calcite also appears to exhibit strong cross-hatched twinning (**Figure 4-6** g). Slight deformation is exhibited as there is kinking of deformation twins in the plagioclase (**Figure 4-6** h). The matrix component makes up 35% and is characterised by quartz, muscovite, chlorite and calcite. Narrow veins containing quartz and chlorite are present in the rocks (**Figure 4-6** i and j). The matrix of the Huis Rivier Formation has a pale green colour, as opposed to the light brown colour seen in the wacke samples of the other formations, possibly due to the large concentration of chlorite.

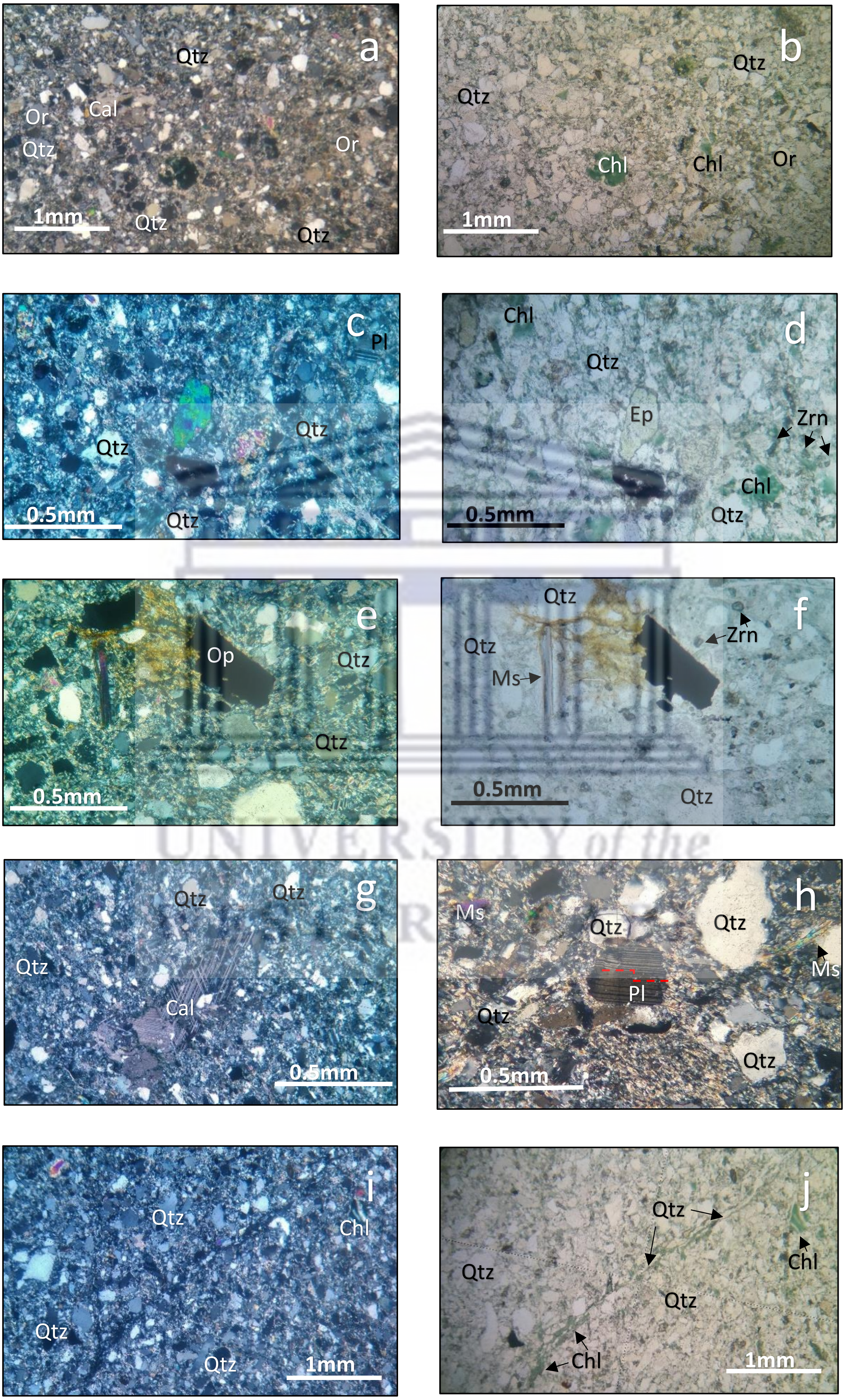
a
Qtz
Or
Cal
Qtz
Or
1mm
Qtz
Qtz
b
Qtz
Qtz
Chl
Chl
Or
1mm
c
Pl
Qtz
Qtz
0.5mm
Qtz
d
Chl
Qtz
Ep
Zrn
Chl
0.5mm
Qtz
e
Op
Qtz
Qtz
0.5mm
f
Qtz
Zrn
Qtz
Ms
0.5mm
Qtz
g
Qtz
Qtz
Qtz
Cal
0.5mm
h
Ms
Qtz
Qtz
Ms
Pl
Qtz
0.5mm
Qtz
i
Qtz
Chl
Qtz
Qtz
1mm
j
Qtz
Chl
Qtz
Qtz
Chl
1mm

Figure 4-6: a and b – Petromicrographs (of the same portion of thin section) displaying the general texture of the wacke of the Huis Rivier Formation, a – xpl, b - ppl. Note pseudomatrix of chlorite (Chl) - sericite defining the framework quartz (Qtz) grain boundaries. c and d – Rare epidote (Ep) grain, c and d are petrographic micrographs of the same portion of thin section, c – xpl light; d – ppl. e and f – Weathering of opaque (Op) minerals, e and f are petrographic micrographs of the same portion of thin section, e – xpl light; f – ppl. g – Anhedral calcite (Cal). h – Plagioclase (Pl) grain exhibiting kinking indicated by the red-dashed line. i and j – Narrow quartz/chlorite vein, i and j are of the same portion of thin section, i – xpl light; j – ppl. Other mineral abbreviations not mentioned in the description: Or – Orthoclase, Zrn – Zircon, Muscovite (Ms).

4.2 Geochemistry

Whole-rock geochemical analysis of sedimentary rocks can yield valuable information on different provenance aspects, such as source-rock composition, amount of transport and recycling, weathering trends and tectonic activity in the source area. Mobile major elements can potentially provide information on syn-depositional processes which alter the sediment. Immobile trace elements, however, remain unchanged during most depositional processes and may retain information on the chemistry of the source rocks.

A total of eight samples were selected for whole-rock geochemical analysis. Whole rock major element results are displayed in **Table 4-1**, major element results are in wt. %.

4.2.1 Major Element Geochemistry

The wacke samples from the Nooitgedagt Member have uniform concentrations. Within the Groenefontein Formation, there is a steady increase in the Al_2O_3, Fe_2O_3 and MgO concentrations from 040916/2 to 040916/5 to 040916/6. Furthermore, within the Groenefontein Formation sample, 040916/2 is more enriched in silica than the other samples.

The Huis Rivier wacke samples are mainly homogenous in the major element concentrations, however, 050916/1 has a slightly lower concentration in CaO. The Huis Rivier Formation is significantly more enriched in CaO, Fe_2O_3, MgO, TiO_2 and SiO_2 than the Nooitgedagt Member and Groenefontein Formation. Although there is an enrichment in the other major elements of the Huis Rivier Formation, there is a significant depletion of silica compared to the Nooitgedagt Member and Groenefontein Formation. There is an increase in Na_2O within the Cango Caves basin. The Na_2O concentration increases from the base (Nooitgedagt Member) to the Groenefontein Formation, and finally to the Huis Rivier Formation at the top (**Table 4-1**).

Table 4-1: Whole-rock major element geochemistry of the samples of the Cango Caves Group of the study area. The major element concentrations of the samples have been compared to that of the Upper Continental Crust (UCC) concentrations after Taylor and McLennan (1995).

MAJOR ELEMENT GEOCHEMISTRY (wt.%)

	040916/2	040916/3	040916/4	040916/5	040916/6	050916/1	050916/2A	050916/2B
SiO_2	79,43	71,83	70,76	72,98	69,20	64,27	63,00	62,87
Al_2O_3	9,66	13,34	15,59	12,97	14,85	15,50	14,54	14,74
TiO_2	0,47	0,63	0,63	0,49	0,45	0,91	1,25	1,19
MgO	0,48	0,58	0,55	0,95	1,05	2,16	2,21	2,22
Fe_2O_3	2,40	3,85	2,02	3,32	4,03	5,64	6,36	6,44
CaO	0,43	0,05	0,09	0,46	0,35	1,68	2,98	3,04
K_2O	2,44	5,41	6,03	3,40	3,55	3,31	2,68	2,72
MnO	0,03	0,00	0,00	0,02	0,03	0,07	0,12	0,11
P_2O_5	0,12	0,10	0,04	0,14	0,13	0,22	0,35	0,34
Cr_2O_3	0,02	0,02	0,02	0,01	0,01	0,02	0,01	0,01
Na_2O	1,87	1,08	0,43	1,76	2,10	2,11	2,27	2,32
LOI	1,69	2,29	3,00	2,59	3,55	3,39	3,50	3,52
TOTAL	99,04	99,18	99,16	99,09	99,30	99,28	99,27	99,52

The wacke samples of the Nooitgedagt Member are enriched in silica in comparison to the UCC composition, there is an enrichment of 10%. There is a slight enrichment in K_2O of the wacke composition compared to the UCC. There is a large deficit in the MgO, CaO and Na_2O concentrations within the Nooitgedagt Member compared to the UCC. Furthermore, concentrations of TiO_2, FeO, K_2O and P_2O_5 are typical of the UCC concentrations.

With regards to the Groenefontein Formation, there is a large deficit in the concentrations of CaO and MgO compared to the UCC. Sample 040916/2 has a 10% enrichment in silica and a 5% deficit in Al_2O_3 compared to the UCC, whereas the other samples have elemental concentrations of the aforementioned elements, that are representative of the UCC. There are slight deficits in the FeO, MnO and Na2O concentrations. TiO_2, K_2O and P_2O_5 elemental concentrations measure the same as UCC concentrations.

The Huis Rivier Formation has elemental concentrations most representative of the UCC. There are slight enrichments in TiO_2 and FeO, but these are low. There are also slight deficits in CaO and Na_2O concentrations (1% respectively).

Sedimentary rock classification was based on discrimination plots from Herron (1988). The diagram compares the silica-aluminium ratio to the iron-potassium ratio within the rock. According to the data represented in **Figure 4-7**, the samples of the Nooitgedagt Member and Groenefontein Formation are classified as wacke and sandstone (litharenite). Of the Nooitgedagt samples, 040916/3 and 040916/4 are classified as wacke. Sample 040916/2 of the Groenefontein Formation has been classified as a litharenite, whereas 040916/5 and 040916/6 are classified as wacke. The Huis Rivier Formation samples plot on the boundary of shale and wacke, although based on the petrography, they are better classified as wacke. Potential reasons for the samples plotting slightly out of the field could be the fine-grained nature of the samples and the alteration of minerals (feldspar and muscovite) to clay minerals.

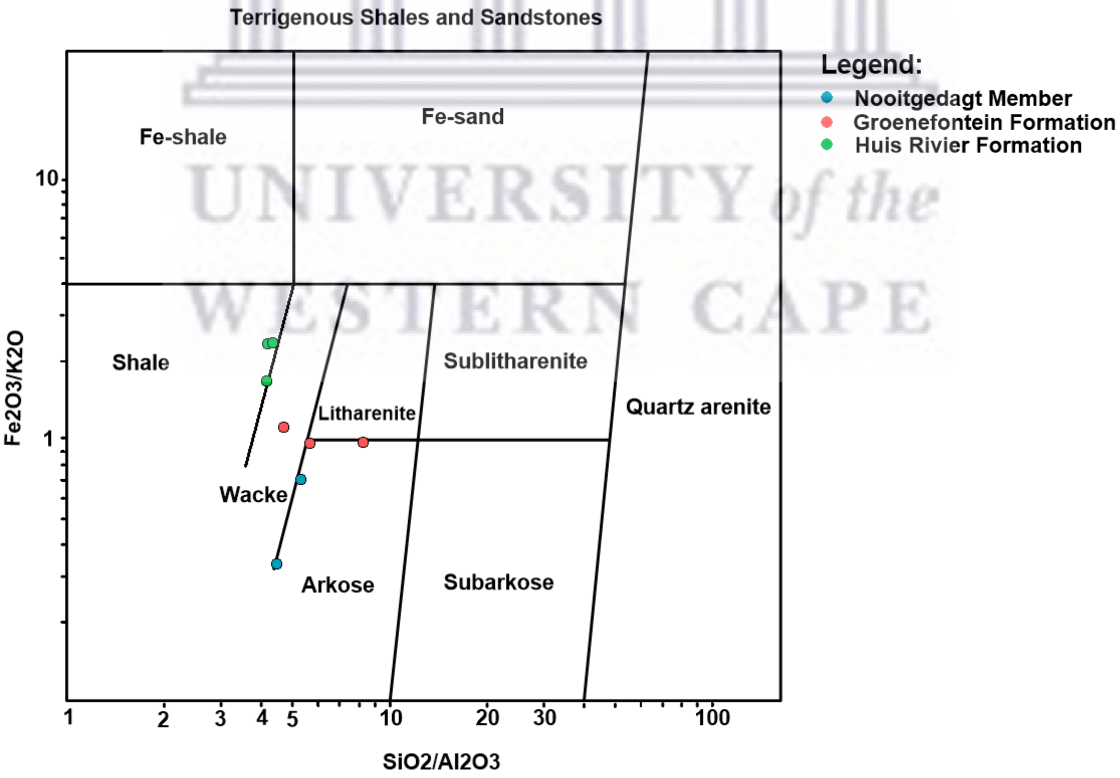

Figure 4-7: Log (SiO_2/Al_2O_3) versus log (Fe_2O_3/K_2O) discrimination diagram of Herron (1988) showing the sedimentary rock classification of the Cango Caves Group samples.

Tectonic setting of the lithologies based on major element concentrations was done according to Roser and Korsch (1986) (**Figure 4-8**). The Nooitgedagt Member plots exclusively within the Passive Margin setting, whereas the Groenefontein Formation plots within the Passive Margin and the boundary of the Passive and Active Continental Margin. Furthermore, the Huis Rivier Formation plots exclusively within the Active Continental Margin field.

Additional major element tectonic discrimination diagrams for sandstones were plotted in accordance with Bhatia and Crook (1986) (**Figure 4-9** a and b). Based on **Figure 4-9** a, the Nooitgedagt Member plots within the Active Continental Margin field and on the boundary of the Active Continental Margin and the Passive Margin. In **Figure 4-9** b, however, only one sample plots within a field and that is the Continental Island Arc. The Groenefontein Formation, in **Figure 4-9** a, plots within the Continental Island Arc field whereas, in **Figure 4-9** b, the samples also plot within the Passive Margin field. The Huis Rivier Formation plots within the Oceanic island arc field in both **Figure 4-9** a and b, however, there are outliers within both **Figure 4-9** a and b.

There are no conclusive results for the tectonic settings of the analysed samples of the Cango Caves Group based on the major elemental concentrations of the samples (**Figure 4-8** and **Figure 4-9**). Discrimination and classification diagrams based on major element concentrations alone are difficult to evaluate as the rocks are highly susceptible to weathering and alteration, therefore, they need to be evaluated with the aid of trace elements which are not as susceptible to alteration. For this reason, trace element geochemical discrimination plots will be used to validate **Figure 4-8** and **Figure 4-9** and provide more conclusive results.

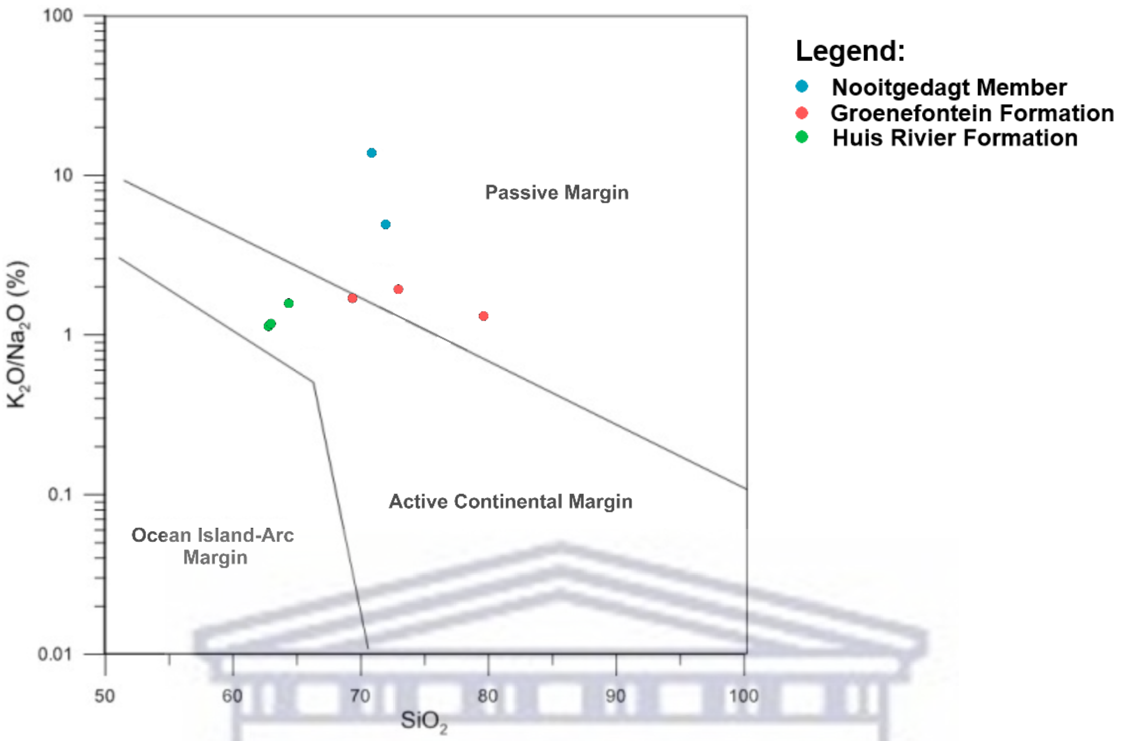

Figure 4-8: SiO2 vs K2O/Na2O discrimination diagram after Roser and Korsch (1986), indicating the geotectonic setting for the studied lithological units.

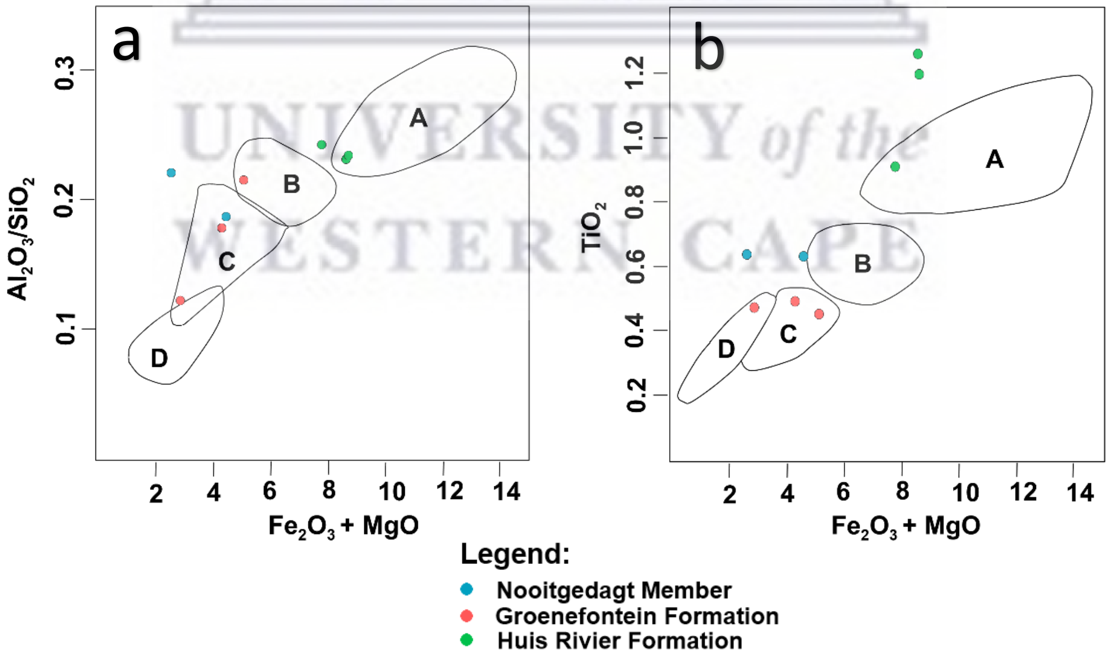

Figure 4-9: Major element composition plots of sands and sandstones for tectonic setting discrimination. a – Al_2O_3 / SiO_2 vs Fe_2O_3 + MgO; b – TiO_2 vs Fe_2O_3 + MgO, after Bhatia (1983). A = Oceanic Island Arc; B = Continental Island Arc; C = Active Continental Margin; D = Passive Margin.

4.2.2 Alteration

According to Nesbitt (2003), the major element composition of clastic sedimentary rocks is affected by three main processes: weathering; transportation and sorting; and diagenesis and metamorphism. These three processes affect mobile elements, therefore, before possible source rocks can be identified, the degree of alteration of the rocks must be determined.

Chemical weathering acts as the main factor affecting the bulk composition (Nesbitt, 2003). Feldspar is the most common mineral in supracrustal clastic sediments and is also the most consistently altered. Feldspar alters to albite and finally illite and kaolinite, resulting in the minerals become increasingly enriched in aluminium (Nesbitt, 2003). Based on these factors, the Chemical Index of Alteration (CIA), after Nesbitt and Young (1982), is most suited to determine the degree of alteration of the rocks. The following formula is applied to calculate CIA using the mole percentage values for oxides (CaO* is the calcium content of silicates):

$$CIA = 100 \times (Al_2O_3 / (Al_2O_3 + Na_2O + CaO^* + K_2O)$$

The ratio is based on the assumption that the dominant process during chemical weathering is the degradation of feldspars and the formation of clay minerals (Goldberg and Humayun, 2010). High CIA values indicate a high degree of alteration.

There are several factors that affect the CIA which need to be considered. These include sediment provenance, hydraulic sorting and post-deformational processes that lead to K^+ addition (K-metasomatism). The contribution of different source rocks to the formation of sediments can be examined using the A-CN-K plot and the Ti /Al ratio. According to Goldberg and Humayun (2010), hydraulic sorting significantly influences the chemical composition of terrigenous sediments due to grain size and sorting, where finer sediments have higher Al concentrations (i.e., clays). Furthermore, larger grain sizes tend to concentrate feldspars, resulting in lowered CIA values. K-metasomatism leads to complexities as it increases the K concentration, which in turn, lowers the CIA.

A further geochemical method used to evaluate chemical alteration or degree of weathering is the K/Cs ratio. This ratio is used to quantify the chemical weathering of feldspar (Naidoo, 2008). The higher the ratio yielded, the lower the degree of alteration of feldspar, as K and Cs are absorbed during chemical weathering and the formation of clay. The addition of K from secondary processes (i.e., K-metasomatism) must also be considered when calculating the ratio, as this results in an increase of K.

The different geological units of the Cango Caves Group have CIA values which average between 55 - 67%. There is slight decrease in CIA values from the bottom of the Cango Caves Group to the top, indicating reduced chemical alteration or K-enrichment. The CIA values of the Nooitgedagt Member range from 63 - 68%.

The Groenefontein Formation has CIA values which range from 59 - 65%. Sample 040916/2 is the anomalous value as it produced the lowest CIA. The other two samples (040916/5 and 040916/6) have homogenous major geochemical concentrations, whereas the above-mentioned sample has a relatively depleted concentration of Al_2O_3 and is enriched in silica. This indicates a lower degree of alteration as the feldspar alterations produce clay minerals (i.e., an increase in Al concentration).

The Huis Rivier Formation has the lowest CIA values with an average of 56% and, therefore, is the least altered from the sampled geological units of the Cango Caves Group.

4.2.3 Weathering

Figure 4-10 displays the general weathering trend of the Cango Caves Group. The Nooitgedagt Member plots towards muscovite compositions, closer to the K-feldspar composition and away from any normal weathering trend, which indicates an increase in secondary K from K-metasomatism. The geochemical data confirms the K-enrichment, mainly with the two wacke samples (that plot the closest to K-feldspar composition with enriched concentrations of K_2O (>5 wt.%)).

The Groenefontein Formation follows the granite normal weathering trend and plots towards illite compositions. The Huis Rivier Formation plots towards illite compositions and suggests compositions between granodiorite (UCC) and granite. The very fine-grained wacke (050916/1) is slightly more enriched in K_2O and plots closer to the granite weathering trend. Furthermore, the collected samples have undergone intermediate weathering (**Figure 4-10**).

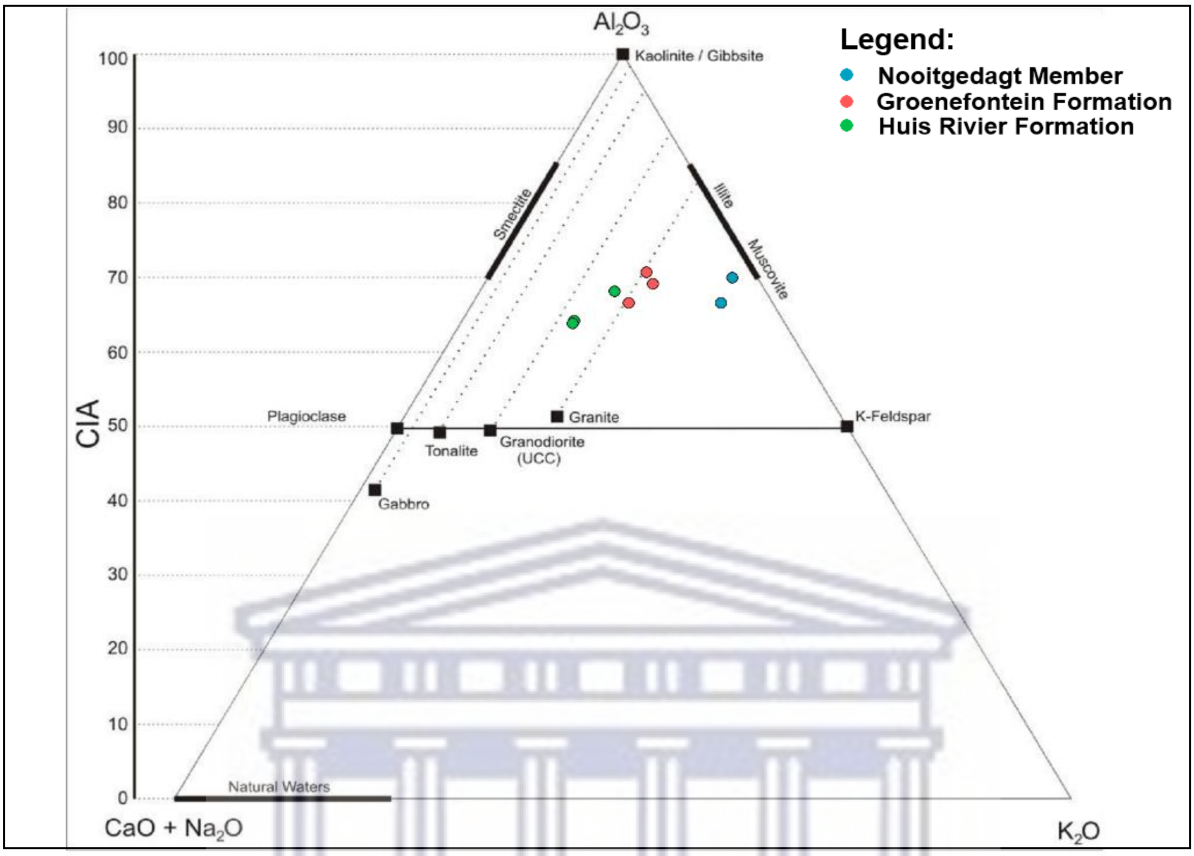

Figure 4-10: CIA diagram showing the general weathering trend of the sampled lithologies of the Cango Caves Group. Modified after Nesbitt and Young (1989).

The two wacke samples of the Nooitgedagt Member have high K/Cs ratios (040916/3 - 21696.19; 040916/4 - 13714.53) (**Figure 4-11**). The wacke samples plot above the typical UCC, whereas the sandstone plots closer, but slightly lower, to the typical UCC value. The high K/Cs ratios and low CIA values could indicate the addition of K from K-metasomatism.

Samples from Groenefontein Formation and the Huis Rivier Formation have ratios which plot between the UCC and the Post-Archean Australian Average Shale (PAAS), after Taylor and McLennan (1985) (**Figure 4-11**).

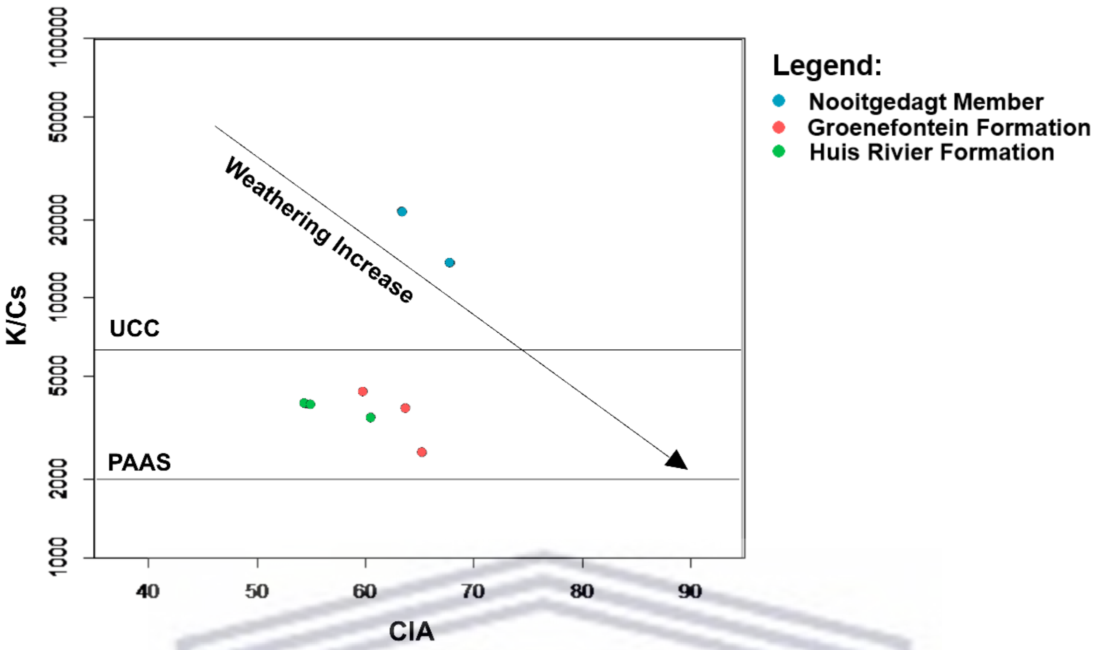

Figure 4-11: K/Cs vs CIA diagram (after McLennan et al., 1993) indicating ratios between UCC and PAAS for the sampled units of the Cango Caves Group.

Another way to compare the evolution of chemical weathering degree is by evaluating the Weathering Index of Parker (WIP), (Parker, 1970), and comparing it to the CIA (González et al., 2017). According to González et al. (2017), the WIP takes into account the transformation of feldspars to clay minerals with respect to the mobility of major alkali and alkaline earth elements. Furthermore, it considers the differential strengths of oxygen bonds and the relation to differential mobility of elements. The WIP is defined by the following formula (Parker, 1970):

$$\text{WIP} = 100 \times [(2Na_2O/0.35) + (MgO/0.9) + (2K_2O/0.25) + (CaO/0.7)]$$

The degree of weathering is inversely proportionate to the WIP values. The degree of weathering can be graphically evaluated by comparing the CIA to the WIP (**Figure 4-12**). The three studied lithological units of the Cango Caves Group fall between the same field (WIP between 30 and 60; CIA between 50 and 70). The samples have undergone intermediate weathering (**Figure 4-12**).

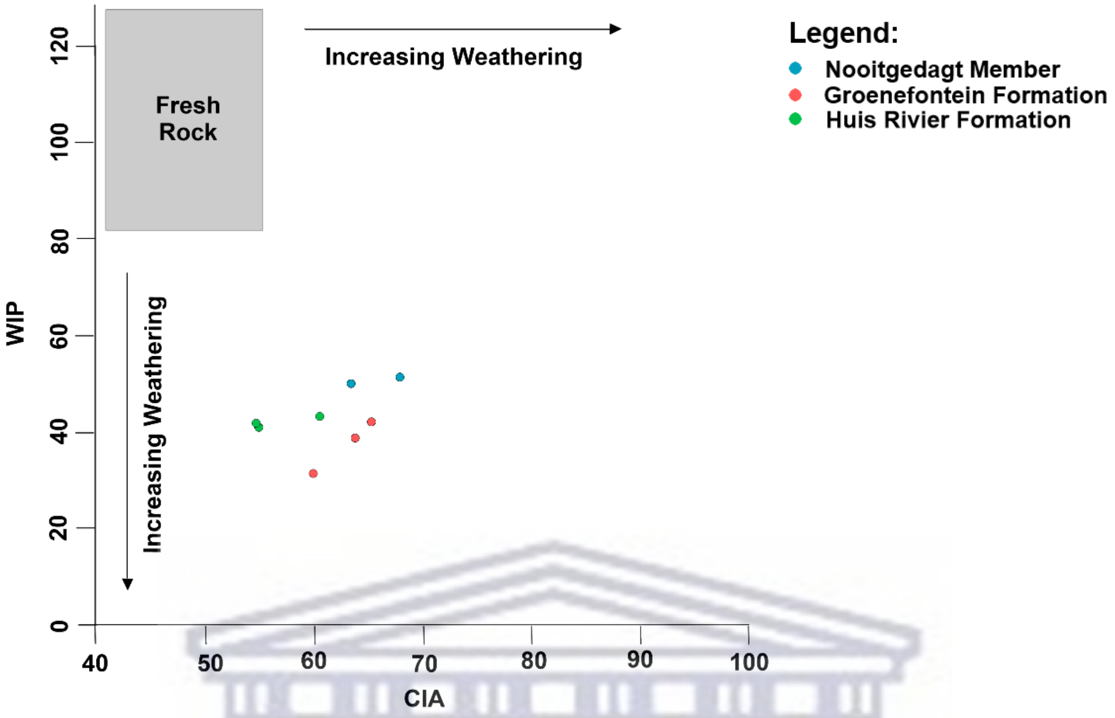

Figure 4-12: Relationship between two weathering proxies, CIA and WIP, for the sedimentary rocks of the Nooitgedagt Member, Groenefontein Formation and Huis Rivier Formation of the Cango Caves Group (after González et al., 2017).

4.2.4 Trace Element Geochemistry

Imperative contributions in interpreting pre-Mesozoic plate settings are provided by the composition of sedimentary rocks. Multiple provenance regions have been destroyed, and the only data available is in the sediments derived from them. The relationship between sediment composition and plate tectonics is therefore a powerful tool for recognising early tectonic settings (Bhatia and Crook, 1986).

Trace elements are useful for determining the tectonic setting of a basin. Notably, the immobile trace elements such as La, Ce, Nd, Y, Th, Zr, Hf, Nd, Ti and Sc are most fit for determining the provenance and tectonic settings of an area. These elements reflect the signature of the parent material as they are transported quantitively into clastic sedimentary rocks during weathering and transportation (Bhatia and Crook, 1986). These trace elements will be used to determine source rock composition, degree of weathering and paleotectonic setting for the Cango Caves Group. The results for the trace element geochemistry are displayed in **Table 4-2**, where trace element concentrations are displayed in parts per million (ppm).

Table 4-2: Whole-rock trace element geochemistry of the samples of the Cango Caves Group of the study area.

TRACE ELEMENT GEOCHEMISTRY (PPM)

	040916/2	040916/3	040916/4	040916/5	040916/6	050916/1	050916/2A	050916/2B
Sc	14,45	17,29	16,9	14,96	16,12	18,51	19,97	19,28
V	41,6	63,25	46,36	53,45	61,39	90,45	99,25	98,55
Cr	144,25	187,9	161	121,9	105,9	152,1	147,75	139,5
Co	4,1	0,97	1,03	6,34	9,07	12,9	13,1	13,11
Ni	15,35	8,5	14,85	17,65	22,15	30,35	26,65	29,55
Cu	14,54	9,01	14,24	18,02	18,5	31,41	22,15	26,39
Zn	35,95	65,6	30,35	59,6	67,25	90,4	88,05	90,1
Rb	102,85	161,15	191,4	153,35	174,05	140,3	109,1	110,95
Sr	96,05	77,5	53,9	104,15	76,3	96,1	300,1	298,5
Y	41,45	32,64	38,17	26,53	31,9	42,5	65,3	62,33
Zr	459,3	371,85	391,3	288,5	197,8	378,6	904,4	795,4
Nb	10,26	18,47	15,63	11,06	11,57	15,71	20,16	19,76
Mo	6,94	9,98	9,12	4,85	3,61	5,36	4,24	3,78
Cs	4,63	2,07	3,65	7,42	11,64	7,85	5,71	5,77
Ba	349,6	939	1007,5	429,95	463,45	449,9	408,6	404,7
Hf	13,8	11,04	11,34	8,76	6,14	10,57	25,94	22,94
Ta	0,72	0,88	0,86	0,73	0,73	0,9	1,34	1,31
Pb	18,89	20,77	39,55	27,14	24,32	18,55	23,66	21,89
Th	19,32	21,16	19,85	12,18	10,71	14,71	32,53	29,09
U	3,82	2,6	2,13	2,71	2,73	3,88	6,34	5,77

According to Winchester and Floyd (1997), the compositional trend of sedimentary rocks can be determined by evaluating the ratios of highly immobile elements, which include the Nb/Y and Zr/Ti ratios (**Figure 4-13**). These four elements are particularly useful as they are highly incompatible and are not significantly affected during weathering and transportation (Fourie, 2012). The sampled rocks from the Cango Caves Group exhibit rhyolitic to rhyodacite source compositions. The wacke of the Nooitgedagt has a rhyolitic source composition. The Groenefontein Formation and Huis Rivier Formation have a spread in the Zr/Ti ratio, these formations exhibit rhyolitic to rhyodacite source compositions.

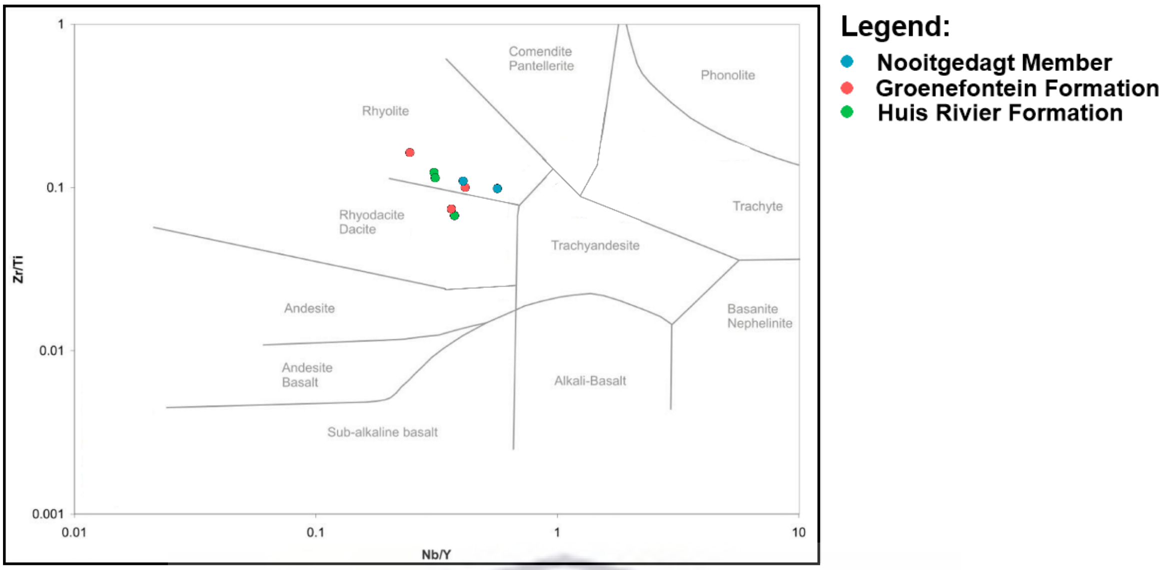

Figure 4-13: Zr/Ti vs Nb/Y discrimination diagram indicating the general composition of sedimentary rocks. After Winchester and Floyd (1997).

Sandstones tend to become enriched in certain trace elements as a result of sediment reworking, namely Ti, Th, Zr and Sc. Sc is a compatible element with a tendency for a less fractionated material, whereas Zr and Th are incompatible elements and increase in concentration with the deposition of more fractionated material. Zr will be enriched over Sc with an increase in sediment reworking. Higher Th/Sc ratios reveal the degree of fractionation of the igneous component included in the detrital mix. Hence, the factors allow for a comparison between the Zr/Sc and Th/Sc ratios (**Figure 4-14**) and provide a good indicator of source compositions (Naidoo, 2008).

Figure 4-14 shows the reworking trend for the samples of the Cango Caves Group which all show similar trends. The Th/Sc ratios of the samples (0.6 - 1.7) indicate that they have an UCC composition and have undergone minor sediment reworking. The Nooitgedagt Member and Groenefontein Formation have similar recycling trends with typical UCC Th/Sc and Zr/Sc ratios. 040916/6 from the middle Nelsrivier Member of the Groenefontein Formation has undergone the lowest degree of reworking with a Th/Sc ratio of 0.66 and Zr/Sc ratio of 12.27. The Huis Rivier Formation shows slightly higher reworking than the other units. The Huis Rivier Formation has high Sc concentrations, but also shows similar UCC concentrations with the one sample (050916/1). Th/Sc and Zr/Sc ratios indicate a less fractionated source component mixed with UCC for the Cango Caves Group.

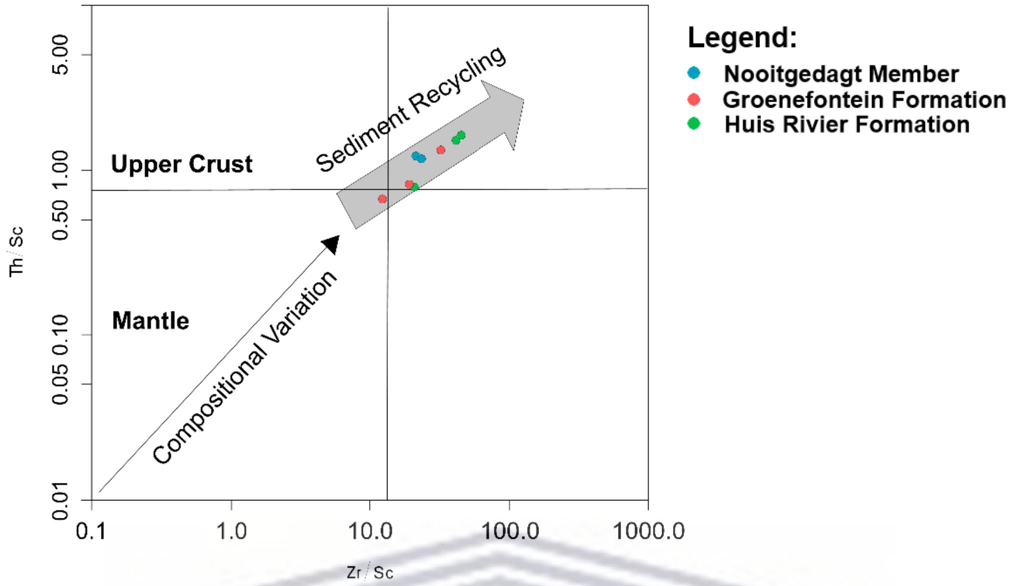

Figure 4-14: Th/Sc vs Zr/Sc ratios of samples of the Cango Caves Group. After McLennan et al. (1990).

Discriminant diagrams based on trace element concentrations are useful for determining the paleotectonic setting in which clastic rocks were deposited. **Figure 4-15** a, b and c are based on the trace element concentrations of La, Th, Sc, Zr and Ti. These trace elements are useful for discriminant diagrams as they are not as susceptible to post sedimentary processes such as diagenesis, metamorphism and fluid flow. Based on the discriminant diagrams in **Figure 4-15**, the sampled rocks of the Cango Caves Group point to a Continental Island Arc setting.

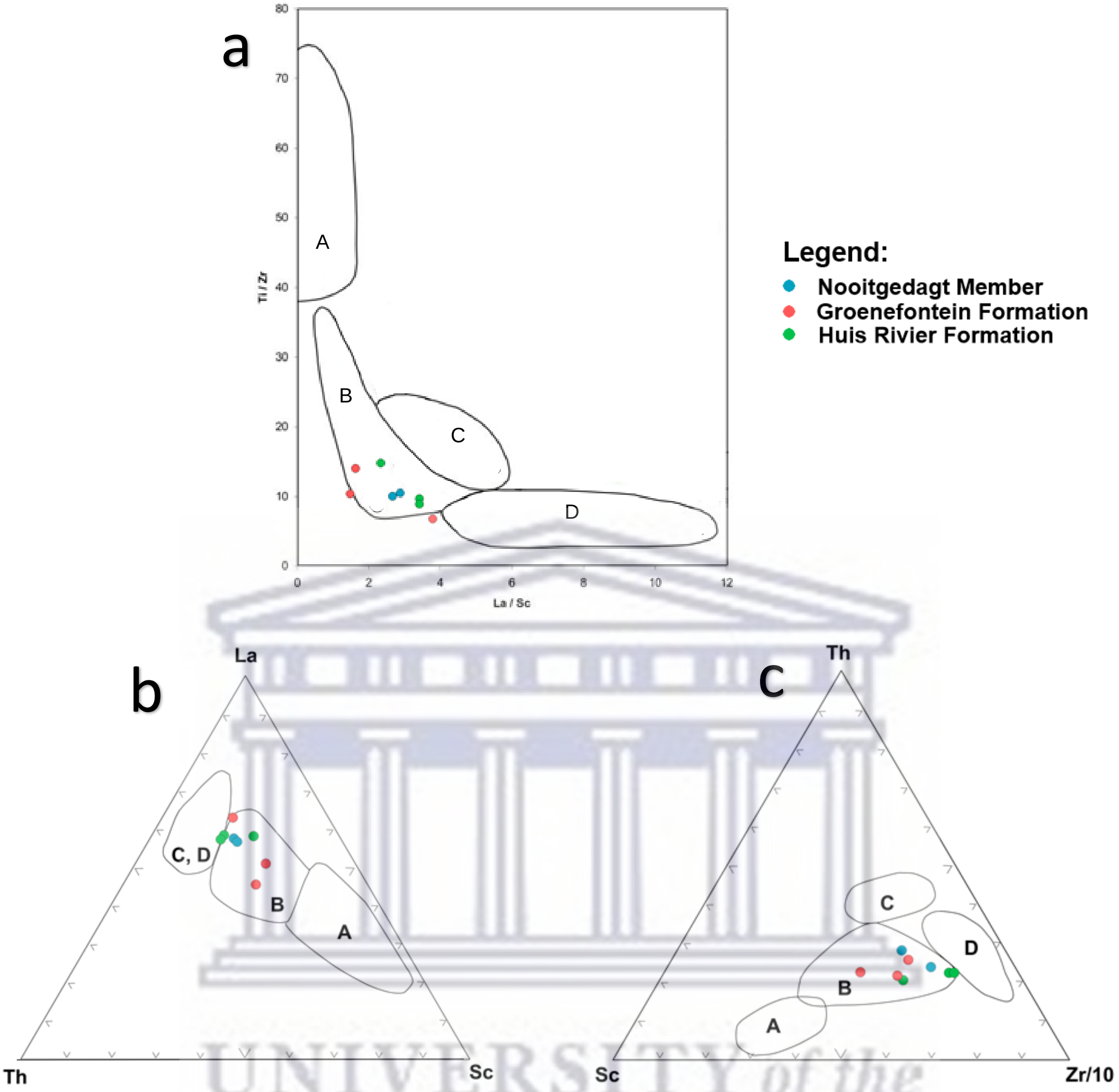

Figure 4-15: Trace element tectonic discriminant diagrams. a – Ti/Zr vs La/Sc; b – Th-La-Sc; c – Sc-Th-Zr/10, after Bhatia and Crook (1986). A = Oceanic Island Arc; B = Continental Island Arc; C = Active Continental Margin; D = Passive Margin.

4.2.5 Rare Earth Element Geochemistry

Chemical changes associated with weathering, erosion, sediment transport, deposition and diagenesis are complicated, however, it has been shown that some elements are transported, in effect quantitatively, in terrigenous components of sediment (McLennan and Taylor, 1991). Of these elements, rare earth elements (REE), Th and Sc, are the most useful for inferring crustal composition, as these elements are not affected by secondary processes (McLennan and Taylor, 1991). The results of the REE geochemical data were normalised to upper continental crust values after Taylor and McLennan (1985). The REE geochemical data, displayed in ppm, for the Cango Caves Group is presented in **Table 4-3**.

Table 4-3: Rare-earth element (REE) geochemistry of the samples of the Cango Caves Group of the study area.

RARE EARTH ELEMENTS (REE) (ppm)

	040916/2	040916/3	040916/4	040916/5	040916/6	050916/1	050916/2A	050916/2B
La	56,41	50,91	47,58	22,08	27,54	44,80	70,13	67,85
Ce	124,90	104,30	96,85	79,80	71,81	94,55	152,90	146,70
Pr	14,77	12,66	11,68	6,69	7,46	11,59	19,06	18,28
Nd	56,45	46,80	44,08	26,12	28,87	44,15	73,70	70,30
Sm	11,82	9,39	8,06	6,32	6,54	9,51	15,60	14,72
Eu	1,36	1,95	1,94	0,95	1,06	1,83	2,07	2,14
Gd	9,76	7,91	7,20	5,54	6,17	8,50	13,42	12,83
Tb	1,46	1,10	1,04	0,87	0,94	1,37	2,02	1,89
Dy	8,88	6,25	6,68	5,19	6,10	7,68	12,06	11,24
Ho	1,74	1,28	1,47	0,98	1,14	1,53	2,50	2,28
Er	5,11	3,65	4,41	3,02	3,45	4,53	7,09	6,88
Tm	0,75	0,49	0,59	0,45	0,48	0,62	0,99	0,98
Yb	4,76	3,28	4,04	2,78	3,26	4,26	6,86	6,51
Lu	0,67	0,52	0,65	0,40	0,48	0,64	1,03	0,98
Σ REE	298,84	250,49	236,27	161,19	165,30	235,56	379,43	363,58
LREE/HREE	7,98	9,15	7,99	7,33	6,46	7,02	7,21	7,29
(La/Sm)n	0,72	0,81	0,89	0,52	0,63	0,71	0,67	0,69
(Eu/Eu*)n	0,60	1,06	1,20	0,75	0,78	0,96	0,67	0,73
(La/Yb)n	0,87	1,14	0,86	0,58	0,62	0,77	0,75	0,76
(Gd/Yb)n	1,19	1,40	1,03	1,15	1,10	1,16	1,13	1,14
Ce/Ce*	1,11	1,01	0,98	1,83	1,34	1,08	1,08	1,07
Ce/Yb	0,90	1,09	0,82	0,99	0,76	0,76	0,77	0,77
Ce/Sm	0,74	0,78	0,84	0,89	0,77	0,70	0,69	0,70
Gd/Lu	1,23	1,28	0,93	1,17	1,08	1,12	1,10	1,10
La/Lu	0,90	1,04	0,78	0,59	0,61	0,75	0,73	0,74

According to Rudnick and Gao (2003), the REE patterns of shales PAAS reflect that of the average upper-continental crust. The Cango Caves Group samples in the study area have REE concentrations similar to that of the upper continental crust normalised concentrations, with a minimal enrichment of Light Rare Earth Elements (LREE) and Heavy Rare Earth Elements (HREE) for certain sampled formations (**Figure 4-16** a).

The wacke samples of the Nooitgedagt Member are slightly enriched in LREE and HREE. The Groenefontein Formation samples are all slightly enriched in HREE, whereas the wacke samples have LREE values similar to the UCC, and the litharenite is slightly enriched in the

LREE. All samples of the Huis Rivier Formation are enriched relative to the normalised UCC, evident by the LREE and HREE values above 1 (**Figure 4-16** a).

The Nooitgedagt Member, Groenefontein Formation and Huis Rivier Formation are characterised by relatively flat REE patterns (La/Lu = 0.78 - 1.044; 0.61 - 0.9; 0.73 - 0.75 respectively) in comparison to the UCC (**Figure 4-16** a). Furthermore, the units are characterised by low La/S values of 0.81 - 0.89; 0.52 - 0.72; 0.67 - 0.71 respectively, and Gd/Lu values of 0.93 - 1.45; 1.08 - 1.23; 1.1 - 1.12 respectively. The low La/Lu value indicates little fractionation or enrichment of LREE relative to HREE.

The samples of the Nooitgedagt Member exhibit moderate-to-strong positive Eu anomalies (1.06 - 1.2 ppm). The Groenefontein Formation exhibits a moderate-to-strong negative Eu anomaly (0.6 - 0.78 ppm), and the Huis Rivier Formation exhibits a weak-to-strong negative Eu anomaly (0.73 - 0.96 ppm).

The spider plot in **Figure 4-16** b shows that the trace element concentrations, of the sampled geological units of the Cango Caves Group, plot relatively close to the UCC (plotting close to 1), with slight enrichments and depletions in certain trace elements. The samples show negative anomalies in the Heavy Field Strength Elements (HFSE) Nb, Ta, Ti and U (strongest negative anomalies are Nb and Ta), with the Light Iron Lithophile Elements (LILE) Sr displaying the largest depletion/negative anomaly.

Furthermore, K shows a negative anomaly in the Groenefontein Formation and the Huis Rivier Formation, whereas in the Nooitgedagt Member it displays a positive anomaly. There is also a slight positive anomaly in HFSE Ti and slight enrichments in Zr, Hf and Y.

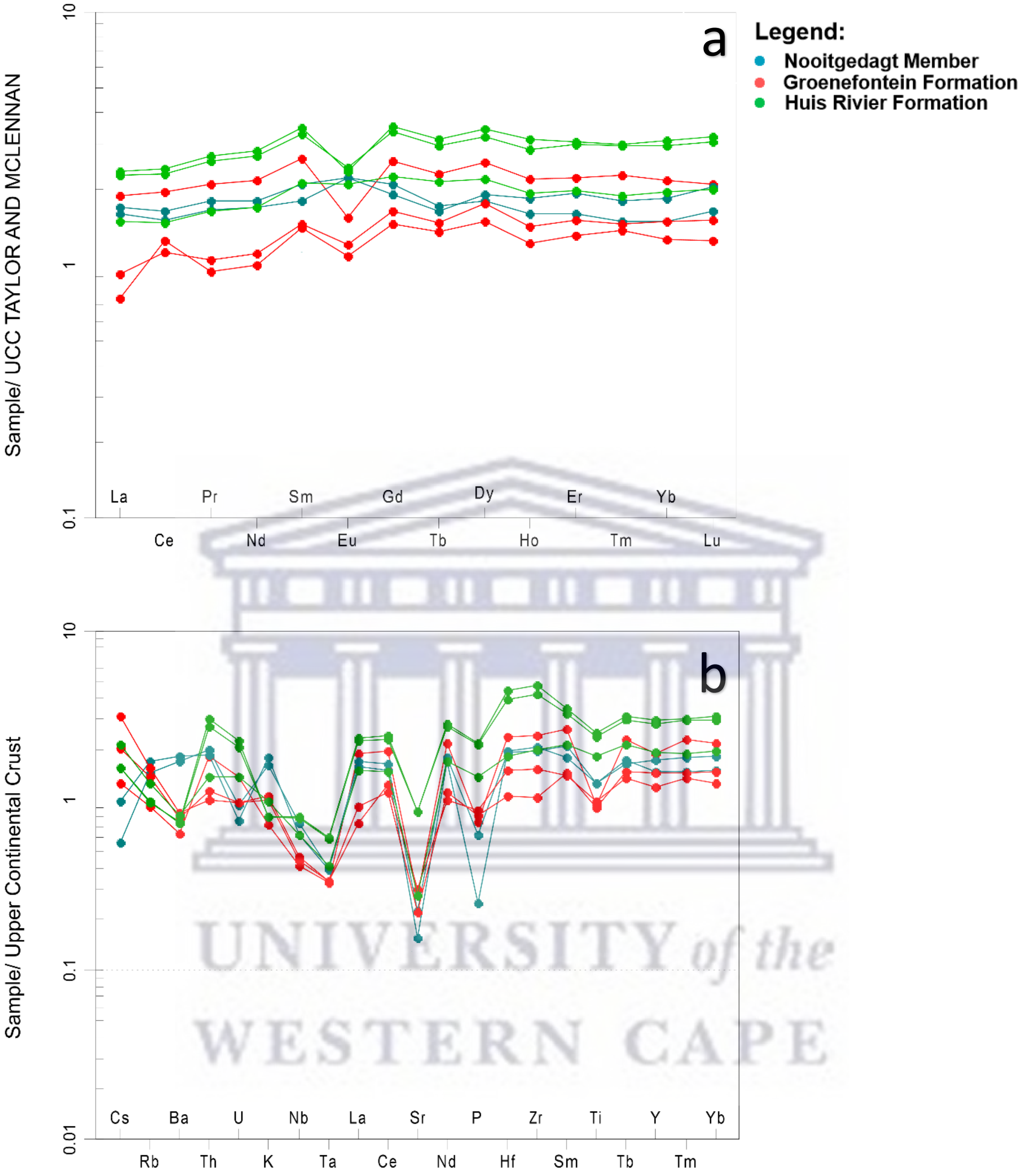

Figure 4-16: a – REE plot of the samples of the Cango Caves Group. b – Trace element spider plot of samples of the Cango Caves Group. Both normalised to UCC concentrations after Taylor and McLennan (1995).

4.2.6 Isotope Geochemistry

Samples from three lithological units from the Cango Caves Group (Nooitgedagt Member, Groenefontein Formation and Huis Rivier Formation) were selected for whole-rock Sm-Nd and Rb-Sr analyses. The results are presented in **Figure 4-17** and **Table 4-4**. The single-stage Nd model ages were calculated using a Sm decay constant of 6.54×10^{-12} $year^{-1}$ (Lugmair and Marti, 1978) and the depleted mantle values of DePaolo (1981). The initial $^{87}Sr/^{86}Sr$ (Sr_I) ratios were calculated using a Rb decay constant of 1.42×10^{-11} $year^{-1}$ (Steiger and Jäger, 1977).

Nooitgedagt Member:

Isotopic data for the Nooitgedagt Member illustrates relatively constant Sm-Nd ratios between 0.11 and 0.12. $^{143}Nd/^{144}Nd$ ratios for the Nooitgedagt Member samples are also constant with ratios of 0.512.

εNd(t) values are within a range that is relatively close to zero, with a minimum value of 0.67 and a maximum value of 1.55. Sample 040916/4 exhibits a positive value of 1.55, indicating a depleted source. Sample 040916/3 has a value of 0.67, pointing towards a depleted source that had some influence from a crustal component. Sm-Nd model ages (T_{DM}) vary from 1.80 - 1.56 Ga, which range from the Paleoproterozoic to the Mesoproterozoic Era.

Groenefontein Formation:

Sm-Nd ratios for the lithologies of the Groenefontein Formation are 0.13, while initial $^{143}Nd/^{144}Nd$ ratios of 0.51 were recorded. εNd(t) values for the samples of the Groenefontein Formation are negative for all the samples. Samples 040916/2, 040916/5 and 040916/6 have εNd(t) values of -3.15, -3.50 and -3.07 respectively. These highly negative εNd(t) values indicate a more enriched source. Sm-Nd model ages (T_{DM}) vary from 1.76 to 1.62 Ga, which indicate a Paleoproterozoic source.

Huis Rivier Formation:

Isotopic data for the Huis Rivier Formation shows constant Sm-Nd ratios of 0.12 and 0.13 for the lithologies, as well as consistent $^{143}Nd/^{144}Nd$ ratios of 0.51. εNd(t) values for 050916/1, 050916/2A and 050916/2B are -3.24, -2.54 and -2.68 respectively. The negative values point to an enriched source. Sm-Nd model ages (T_{DM}) vary from 1.69 to 1.56 Ga, which indicate a Paleoproterozoic source.

Table 4-4: Whole rock isotopic data for the Cango Caves Group of the study area.

Sample	Formation	Sm	Nd	$^{143}Nd/^{144}Nd$	$^{147}Sm/^{144}Nd$	2s.e.	n	Epsilond(0)	Nd(t)	T(ma)	CHUR (t)	End(t)	$^{87}Sr/^{86}Sr$	2s.e.	n	TDM	TCHUR	Rb	Sr
040916/2	Groenefontein	12.6	60.1	0.512223	0.1265	0.000004	76	-7.93	0.51177	550.00	0.51193	-3.155873	0.736122	0.000011	77	1.6177	0.9001	102.85	96.05
040916/3	Nooitgedagt	15.8	80.6	0.512109	0.1187	0.000004	76	-10.16	0.51125	1100.00	0.51122	0.667185	0.761770	0.000009	77	1.6684	1.0336	161.15	77.5
040916/4	Nooitgedagt	14.5	78.6	0.512100	0.1112	0.000003	74	-10.34	0.51130	1100.00	0.51122	1.5502	0.768330	0.000009	76	1.5599	0.9592	191.4	53.9
040916/5	Groenefontein	6.8	30.7	0.512234	0.1344	0.000003	76	-7.72	0.51175	550.00	0.51193	-3.501327	0.742820	0.000008	73	1.7583	0.9879	153.35	104.15
040916/6	Groenefontein	7.1	33.3	0.512234	0.1281	0.000004	76	-7.73	0.51177	550.00	0.51193	-3.069809	0.753517	0.000014	78	1.6300	0.8986	174.05	76.3
050916/1	Huis Rivier	9.1	42.9	0.512218	0.1287	0.000003	74	-8.04	0.51174	570.00	0.51190	-3.239953	0.742548	0.000009	77	1.6685	0.9409	140.3	96.1
050916/2A	Huis Rivier	15.8	76.5	0.512239	0.1248	0.000002	77	-7.62	0.51177	570.00	0.51190	-2.541009	0.724543	0.000010	78	1.5603	0.8455	109.1	300.1
050916/2B	Huis Rivier	15.4	74.6	0.512231	0.1245	0.000004	77	-7.78	0.51177	570.00	0.51190	-2.677816	0.724821	0.000009	77	1.5684	0.8589	110.95	298.5

- ε Nd(t) = (($^{143}Nd/^{144}Nd(i)/^{143}Nd/^{144}Nd(CHUR, t)$)-1) x 10000

- TDM = 1/ (λ) × ln (1+ ($^{143}Nd/^{144}Nd(0)–^{143}Nd/^{144}Nd(DM)/^{147}Sm/^{144}Nd–^{147}Sm/^{144}Nd$ (DM))) × 0,000000001 (after DePaolo, 1981) where ($^{143}Nd/^{144}Nd$)DM = 0.51351, ($^{147}Sm/^{144}Nd$)DM = 0.2136

- TCHUR = 1/ (λ) ×ln (1+ ($^{143}Nd/^{144}Nd(0)–^{143}Nd/^{144}Nd$ (CHUR, t))/$^{147}Sm/^{144}Nd–^{147}Sm/^{144}Nd$ (CHUR, t)) × 109 (after DePaolo, 1981) where ($^{143}Nd/^{144}Nd$)(CHUR, t) = 0.512638, ($^{147}Sm/^{144}Nd$)(CHUR, t) = 0.1967

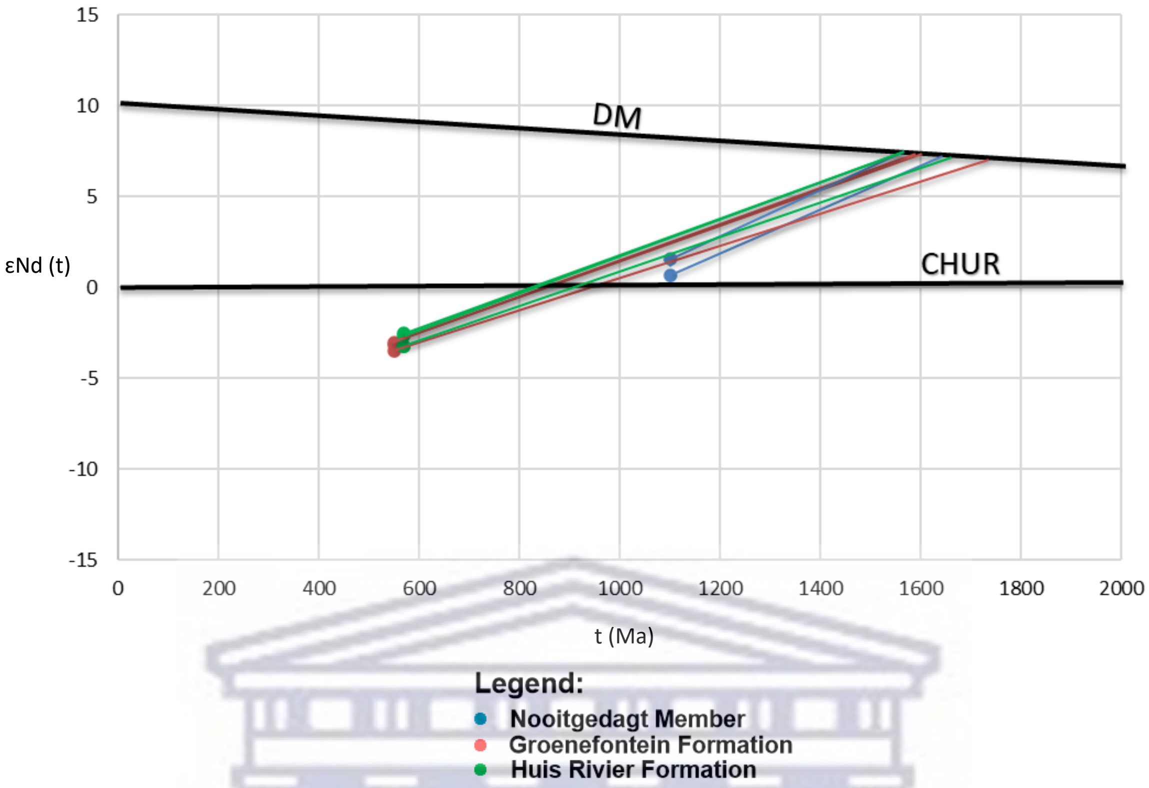

Figure 4-17: εNd (t) vs Age (Ma) for the Nooitgedagt Member, Groenefontein Formation and Huis Rivier Formation of the Cango Caves Group (Eglington, 2006).

4.3 U-Pb Geochronology

The Matjies River Formation (basal Nooitgedagt Member), Groenefontein Formation and the Huis Rivier Formation of the Cango Caves Group were dated. The Matjies River Formation and the Groenefontein Formation were sampled from the central Kango Inlier, whereas the Huis Rivier Formation was sampled from the west of the Kango Inlier. A description of the resultant U-Pb ages from the zircon grains for the sampled formations of the Cango Caves Group are described in this section.

Uncertainties on individual analyses in data tables are reported at 2 σ level and mean ages for pooled U/Pb analyses are quoted with 90%. To eliminate uncertainty, dates with discordance greater than 10% are not used in determining the weighted mean ages.

4.3.1 Nooitgedagt Member:

One sample from the Nooitgedagt Member of the Matjies River Formation was dated, 040916/3. The sample outcrops in the central zone of the Kango Inlier. **Appendix A** presents the U-Th-Pb isotopic analyses performed on zircon grains from 040916/3. The zircon grains from the Nooitgedagt Member are euhedral to subhedral and range in size from ~100 - 400 µm. The zircons are transparent and display percussion marks caused by abrasion from transportation. The cathodoluminescence (CL) imaging of the grains show a mix of zircons displaying concentric zonation patterns and zircons with no zonation (**Figure 4-18)**.

A total of 114 U-Th-Pb analyses on zircon grains from 040916/3 were completed. Twenty-four of these analyses did not pass the <10% discordancy test. 040916/3 produced a U-Pb Concordia age of 1077 ± 3 Ma, with minimum and maximum ages of 1009 and 1135 Ma, respectively (**Figure 4-19)**.

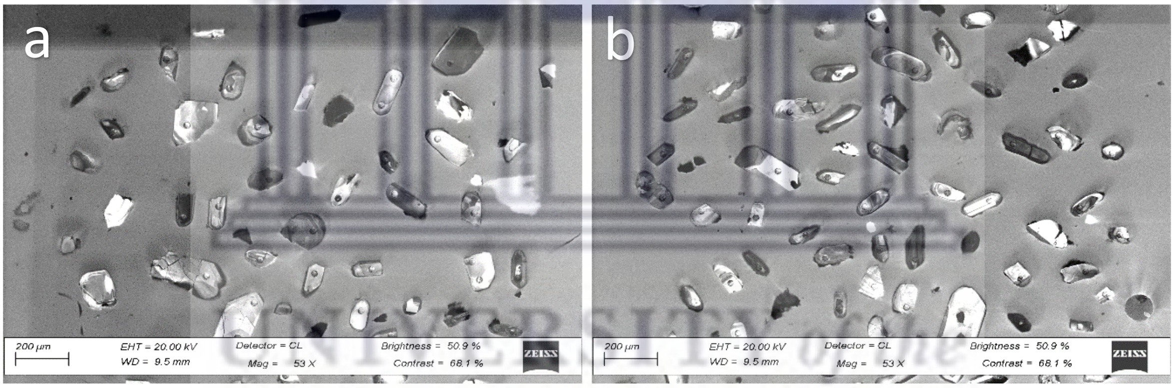

Figure 4-18: Cathodoluminescence images for 040916/3 from the Nooitgedagt Member of the Matjies River Formation.

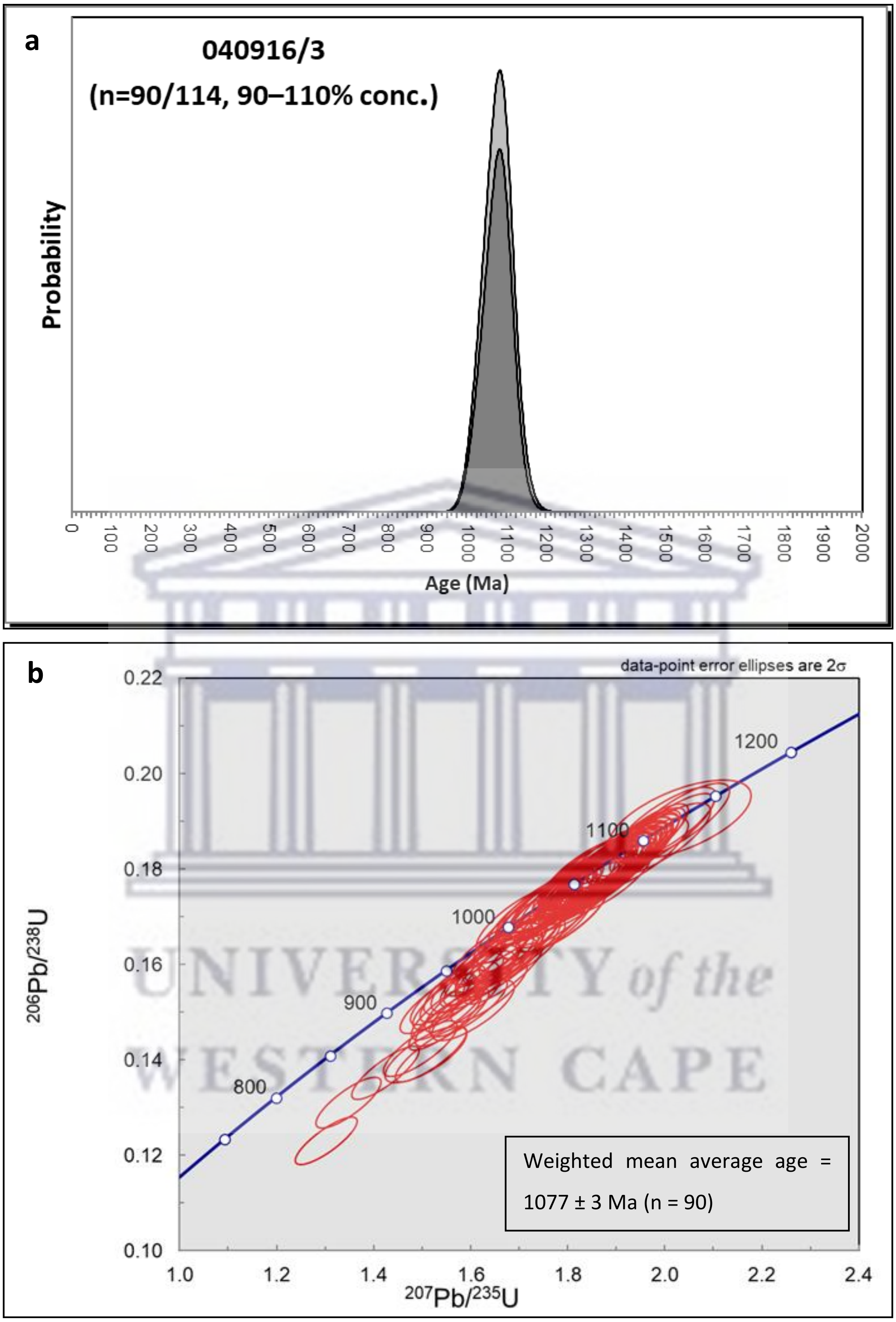

Figure 4-19: a – Probability distribution of sample 040916/3 from the middle Nooitgedagt Member of the Matjies River Formation. b – Concordia diagram of 040916/3 showing the $^{206}Pb/^{238}U$ ages of zircons: data-point ellipses are plotted at 2σ.

4.3.2 Groenefontein Formation:

Three samples from the Groenefontein Formation were dated, including 040916/2, 040916/5 and 040916/6. Samples 040916/2 and 040916/5 were sampled from the central – northern zone of the Kango Inlier. These samples are from the lower Nelsrivier Member of the Groenefontein Formation. 040916/6 was sampled within the central – eastern zone of the inlier and was sampled from the middle Nelsrivier Member.

Zircons from the Groenefontein Formation are more homogenous than the Nooitgedagt Member in terms of size, colour, shape and other morphologically distinguishing criteria. This is due to longer transportation distances and sedimentary mixing during the deposition. The zircon grains are subrounded and vary in size from ~100 - 200 µm. The zircons display strong concentric zonation (**Figure 4-20**, **Figure 4-21**, **Figure 4-22)**.

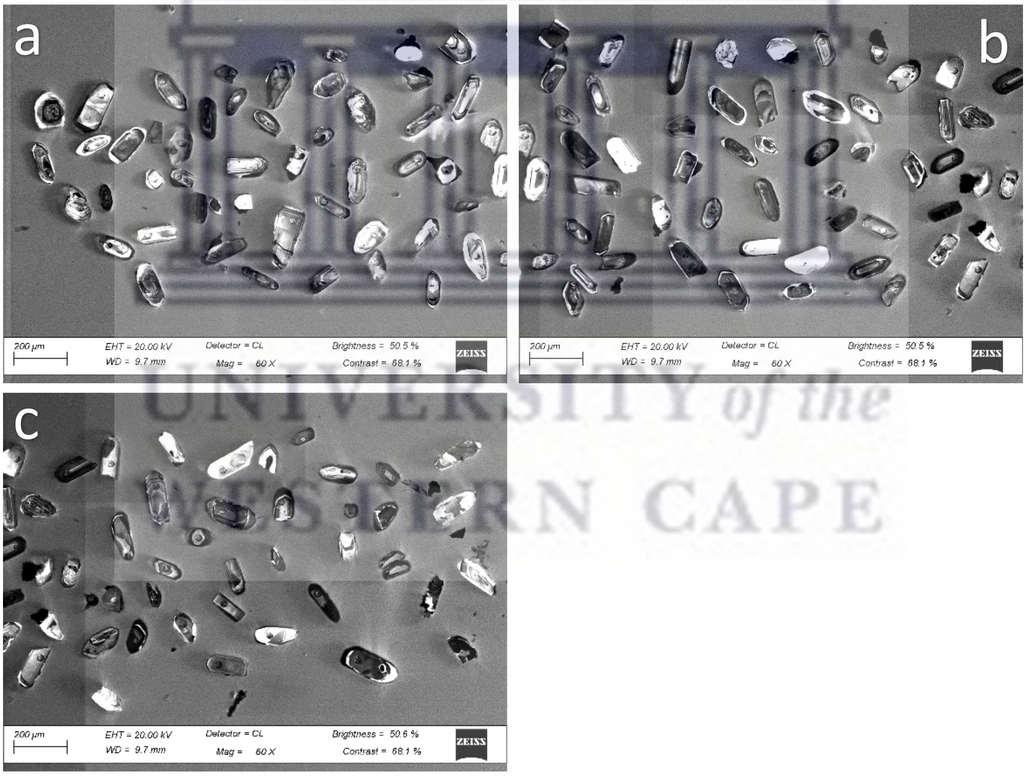

Figure 4-20: Cathodoluminescence images for 040916/2 from the lower Nelsrivier Member of the Groenefontein Formation.

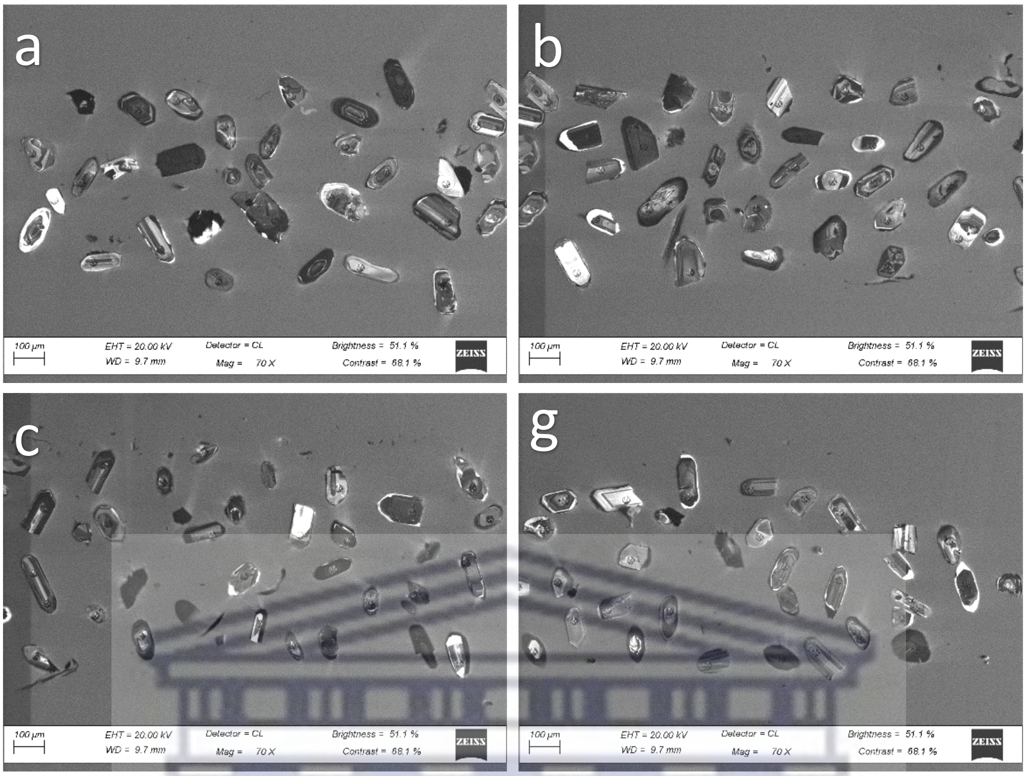

Figure 4-21: Cathodoluminescence Images for 040916/5 from the lower Nelsrivier Member of the Groenefontein Formation.

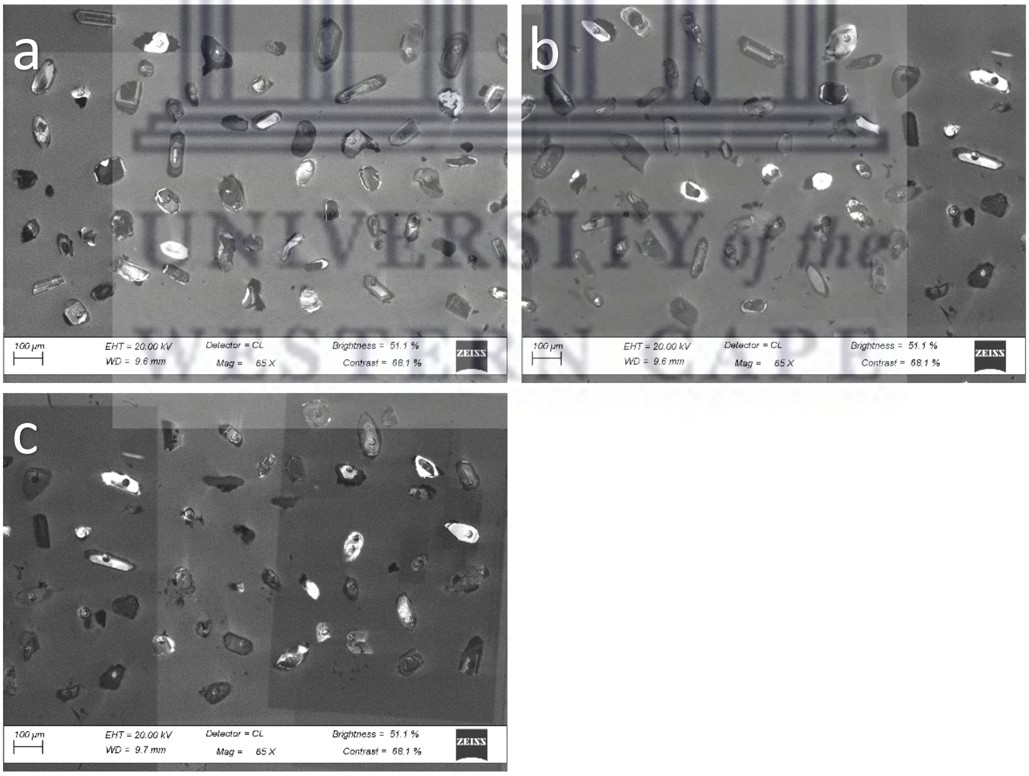

Figure 4-22: Cathodoluminescence images for 040916/6 from the middle Nelsrivier Member of the Groenefontein Formation.

A total of 100 U-Th-Pb analyses on zircon grains from 040916/2 were completed. **Appendix B** presents the U-Th-Pb isotopic analyses results performed on zircon grains from 040916/2. Nineteen of these analyses did not pass the <10% discordancy test. A U-Pb Concordia age of 1003 ± 10.3 Ma was produced by 040916/2, with a minimum age of 548 Ma and a maximum age of 1874 Ma recorded (**Figure 4-23**).

A total of 92 U-Th-Pb analyses on zircon grains from 040916/5 were completed, of which 30 analyses did not pass the <10% discordancy test. **Appendix C** presents the U-Th-Pb isotopic analyses results performed on zircon grains from 040916/5. A U-Pb Concordia age of 1047 ± 5.6 Ma was produced by 040916/5, with a minimum age of 552 Ma and a maximum of 1886 Ma (**Figure 4-24**).

A total of 94 U-Th-Pb analyses on zircon grains from 040916/6 were completed, of which 34 analyses did not pass the <10% discordancy test. **Appendix D** presents the U-Th-Pb isotopic analyses results performed on zircon grains from 040916/6. A U-Pb Concordia age of 1047 ± 8 Ma was produced by 040916/2, with a minimum age of 540 Ma and a maximum of 2708 Ma recorded (**Figure 4-25**).

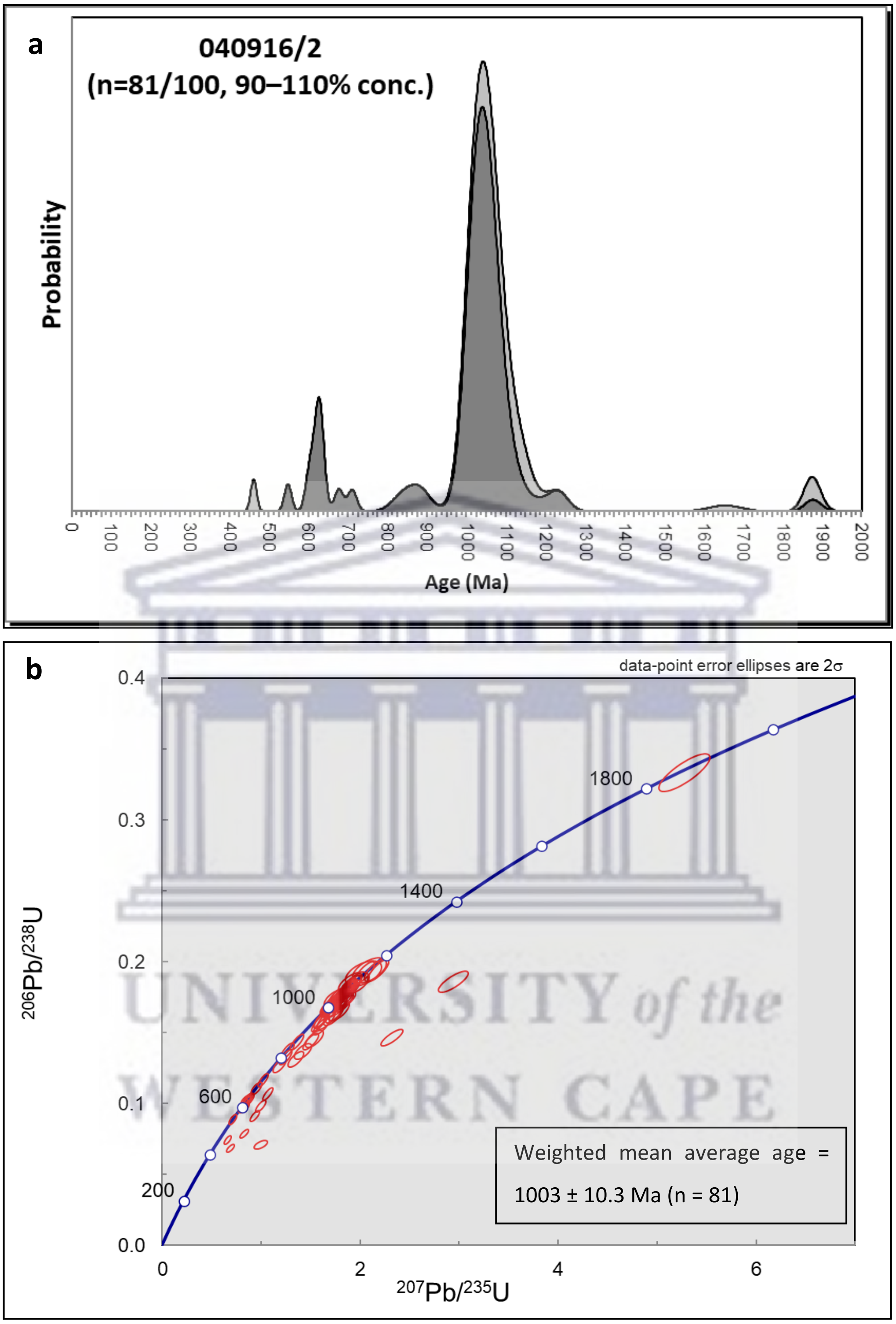

Figure 4-23: a – Probability distribution of sample 040916/2 from the lower Nelsrivier Member of the Groenefontein Formation. b – Concordia diagram of 040916/2 showing the ^{206}Pb/^{238}U ages of zircons: data-point ellipses are plotted at 2σ.

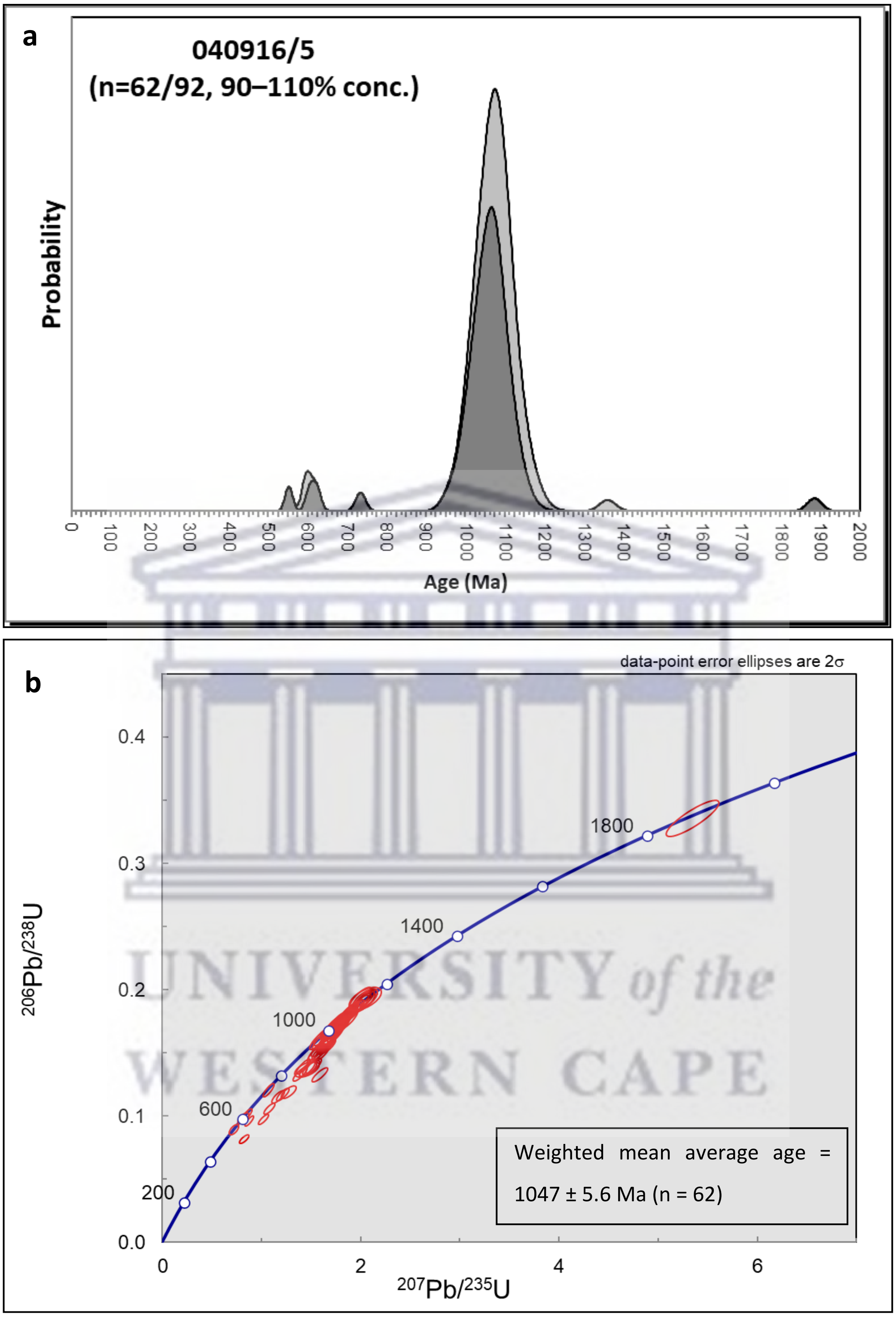

Figure 4-24: a – Probability distribution of sample 040916/5 from the lower Nelsrivier Member of the Groenefontein Formation. b – Concordia diagram of 040916/5 showing the ^{206}Pb/^{238}U ages of zircons: data-point ellipses are plotted at 2σ.

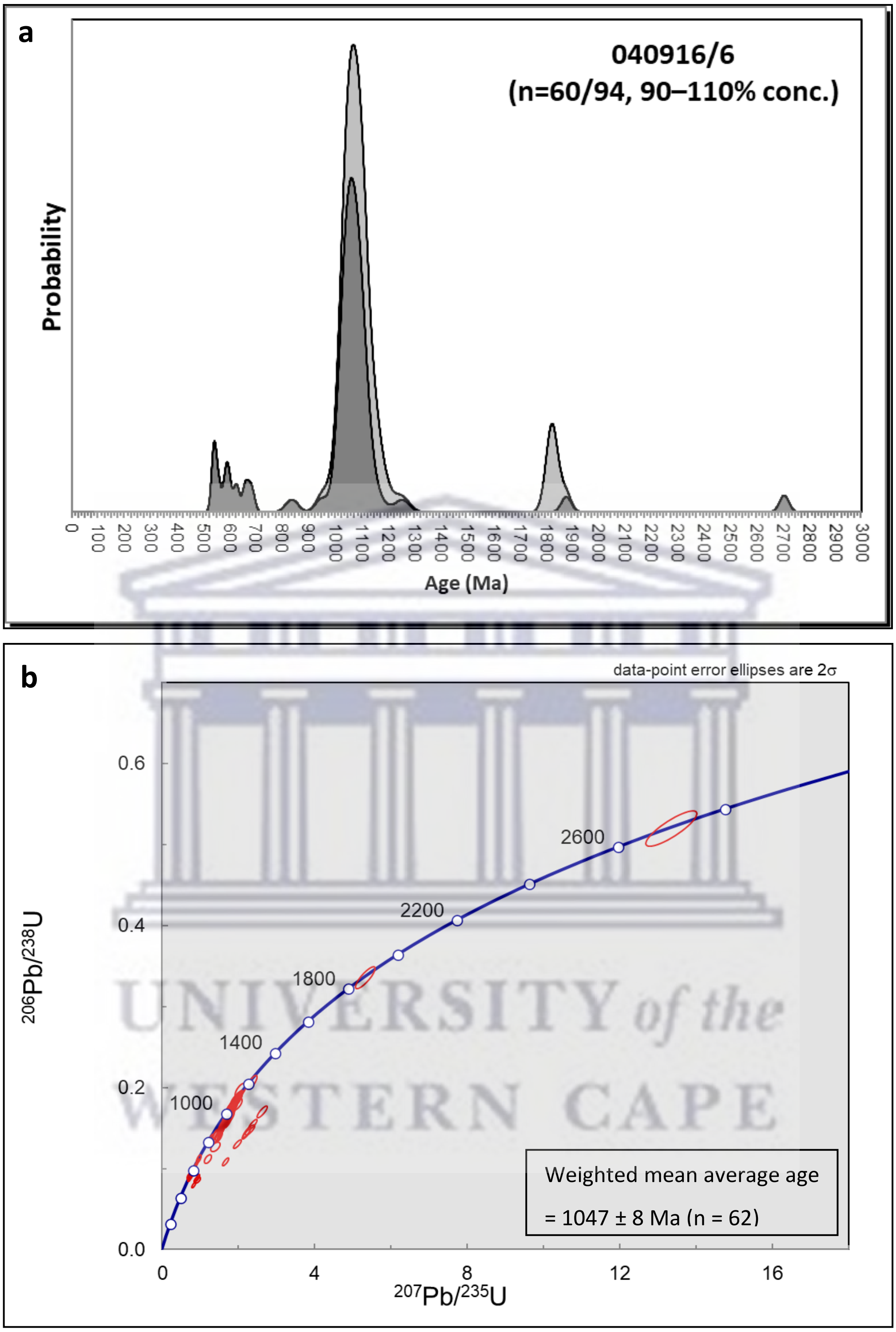

Figure 4-25: a – Probability distribution of sample 040916/6 from the middle Nelsrivier Member of the Groenefontein Formation. b – Concordia diagram of 040916/6 showing the $^{206}Pb/^{238}U$ ages of zircons: data-point ellipses are plotted at 2σ.

4.3.3 Huis Rivier Formation

Two samples from the Huis Rivier Formation were dated, including 050916/1 and 050916/2B. Both samples were sampled from the eastern zone of the Kango Inlier.

The zircons from the Huis Rivier Formation are homogenous. The grains are subrounded to rounded and exhibit little to no zonation. The grains are ~100 µm in size with minor longer elongated zircon grains (**Figure 4-26**, **Figure 4-27**).

A total of 80 U-Th-Pb analyses on zircon grains from 050916/1 were completed. **Appendix E** presents the U-Th-Pb isotopic analyses results performed on zircon grains from 050916/1. Seventeen of these analyses did not pass the <10% discordancy test. The analyses are plotted on Concordia diagrams (**Figure 4-28**). 050916/1 produced a U-Pb Concordia age of 847 ± 17.1 Ma. The sample produced a minimum age of 550 Ma and a maximum age of 1149 Ma.

A total of 107 U-Th-Pb analyses on zircon grains from 050916/2B were completed, of which 15 analyses did not pass the <10% discordancy test. **Appendix F** presents the U-Th-Pb isotopic analyses results performed on zircon grains from 050916/2B. The analyses are plotted on Concordia diagrams (**Figure 4-29**). 050916/2B produced a U-Pb Concordia age of 872 ± 8.2 Ma. The sample produced a minimum age of 558 Ma and a maximum age of 2427 Ma.

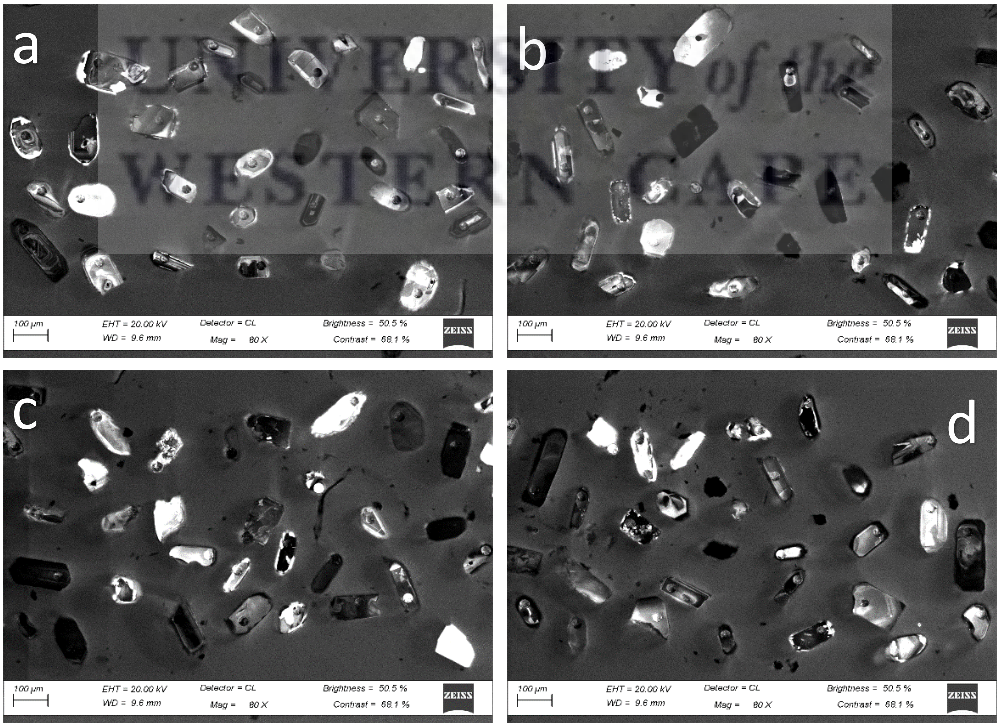

Figure 4-26: Cathodoluminescence images for 050916/1 from the Huis Rivier Formation.

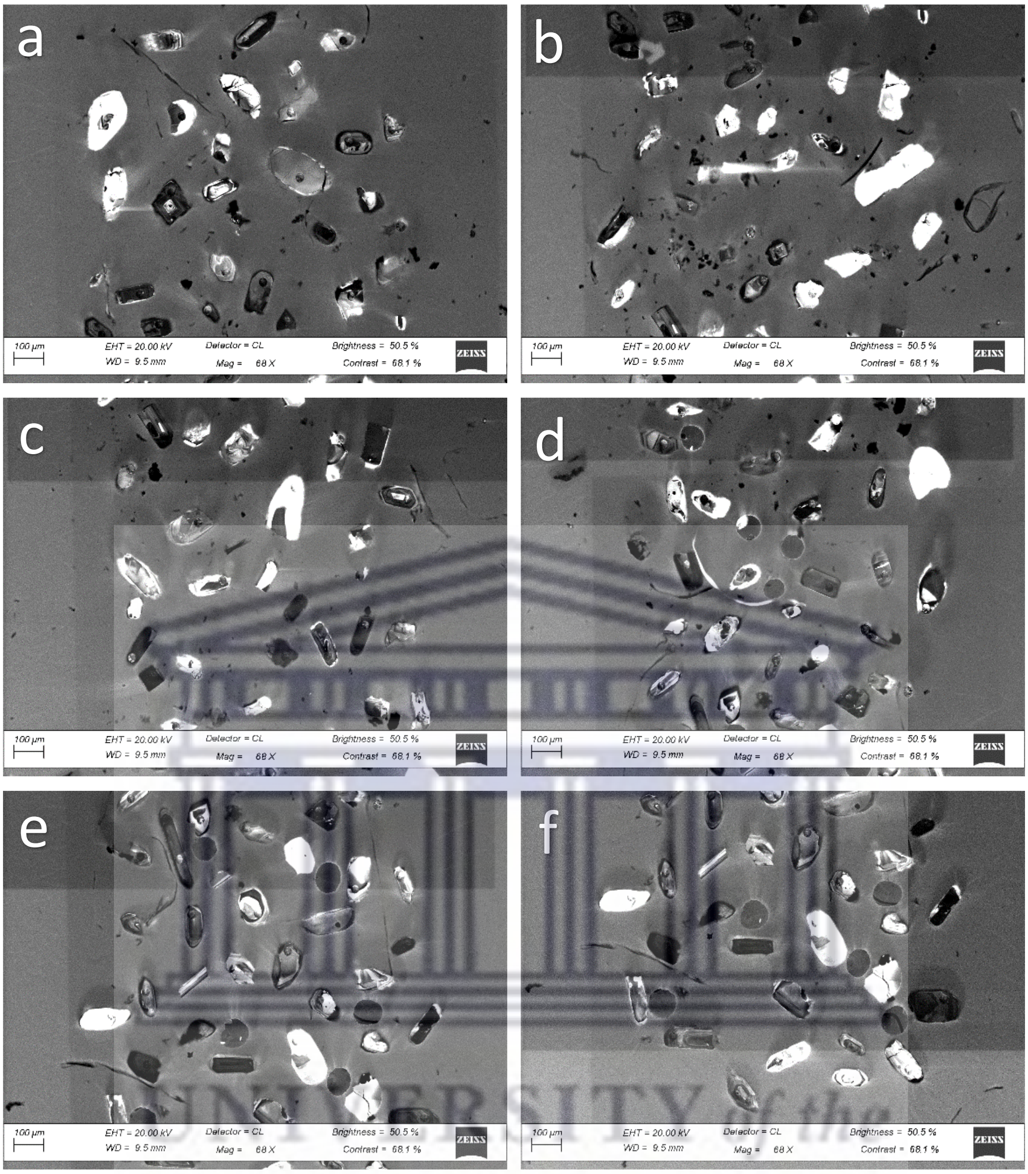

Figure 4-27: Cathodoluminescence images for 050916/2B from the Huis Rivier Formation.

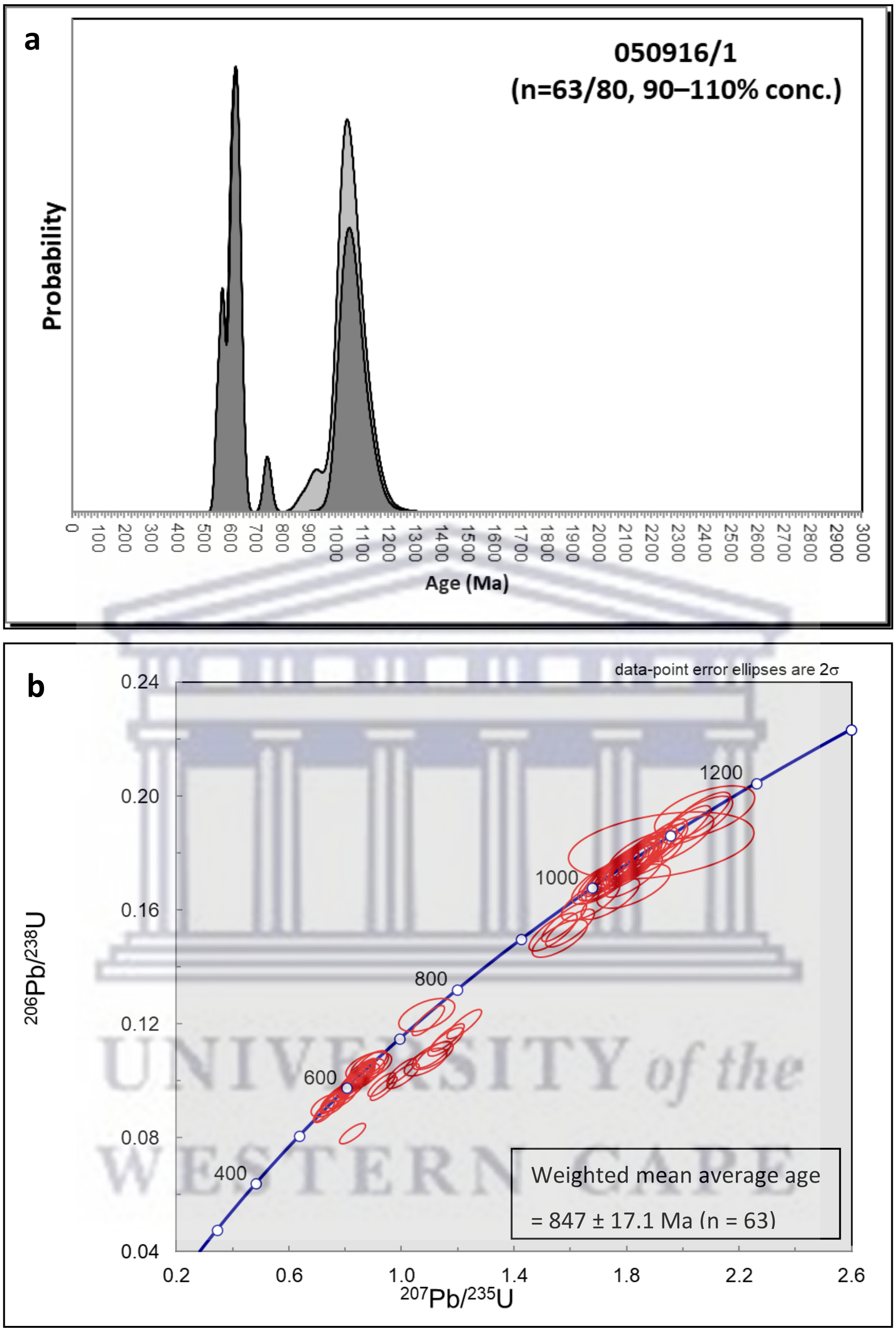

Figure 4-28: a – Probability distribution of sample 050916/1 from the Huis Rivier Formation. b – Concordia diagram of 050916/1 showing the $^{206}Pb/^{238}U$ ages of zircons: data-point ellipses are plotted at 2σ.

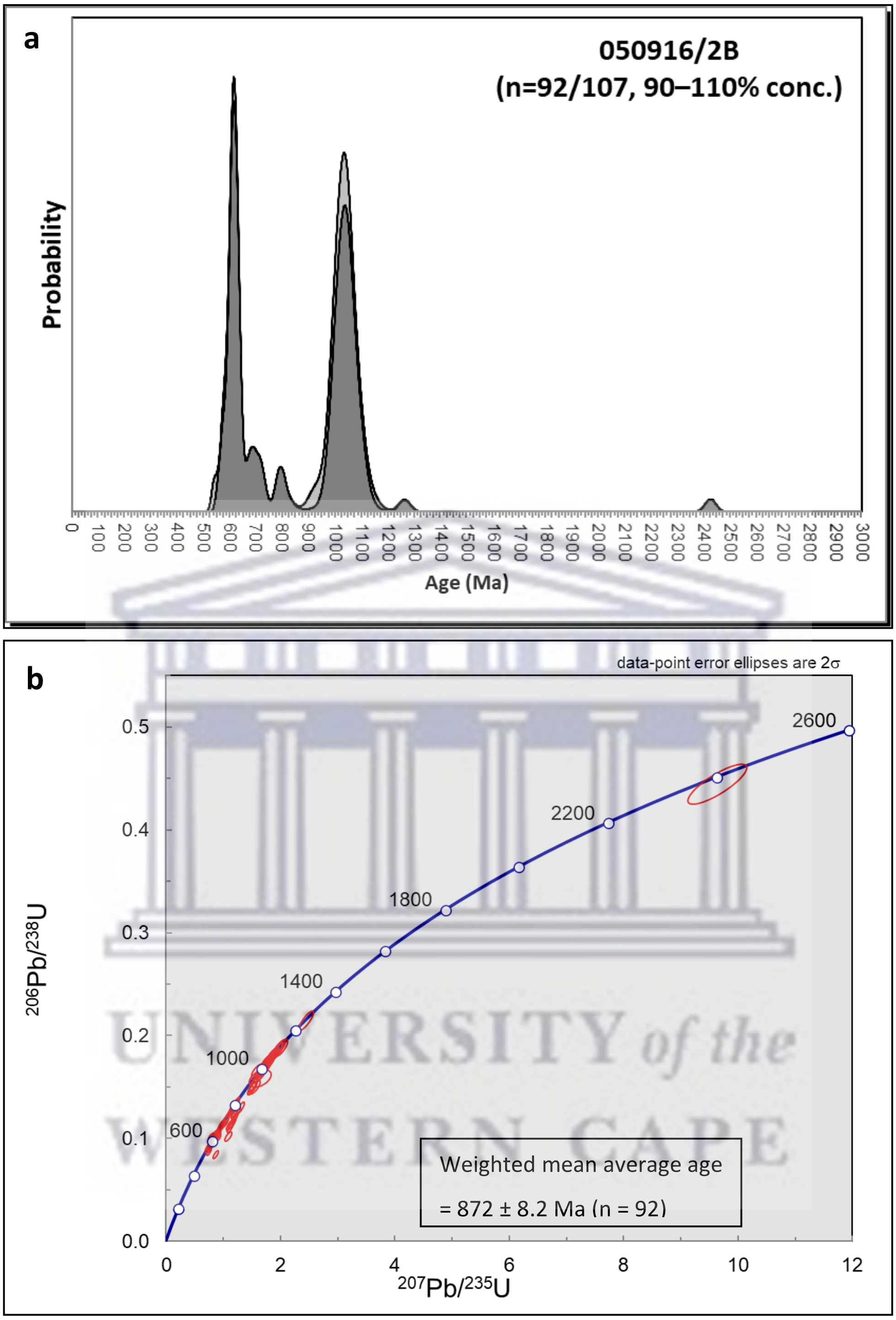

Figure 4-29: a – Probability distribution of sample 050916/2B from the Huis Rivier Formation. b – Concordia diagram of 050916/2B showing the $^{206}Pb/^{238}U$ *ages of zircons: data-point ellipses are plotted at 2σ.*

5. DISCUSSION

5.1 Petrography

The physical, chemical and biological properties of sedimentary rocks are influenced by the provenance and depositional environment. The provenance and depositional environments are a result of the geological and tectonic history of the area in which the sediments accumulate (Boggs and Boggs, 2009). For this reason, the characteristics of sediments, such as grain size and sorting, are important when trying to understand the depositional evolution of sedimentary rocks (Visher, 1969). Sediment characteristics reflect the depositional environment and sediment from different sedimentary environments exhibit unique grain properties.

The wacke samples of the Nooitgedagt Member are poorly sorted and comprised of subangular fine to very-fine-grained sand sized particles and larger rounded clasts. The texture of these rocks suggests rapid deposition close to the source from which the sediments were weathered and eroded, most likely due to submarine avalanches on the edge of the continental shelf (Serra, 1986).

Microcline being present within the rocks of the Nooitgedagt Member suggests that the sediments were derived from an igneous source. The presence of sericite in the rocks suggests they have undergone hydrothermal alteration (Haldar and Tisljar, 2014). Based on the petrographic results, the base of the Nooitgedagt Member is therefore comprised of rocks which have been deposited on the edge of a continental margin, from sediments which have been rapidly deposited and buried near the source from which it was weathered.

The rocks of the Groenefontein Formation are texturally immature. They are poorly sorted, and the mineral grains are subangular at the base, whereas in the middle of the formation, the grains are more subrounded. The grains are fine grained at the base of the formation, whereas in the middle the mineral grains are very-fine grained. The fining up within the Groenefontein Formation suggests that there was a deepening of the sedimentary basin (Serra, 1986). Another explanation is that an initial rapid deposition closer to the source was followed by the deposition of sediment that had undergone a longer transportation time.

The large amounts of quartz veins and sericitic alteration suggests hydrothermal alteration of the Groenefontein Formation rocks (Haldar and Tisljar, 2014). Further evidence of hydrothermal infiltration and alteration is presented by the oxidation weathering exhibited in the block samples as well as in the thin sections.

The Huis Rivier Formation samples are fine to very-fine grained and are moderately sorted. Additionally, turbidites were found in the wacke samples. Based on the texture of the rocks and presence of turbidites, the rocks were most likely deposited in a deepening basin by turbiditic currents (Serra, 1986).

There is a high degree of alteration within the rocks of the Huis Rivier Formation, evident by chloritisation, seritisation and weathering of opaque minerals (Haldar and Tisljar, 2014). Chloritisation is often associated with low-grade metamorphism (Morad et al., 1994). This provides evidence for the low-grade greenschist metamorphism experienced by the rocks of the Cango Caves Group. There is evidence of deformation from compressional forces within the Huis Rivier Formation, evident by kinking of deformation twins in plagioclase and the cross-hatched twinning in the calcite.

The sampled rocks from the Cango Caves Groups have been classified as either wacke or litharenite. Based on the petrographic results, it can be determined that the rocks of the Cango Caves Group are highly altered (due to hydrothermal alteration) and were deposited in a deepening basin, initially caused by rapid deposition from nearby sources followed by increased transportation times as the basin deepened.

The presence of sericite in all the rocks suggests that the sediments of the Cango Caves Group were sourced from igneous material (Haldar and Tisljar, 2014). The Namaqua basement rocks which underlie the Cango Caves Group could be a possible provenance source (Naidoo et al., 2013).

5.2 Geochemistry

5.2.1 Alteration

Weathering patters were determined by CIA calculations and were cross-checked using K/Cs ratios and WIP.

Based on the high K/Cs ratios, low CIA and the high K concentrations, it is clear that the Nooitgedagt Member has undergone a degree of K-metasomatism. The WIP vs CIA plot (**Figure 4-12**) also indicates that the lithological successions of the Cango Caves Group have undergone moderate degrees of weathering. CIA values for the Cango Caves Group indicate moderate degrees of weathering. Within the Cango Caves Group, there is a gradual decrease in the degree of weathering from the Nooitgedagt Member, the lowest succession, to the Huis Rivier Formation, at the top.

Therefore, the Cango Caves Group has undergone moderate degrees of weathering, possibly with rapid sedimentation rates over short transportation distances. This is in agreement with the petrographic observations.

5.2.2 Sediment provenance and tectonic setting

An overview of the REE patterns for each Formation is illustrated in **Figure 4-16**.

The rocks of the Cango Caves Group are characterised by relatively flat REE patterns. The REE concentrations are similar to the upper continental crust normalised concentrations after Taylor and McLennan (1985). There are slight enrichments and depletions with regards to the LREE and HREE. The Nooitgedagt Member is enriched in LREE and HREE relative the UCC. The positive Eu anomaly for the Nooitgedagt Member is possibly due to the enrichment of K within the samples.

The Groenefontein Formation samples are all slightly enriched in HREE. The wacke samples have LREE values similar to the UCC and the litharenite is slightly enriched in the LREE. The Huis Rivier Formation is enriched in LREE and HREE relative to the UCC. Both the Groenefontein and Huis Rivier formations exhibit moderate-to strong-negative Eu anomalies, indicating an overall upper-continental felsic provenance for these formations. Overall, the

Cango Caves Group is characterised by low La/Lu values, which indicate that the rocks have undergone little fractionation.

The Zr/Sc and Th/Sc ratios (**Figure 4-14**) are good indicators of source compositions. The Nooitgedagt Member and the Groenefontein Formation show typical upper crustal Th/Sc vs Zr/Sc ratios and have therefore experienced minimal reworking. In contrast, the Huis Rivier Formation has high Sc concentrations, which indicates less fractionated source components mixed with UCC concentrations. The rocks have therefore undergone minimal reworking.

The isotope geochemistry results indicate that a less fractionated (mafic to intermediate) source appears to be the main source component for the Cango Caves Group. Source rocks, which were eroded and weathered to form the rocks of the Cango Caves Group, are likely to have been granitic or granodioritic. There is a change from a granitic source for the Nooitgedagt Member (lower stratigraphical unit) to a mixture between granitic and granodioritic sources for the Groenefontein and Huis Rivier formations.

The tectonic setting of the Cango Caves Group was interpreted using the plots of La/Sc vs Ts/Zr, La-Th-Sc and Th-Sc-Zr/10, after Bhatia and Crook (1986) (**Figure 4-15**). The tectonic setting of the Nooitgedagt Member points to a Continental Island Arc source. The Groenefontein Formation also appears to have a Continental Island Arc to Active Continental Margin provenance source (**Figure 4-15**). The Huis Rivier Formation has also undergone minor reworking of the detrital material and points to a Continental Island Arc with a tendency towards the Passive Margin setting.

5.3 Geochronology

U-Pb analysis of detrital zircons was used to determine absolute ages of the Nooitgedagt Member of the Matjies River Formation, the Nelsrivier Member of the Groenefontein Formation Groenefontein Formation and Huis Rivier Formation, of the Cango Caves Group. The zircons were analysed using laser ablation-single collector-magnetic sector field ICP-MS.

The U-Pb ages for Nooitgedagt Member of the Matjies River Formation are only Mesoproterozoic, ranging between 1000 and 1150 Ma. This study produced a Concordia $^{206}Pb/^{238}U$ age of 1077 Ma. The determined age falls within ages, after Naidoo (2008), of 1070 to 1268 Ma for the Nooitgedagt Member. U/Pb isotope dating of detrital zircons, from Barnett et al. (1997), suggests that the gneisses of the Mesoproterozoic Namaqua-Natal Mobile Belt (1100 Ma) are possible source rocks for the Nooitgedagt Member.

Eglington (2006) recorded ages from ~1200 - 1300 Ma for the Natal sub-province. These ages produced by Barnett et al. (1997) and Eglington (2006) for the Namaqua-Natal Mobile Belt align with age data of the Nooitgedagt Member from this study, and there is no other evidence of mixing of any other source material for the Nooitgedagt Member. For this reason, sediments from the Nooitgedagt Member were most likely only supplied by the Namaqua-Natal Mobile Belt.

The Groenefontein Formation produced $^{206}Pb/^{238}U$ ages of ~1003 - 1047 Ma. These detrital ages represent the source material. The $^{206}Pb/^{238}U$ ages suggests that the Groenefontein Formation was sourced from the Namaqua Natal Mobile Belt. A younger age of ~540 - 552 Ma was also produced for detrital zircons of the Groenefontein Formation.

The younger ages most likely reflect a younger source material and more closely reflect the depositional age of the Groenefontein Formation. These zircon ages suggest an input of detritus from Pan-African-age terranes proximal to the Kango Inlier. These ages closely correlate with ages of the Cape Granite Suite of 555 - 510 Ma (Scheepers and Armstrong, 2002). The Groenefontein Formation was, therefore, most likely sourced from granitoids from the Namaqua Natal Mobile Belt, with an influence of granitic or granodioritic material from a Pan-African source.

The Huis Rivier Formation produced $^{206}Pb/^{238}U$ ages of ~847 - 872 Ma with older detrital of Namaqua Natal Mobile Belt ages. A younger age of ~550 - 558 Ma was also produced for detrital zircons of the Huis Rivier Formation.

As with the Groenefontein Formation, the younger ages most likely reflect a younger source material and more closely reflect the depositional age of the Huis Rivier Formation. The younger detrital ages suggest there was an influence of material of Pan-African ages. The ages correlate with the Cape Granite Suite of 555 - 510 Ma (Scheepers and Armstrong, 2002). The Huis Rivier Formation was most likely sourced from granitoids from the Namaqua-Natal Mobile Belt with an influence of granitic or granodioritic material from a Pan-African source.

The Groenefontein and Huis Rivier formations were deposited above the Groenefontein Unconformity. The Mesoproterozoic and Neoproterozoic ages for these formations imply that after the Groenefontein Unconformity, a new source area started to supply sediments of the Groenefontein Formation. This supply increased during the deposition of the Huis Rivier Formation.

The zircon ages indicate that prior to the formation of the Groenefontein Unconformity, i.e., during deposition of the Matjies River Formation, supply of sediments only occurred from a northern and eastern source area, namely from the Mesoproterozoic Namaqua-Natal Mobile Belt (Naidoo et al., 2013; Nel et al., 2018). After the formation of the Groenefontein Unconformity, another new source area also started to supply sediments of Neoproterozoic age. This source area presumably represents the Terra Australis Orogen (TAO) located to the south of the Kango Inlier (Cawood, 2005; Naidoo et al., 2013) and played an increasingly important role during the deposition of the Cango Caves Group.

5.4 Basin Evolution

This section will discuss the basin evolution of the lower Kango Inlier based on the petrographic, geochemical and geochronological data of the Cango Caves Group.

The Cango Caves Group was deposited in a deepening basin, initially from rapid deposition from nearby sources followed by increased transportation times as the basin deepened. Rapid deposition for the Cango Caves Group is supported by Naidoo (2008), which states that a period of rapid deepening of the basin allowed for rapid sedimentary rates for the Cango Caves Group following a period of transgression.

The Nooitgedagt Member was deposited in a shallow marine to marine shelf environment. This was followed by the Kombuis Member which predominantly accumulated on a shelf (Germs et al., 2009). The deposition of the Matjies Rivier Formation was followed by the Groenefontein Unconformity and by tectonic extension and the deepening of the basin, into which the Groenefontein Formation and Huis Rivier turbidites were deposited.

The basin evolution is discussed below:

Naidoo (2008) suggests the most reliable scenario for the basin development involves the TAO. The Orogeny was an Active Continental Margin to the south of Gondwana, which was related to peri-Gondwana terranes such as Patagonia and the Falkland Islands (Cawood, 2005). Subduction related to the TAO was at ~570 Ma (Cawood, 2005).

Paleocurrent data from Le Roux (1977) indicate that the Huis Rivier Formation was sourced mainly from the north and south (also sourced from the east). The southern source for the Huis Rivier Formation supports this scenario as long as no arc-related succession is found to the south of South Africa (Naidoo, 2008).

Petrographic, geochemical and isotopic evidence of the Cango Caves Group, from Naidoo et al., (2013), supports the scenario of a TAO, as a young, evolving foreland basin.

For the abovementioned reasons, evidence from previous work and this study suggest the Cango Caves Group was most likely deposited in a foreland basin related to subduction driven processes along southern Gondwana with TAO influencing subduction processes. Subduction related to the TOA resulted in the progressive deepening of the foreland basin and the deposition of the Cango Caves Group. Tectonic processes by the TAO exhumed rocks of the Natal Belt (Naidoo et al., 2013), which were eroded to form the source rocks of the Cango Caves Group. Furthermore, there is evidence of Pan-African aged source material within the Cango Caves Group (Groenefontein and Huis Rivier Formations) which indicate that, during the deposition of the Cango Caves Group, there was an increased influence from the Pan-African orogeny.

6. CONCLUSION

A provenance study was conducted on the Cango Caves Group with a focus on the Nooitgedagt Member of the Matjies River Formation, the Nelsrivier Member of the Groenefontein Formation, and the Huis Rivier Formation. The provenance study was achieved by quantifying the mineralogical, geochemical, isotopic and geochronological compositions of the rocks. The final aim was to attempt to decipher the crustal evolution of the Cango Caves Group and basin evolution of the lower Kango Inlier.

Based on the petrographic analysis, the Cango Caves Group was determined to have been initially deposited by rapid deposition from nearby sources, followed by increased transportation times as the basin deepened. The rocks have undergone hydrothermal alteration based on the large number of quartz veins, chloritisation and seritisation. The presence of sericite in all the rocks suggests that the sediments of the Cango Caves Group were sourced from igneous material.

The geochemical and petrographic results indicate moderate degrees of weathering for the Cango Caves Group. There is a gradual decrease in the degree of weathering from the Nooitgedagt Member, the lowest succession, to the Huis Rivier Formation, at the top. Thus, indicating lower sedimentation rates and greater transportation distances in the younger units of the Cango Caves Group.

Overall, the Cango Caves Group is characterised by low La/Lu values, therefore indicating that the rocks had undergone little fractionation. The results indicate that a mafic/intermediate source appears to be the main source component for the Cango Caves Group. Source rocks, which were eroded and weathered to form the rocks of the Cango Caves Group, are likely to have been granitic or granodioritic. The rocks appear to have been sourced from granitoids of the Namaqua-Natal Mobile Belt from sources to the east, north and south of the basin.

Provenance-indicating discrimination diagrams show sources from mixed tectonic settings for the Cango Caves Group. A Continental Island Arc source was determined for the Nooitgedagt Member; a Continental Island Arc to Active Continental Margin provenance source was determined for the Groenefontein Formation; and a Continental Island Arc with a tendency towards the Passive Margin source was determined for the Huis Rivier Formation.

The zircon ages for Nooitgedagt Member of the Matjies River Formation are only Mesoproterozoic, between 1000 and 1150 Ma. This study produced a Concordia $^{206}Pb/^{238}U$ age of 1077 ± 3 Ma. This indicate that the sediments of the Nooitgedagt Member of the Matjies River Formation were only source from the Namaqua-Natal Mobile Belt.

The Groenefontein and Huis Rivier Formations were deposited after the Groenefontein Unconformity and produced both Mesoproterozoic and Neoproterozoic ages. The Groenefontein and Huis Rivier Formations produced Concordia ages of ~1003 - 1047 Ma and ~847 - 872 Ma, respectively. The Groenefontein formation produced younger detrital ages of ~540 - 552 Ma, and the Huis Rivier formation produced younger detrital ages of ~550 - 558 Ma. These younger detrital ages more closely reflect the depositional ages.

The zircon ages indicate that prior to the formation of the Groenefontein Unconformity, supply of sediments only occurred from the Mesoproterozoic Namaqua-Natal Mobile Belt. These sediments were sourced from a northern and eastern source area (Nel et al., 2018). After formation of the Groenefontein Unconformity another new source area also started to supply sediments of Neoproterozoic age. This source area presumably represents the TAO located to the south of the Kango Inlier (Cawood, 2005; Naidoo et al., 2013) and played an increasingly important role during the deposition of the Cango Caves Group.

The evolution of the Kango Inlier most likely began from an erosional setting which initiated the deposition of the basal Nooitgedagt Member of the Cango Caves Group. Subsequent to the deposition of the Kombuis Member, extension within the basin was governed by subduction related to the southern Pan-African orogeny, creating a foreland basin. Extension was coupled with the progressive deepening of the basin as the rest of the Cango Caves Group was deposited. Subduction was presumably related to the TAO along southern Gondwana.

The TAO exhumed rocks of the Namaqua-Natal Mobile Belt, which were eroded to form source rocks of the Cango Caves Group. Furthermore, source material of Pan-African age within the Cango Caves Group (Groenefontein and Huis Rivier Formations) indicates that, during the deposition of the Cango Caves Group, there was an increased influence from the Pan-African orogeny.

Progressive subduction along southern Gondwana resulted in the folding of the Cango Caves Group, this was followed by uplift and the deposition of the Kansa Group sediments (Germs et al., 2009).

REFERENCES

Barnett, W., Armstrong, R.A. and de Wit, M.J. (1997). Stratigraphy of the upper Neoproterozoic Kango and lower Palaeozoic Table Mountain groups of the Cape fold belt revisited. *South African Journal of Geology*, 100(3), pp. 237-250.

Bhatia, M. R., Crook, K. A. (1986). Trace element characteristics of graywackes and tectonic setting discrimination of sedimentary basins. *Contributions to Mineralogy and Petrology*, 92(2), pp. 181-193.

Bhatia, M.R. (1983). Plate tectonics and geochemical composition of sandstones. *The Journal of Geology*, 91(6), pp. 611-627.

Boggs Jr, S. and Boggs, S. (2009). *Petrology of sedimentary rocks*. Cambridge University Press.

Cawood, P.A. (2005). Terra Australis Orogen: Rodinia breakup and development of the Pacific and Iapetus margins of Gondwana during the Neoproterozoic and Paleozoic. *Earth-Science Reviews*, 69(3-4), pp. 249-279.

Cornell, D. H., Zack, T., Andersen, T., Corfu, F., Frei, D. and Van Schijndel, V. (2016). Th-U- Pb zircon geochronology of the Paleoproterozoic Hartley Formation porphyry by six methods, with age uncertainty approaching 1 Ma. *South African Journal of Geology*, 119, pp. 473-494.

DePaolo, D. (1981). A neodymium and strontium isotopic study of the Mesozoic calc-alkaline granitic batholiths of Sierra Nevada and Peninsular Ranges, California. *Journal Geophysical Research*, 68, pp. 470-488.

Eglington, B. (2006). Evolution of the Namaqua-Natal Belt, southern Africa – A geochronological and isotope geochemical review. *Journal of African Earth Sciences*, 46(1-2), pp. 93-111.

Fölling, P.G. and Frimmel, H.E. (2002). Chemostratigraphic correlation of carbonate successions in the Gariep and Saldania Belts, Namibia and South Africa. *Basin Research*, 14(1), pp. 69-88.

Fourie, P.H. (2012). *Provenance and Paleotectonic Setting of the Devonian Bokkeveld Group, Cape Supergroup, South Africa* (Published M.Sc. thesis). University of Johannesburg, South Africa.

Frei, D. and Gerdes, A. (2009). Precise and accurate in situ U–Pb dating of zircon with high sample throughput by automated LA-SF-ICP-MS. *Chemical Geology*, 261, pp. 261-270.

Frimmel, H.E. (2009). Trace element distribution in Neoproterozoic carbonates as palaeoenvironmental indicator. *Chemical Geology*, 258(3-4), pp. 338-353.

Frimmel, H.E., Fölling, P.G. and Diamond, R. (2001). Metamorphism of the Permo-Triassic Cape Fold Belt and its basement, South Africa. *Mineralogy and Petrology*, 73(4), pp. 325-346.

Gaucher, C. and Germs, G.J. (2006). Recent advances in South African Neoproterozoic-Early Palaeozoic biostratigraphy: correlation of the Cango Caves and Gamtoos Groups and acritarchs of the Sardinia Bay Formation, Saldania Belt. *South African Journal of Geology*, 109(1-2), pp. 193-214.

Germs, G.J.B., Miller, R.McG., Frimmel, H.E., Gaucher, C. (2009). Syn- to late-orogenic sedimentary basins of southwestern Africa. Neoproterozoic to Early Palaeozoic evolution of Southwestern Africa. In: Gaucher, C., Sial, A.N., Halverson, G.P., Frimmel, H.E. (Eds.): Neoproterozoic-Cambrian tectonics, global change and evolution: a focus on southwestern Gondwana. *Developments in Precambrian Geology*, 16, Elsevier, pp. 183-203.

Goldberg, K. and Humayun, M. (2010). The applicability of the Chemical Index of Alteration as a paleoclimatic indicator: An example from the Permian of the Paraná Basin, Brazil. *Palaeogeography, Palaeoclimatology, Palaeoecology*, 293(1-2), pp. 175-183.

González, P.A.A., Garban, G., Hauser, N. and Gigena, L. (2017). Geochemistry of metasedimentary rocks from the Puncoviscana Complex in the Mojotoro Range, NW Argentina: Implications for provenance and tectonic setting. *Journal of South American Earth Sciences*, 78, pp. 250-263.

Gresse, P.G., Chemale, F., Da Silva, L.C., Walraven, F. and Hartmann, L.A. (1996). Late-to post-orogenic basins of the Pan-African–Brasiliano collision orogen in southern Africa and southern Brazil. *Basin Research*, 8(2), pp. 157-171.

Grunow, A., Hanson, R. and Wilson, T. (1996). Were aspects of Pan-African deformation linked to Iapetus opening? *Geology*, 24(12), pp. 1063-1066.

Haldar, S.K. and Tisljar, J. (2014). *Introduction to Mineralogy and Petrology*. Elsevier.

Hartnady, C.J.H., Newton, A.R. and Theron, J.N. (1974). The stratigraphy and structure of the Malmesbury Group in the southwestern Cape. *Precambrian Research Unit*, University of Cape Town, Bulletin 15, pp. 193-213.

Herron, M.M. (1988). Geochemical classification of terrigenous sands and shales from core or log data. *Journal of Sedimentary Petrology,* 58, pp. 829-829.

Le Roux, J.P. (1977). *The stratigraphy, sedimentology and structure of the Cango Group north of Oudtshoorn, C.P* (Unpublished M.Sc. thesis). University of Stellenbosch, South Africa.

Le Roux, J.P., Gresse, P.G. (1983). The sedimentary–tectonic realm of the Kango Group. *Special Publication of the Geological Society of South Africa,* 12, pp. 33–45.

Ludwig, K.R. (2003). Isoplot/Ex version 3: a Geochronological toolkit for Microsoft Excel. *Berkeley Geochronology Centre*.

Lugmair, G. W., Marti, K. (1978). Lunar initial ^{143}Nd/^{144}Nd: differential evolution of the lunar crust and mantle. *Earth and Planetary Science Letters*, 39(3), pp. 349-357.

McLennan, S.M. and Taylor, S.R. (1991). Sedimentary rocks and crustal evolution: tectonic setting and secular trends. *The Journal of Geology*, 99(1), pp. 1-21.

McLennan, S.M., Hemming, S., McDaniel, D.K. and Hanson, G.N. (1993). Geochemical approaches to sedimentation, provenance, and tectonics. *Special Papers-Geological Society of America*, pp. 21-21.

McLennan, S.M., Taylor, S.R., McCulloch, M.T. and Maynard, J.B. (1990). Geochemical and Nd Sr isotopic composition of deep-sea turbidites: crustal evolution and plate tectonic associations. *Geochimica et cosmochimica acta*, 54(7), pp. 2015-2050.

Morad, S., Ismail, H.B., De Ros, L.F., Al-Aasm, I.S. and Serrhini, N.E. (1994). Diagenesis and formation water chemistry of Triassic reservoir sandstones from southern Tunisia. *Sedimentology*, 41(6), pp. 1253-1272.

Naidoo, T. (2008). *Provenance of the Neoproterozoic to Early Paleozoic Kango Inlier, Oudtshoorn, South Africa* (Unpublished M.Sc. thesis). University of Johannesburg, South Africa.

Naidoo, T., Zimmermann, U. and Chemale Jr, F. (2013). The evolution of Gondwana: U–Pb, Sm–Nd, Pb–Pb and geochemical data from Neoproterozoic to Early Palaeozoic successions of the Kango Inlier (Saldania Belt, South Africa). *Sedimentary Geology*, 294, pp. 164-178.

Nel, R., Germs, G.J.B., Praekelt, H.E. and Odendaal, A.I. (2018). Re-examination and reinterpretation of the stratigraphy of the Matjies River Formation, Cango Caves Group, Neoproterozoic to early Palaeozoic Saldania Belt, South Africa. *South African Journal of Geology*, 121(4), pp. 451-462.

Nesbitt, H.W. (2003). Geochemistry of sediments and sedimentary rocks: evolutionary considerations to mineral deposit-forming environments, petrogenesis of siliciclastic sediments and sedimentary rocks. *In: Lentz, D.R. (Ed.), Geological Association of Canada*, 4, pp. 39-51.

Nesbitt, H.W. and Young, G.M. (1989). Formation and diagenesis of weathering profiles. *The Journal of Geology*, 97(2), pp. 129-147.

Praekelt, H.E., Germs, G.J.B. and Kennedy, J.H. (2008). A distinct unconformity in the Cango Caves Group of the Neoproterozoic to early Paleozoic Saldania Belt in South Africa: its regional significance. *South African Journal of Geology*, 111(4), pp. 357-368.

Roser B.P. and Korsch R.J. (1986). Determination of tectonic setting of sandstone-mudstone suites using SiO_2 and K20/Na_2O ratio. *The Journal of Geology*, 94, pp. 635-650.

Rozendaal, A., Gresse, P.G., Scheepers, R. and Le Roux, J.P. (1999). Neoproterozoic to early Cambrian crustal evolution of the Pan-African Saldania belt, South Africa. Pr*ecambrian research*, 97(3-4), pp. 303-323.

Rudnick, R. L. and Gao, S. (2003). Composition of the continental crust. *The crust*, 3, pp. 1-64.

Scheepers, R. and Armstrong, R. (2002). New U-Pb SHRIMP zircon ages of the Cape Granite Suite: implications for the magmatic evolution of the Saldania Belt. *South African Journal of Geology*, 105(3), pp. 241-256.

Serra, O. (1986). Information on Depositional Sedimentary Environments (Formation of sedimentary rocks). *Developments in Petroleum Science*, 15, pp. 215-339.

Steiger, R. H. and Jäger, E. (1977). Subcommission on geochronology: convention on the use of decay constants in geo-and cosmochronology. *Earth and planetary science letters*, 36(3), pp. 359-362.

Taylor, S.R. and McLennan, S.M. (1985). The continental crust: its composition and evolution.

Taylor, S.R. and McLennan, S.M. (1995). The geochemical evolution of the continental crust. *Reviews of geophysics*, 33(2), pp. 241-265.

Van Staden, A., Naidoo, T., Zimmermann, U. and Germs, G.J. (2006). Provenance analysis of selected clastic rocks in Neoproterozoic to lower Paleozoic successions of southern Africa from the Gariep Belt and the Kango Inlier. *South African Journal of Geology*, 109(1-2), pp. 215-232.

Visher, G.S. (1969). Grain size distributions and depositional processes. *Journal of Sedimentary Research*, 39(3).

Von Veh, M.W. (1983). Aspects of sedimentation, structure and tectonic evolution in the Tygerberg Terrane, southwestern Cape Province. *Precambrian Research Unit*, University of Cape Town, Bulletin, 32: 88 pp.

Winchester, J.A. and Floyd, P.A. (1977). Geochemical discrimination of different magma series and their differentiation products using immobile elements. *Chemical geology*, 20, pp. 325-343.

APPENDIX LIST

Appendix A – LA-ICP-MS U-Pb geochronological data for zircons of sample 040916/3

Appendix B – LA-ICP-MS U-Pb geochronological data for zircons of sample 040916/2

Appendix C – LA-ICP-MS U-Pb geochronological data for zircons of sample 040916/5

Appendix D – LA-ICP-MS U-Pb geochronological data for zircons of sample 040916/6

Appendix E – LA-ICP-MS U-Pb geochronological data for zircons of sample 040916/1

Appendix F – LA-ICP-MS U-Pb geochronological data for zircons of sample 040916/2B

Appendix A - LA-ICP-MS U-Pb geochronological data for zircons of sample 040916/3

040916/3							**RATIOS**							**AGES [Ma]**						**Conc.**
Sample	**Analysis**	**U [ppm]**[a]	**Pb [ppm]**[a]	**Th [ppm]**	**^{206}Pb/^{204}Pb**	**Th/U meas**	**^{207}Pb/^{235}U**[b]	**2 σ**[d]	**^{206}Pb/^{238}U**[b]	**2 σ**[d]	**rho**[c]	**^{207}Pb/^{206}Pb**[e]	**2 σ**[d]	**^{207}Pb/^{235}U**	**2 σ**	**^{206}Pb/^{238}U**	**2 σ**	**^{207}Pb/^{206}Pb**	**2 σ**	%
040916/3	A_276	137	24	68	15861	0.50	1.828	0.076	0.1765	0.0058	0.79	0.0751	0.0019	1056	44	1048	35	1072	51	98
040916/3	A_277	140	26	57	116118	0.41	2.001	0.085	0.1895	0.0063	0.78	0.0766	0.0021	1116	48	1119	37	1110	54	101
040916/3	A_278	230	41	130	179850	0.56	1.851	0.075	0.1782	0.0059	0.82	0.0753	0.0018	1064	43	1057	35	1077	47	98
040916/3	A_279	1318	203	635	3348	0.48	1.638	0.064	0.1542	0.0051	0.84	0.0771	0.0016	985	39	924	30	1122	42	82
040916/3	A_280	131	23	89	15098	0.68	1.865	0.078	0.1778	0.0059	0.79	0.0761	0.0020	1069	45	1055	35	1098	52	96
040916/3	A_281	268	49	142	12758	0.53	1.898	0.077	0.1814	0.0060	0.82	0.0759	0.0018	1081	44	1075	35	1092	46	98
040916/3	A_282	450	82	49	16123	0.11	1.908	0.076	0.1828	0.0060	0.83	0.0757	0.0017	1084	43	1082	36	1088	44	99
040916/3	A_283	160	27	97	119842	0.60	1.740	0.072	0.1710	0.0057	0.80	0.0738	0.0018	1024	42	1018	34	1036	50	98
040916/3	A_284	221	40	88	173133	0.40	1.854	0.075	0.1790	0.0059	0.81	0.0751	0.0018	1065	43	1062	35	1071	48	99
040916/3	A_285	161	29	89	8558	0.55	1.845	0.076	0.1775	0.0059	0.80	0.0754	0.0019	1062	44	1053	35	1079	50	98
040916/3	A_286	208	37	64	3647	0.31	1.876	0.076	0.1805	0.0060	0.81	0.0754	0.0018	1073	44	1069	35	1079	48	99
040916/3	A_287	460	83	75	364748	0.16	1.891	0.075	0.1812	0.0060	0.83	0.0757	0.0017	1078	43	1073	35	1087	44	99
040916/3	A_288	681	111	230	5488	0.34	1.713	0.067	0.1630	0.0054	0.84	0.0762	0.0016	1013	40	973	32	1101	43	88
040916/3	A_289	124	22	79	13688	0.63	1.879	0.079	0.1776	0.0059	0.79	0.0768	0.0020	1074	45	1054	35	1115	51	95
040916/3	A_290	219	40	115	173063	0.52	1.888	0.077	0.1802	0.0060	0.81	0.0760	0.0018	1077	44	1068	35	1096	47	97
040916/3	A_293	345	63	156	4650	0.45	1.923	0.077	0.1822	0.0060	0.83	0.0765	0.0017	1089	44	1079	36	1109	45	97
040916/3	A_294	539	66	307	2797	0.57	1.302	0.052	0.1231	0.0041	0.83	0.0767	0.0017	847	34	748	25	1114	45	67
040916/3	A_295	273	48	253	209106	0.93	1.830	0.074	0.1753	0.0058	0.82	0.0757	0.0018	1056	43	1041	34	1087	47	96
040916/3	A_296	267	35	291	47110	1.09	1.347	0.055	0.1311	0.0043	0.81	0.0746	0.0018	866	35	794	26	1057	48	75
040916/3	A_297	134	23	77	-49806	0.57	1.700	0.072	0.1693	0.0056	0.79	0.0728	0.0019	1008	43	1008	33	1009	53	100
040916/3	A_298	158	26	102	1919	0.65	1.643	0.068	0.1624	0.0054	0.80	0.0734	0.0018	987	41	970	32	1024	51	95
040916/3	A_299	322	60	125	32657	0.39	1.946	0.078	0.1853	0.0061	0.83	0.0762	0.0017	1097	44	1096	36	1099	45	100
040916/3	A_300	505	94	139	411010	0.28	1.954	0.078	0.1862	0.0061	0.83	0.0761	0.0017	1100	44	1100	36	1098	44	100
040916/3	A_301	76	12	55	52079	0.72	1.605	0.071	0.1565	0.0052	0.75	0.0744	0.0022	972	43	937	31	1052	59	89
040916/3	A_302	689	120	497	524876	0.72	1.787	0.070	0.1744	0.0058	0.84	0.0743	0.0016	1041	41	1036	34	1051	43	99
040916/3	A_303	687	108	636	40083	0.93	1.622	0.064	0.1579	0.0052	0.84	0.0745	0.0016	979	39	945	31	1055	44	90
040916/3	A_304	160	29	95	6159	0.60	1.895	0.078	0.1805	0.0060	0.81	0.0762	0.0019	1079	44	1069	35	1100	49	97
040916/3	A_305	407	76	35	17441	0.09	1.991	0.085	0.1863	0.0062	0.78	0.0775	0.0021	1113	47	1101	37	1135	53	97
040916/3	A_306	392	59	661	257278	1.69	1.554	0.062	0.1503	0.0050	0.83	0.0750	0.0017	952	38	903	30	1067	46	85
040916/3	A_307	363	57	134	9885	0.37	1.615	0.065	0.1576	0.0052	0.83	0.0743	0.0017	976	39	943	31	1050	46	90
040916/3	A_310	271	48	96	211309	0.36	1.863	0.075	0.1788	0.0059	0.82	0.0756	0.0017	1068	43	1061	35	1083	46	98
040916/3	A_311	203	36	109	8062	0.53	1.844	0.075	0.1774	0.0059	0.81	0.0754	0.0018	1061	43	1053	35	1079	48	98
040916/3	A_312	858	151	241	11179	0.28	1.834	0.072	0.1755	0.0058	0.84	0.0758	0.0016	1058	42	1042	34	1090	43	96
040916/3	A_313	770	109	3180	6242	4.13	1.519	0.060	0.1412	0.0047	0.83	0.0780	0.0017	938	37	851	28	1148	43	74
040916/3	A_314	442	82	78	356105	0.18	1.937	0.077	0.1849	0.0061	0.83	0.0760	0.0017	1094	44	1094	36	1094	44	100
040916/3	A_315	149	23	109	1770	0.73	1.585	0.067	0.1560	0.0052	0.79	0.0737	0.0019	964	40	934	31	1033	52	90
040916/3	A_316	393	72	136	25792	0.35	1.933	0.078	0.1844	0.0061	0.82	0.0760	0.0018	1093	44	1091	36	1096	46	100
040916/3	A_317	272	42	161	181606	0.59	1.553	0.063	0.1536	0.0051	0.82	0.0733	0.0017	952	39	921	31	1023	47	90
040916/3	A_318	120	20	62	88588	0.52	1.786	0.076	0.1696	0.0057	0.79	0.0764	0.0020	1040	44	1010	34	1105	52	91
040916/3	A_319	410	75	70	88218	0.17	1.935	0.077	0.1841	0.0061	0.83	0.0762	0.0017	1093	44	1089	36	1101	45	99
040916/3	A_320	147	27	94	6732	0.64	1.920	0.080	0.1833	0.0061	0.80	0.0760	0.0019	1088	45	1085	36	1094	50	99
040916/3	A_321	440	77	105	8424	0.24	1.810	0.072	0.1756	0.0058	0.83	0.0747	0.0017	1049	42	1043	35	1062	45	98
040916/3	A_322	500	91	131	5516	0.26	1.913	0.076	0.1828	0.0061	0.83	0.0759	0.0017	1086	43	1082	36	1093	44	99
040916/3	A_323	172	29	68	125257	0.40	1.751	0.073	0.1678	0.0056	0.81	0.0757	0.0019	1028	43	1000	33	1087	49	92
040916/3	A_324	316	54	139	234503	0.44	1.722	0.070	0.1705	0.0057	0.82	0.0733	0.0017	1017	41	1015	34	1021	47	99
040916/3	A_327	239	43	113	14721	0.47	1.881	0.076	0.1788	0.0059	0.82	0.0763	0.0018	1074	44	1060	35	1103	47	96
040916/3	A_328	1193	176	1086	4840	0.91	1.547	0.061	0.1480	0.0049	0.84	0.0758	0.0016	949	37	890	29	1090	43	82
040916/3	A_329	534	84	230	4431	0.43	1.666	0.067	0.1581	0.0052	0.83	0.0765	0.0017	996	40	946	31	1107	44	85
040916/3	A_330	388	69	53	17819	0.14	1.872	0.080	0.1787	0.0060	0.79	0.0760	0.0020	1071	46	1060	35	1095	53	97
040916/3	A_331	324	52	213	224929	0.66	1.667	0.067	0.1598	0.0053	0.82	0.0757	0.0017	996	40	956	32	1086	46	88
040916/3	A_332	923	127	776	5293	0.84	1.424	0.057	0.1373	0.0046	0.84	0.0752	0.0016	899	36	829	28	1075	44	77
040916/3	A_333	130	23	109	3592	0.84	1.833	0.086	0.1770	0.0060	0.73	0.0751	0.0024	1057	50	1050	36	1072	65	98
040916/3	A_334	244	37	260	5171	1.06	1.595	0.065	0.1511	0.0050	0.81	0.0766	0.0018	968	40	907	30	1110	47	82
040916/3	A_335	123	21	57	6492	0.46	1.771	0.075	0.1722	0.0058	0.79	0.0746	0.0019	1035	44	1024	34	1058	52	97
040916/3	A_336	92	16	50	10255	0.55	1.843	0.080	0.1794	0.0060	0.77	0.0745	0.0020	1061	46	1064	36	1056	55	101

040916/3							RATIOS							AGES [Ma]						Conc.
Sample	**Analysis**	**U [ppm]^{a}**	**Pb [ppm]^{a}**	**Th [ppm]**	**^{206}Pb/^{204}Pb**	**Th/U meas**	**^{207}Pb/^{235}U^{b}**	**2 σ^{d}**	**^{206}Pb/^{238}U^{b}**	**2 σ^{d}**	**rho^{c}**	**^{207}Pb/^{206}Pb^{e}**	**2 σ^{d}**	**^{207}Pb/^{235}U**	**2 σ**	**^{206}Pb/^{238}U**	**2 σ**	**^{207}Pb/^{206}Pb**	**2 σ**	%
040916/3	A_337	512	91	103	7584	0.20	1.853	0.074	0.1768	0.0059	0.83	0.0760	0.0017	1064	43	1049	35	1095	45	96
040916/3	A_338	689	121	144	524392	0.21	1.820	0.072	0.1755	0.0058	0.84	0.0752	0.0016	1053	42	1042	35	1074	44	97
040916/3	A_339	173	27	179	115912	1.03	1.576	0.066	0.1541	0.0052	0.80	0.0742	0.0019	961	40	924	31	1046	51	88
040916/3	A_340	187	33	64	41818	0.34	1.833	0.076	0.1770	0.0059	0.81	0.0751	0.0018	1057	44	1051	35	1071	49	98
040916/3	A_341	125	22	70	2204	0.56	1.883	0.080	0.1794	0.0060	0.79	0.0761	0.0020	1075	45	1064	36	1098	52	97
040916/3	A_349	232	43	87	3696	0.37	1.949	0.081	0.1832	0.0061	0.81	0.0772	0.0019	1098	46	1084	36	1125	49	96
040916/3	A_350	254	39	135	4955	0.53	1.559	0.064	0.1527	0.0051	0.81	0.0741	0.0018	954	39	916	31	1044	48	88
040916/3	A_351	369	65	212	282140	0.58	1.827	0.074	0.1768	0.0059	0.82	0.0749	0.0017	1055	43	1050	35	1066	46	98
040916/3	A_352	87	14	69	61198	0.80	1.694	0.075	0.1635	0.0055	0.76	0.0752	0.0021	1006	44	976	33	1073	57	91
040916/3	A_353	647	113	623	13637	0.96	1.830	0.073	0.1745	0.0058	0.83	0.0761	0.0017	1056	42	1037	35	1097	44	94
040916/3	A_354	133	22	96	93277	0.72	1.670	0.071	0.1626	0.0055	0.79	0.0745	0.0019	997	42	971	33	1055	52	92
040916/3	A_355	168	27	129	3119	0.77	1.655	0.069	0.1603	0.0054	0.80	0.0748	0.0019	991	42	959	32	1064	51	90
040916/3	A_356	355	65	79	12252	0.22	1.919	0.078	0.1835	0.0061	0.82	0.0758	0.0017	1088	44	1086	36	1090	46	100
040916/3	A_357	88	14	64	61436	0.73	1.659	0.073	0.1608	0.0054	0.77	0.0749	0.0021	993	44	961	33	1064	57	90
040916/3	A_358	307	54	67	234844	0.22	1.841	0.075	0.1771	0.0059	0.82	0.0754	0.0018	1060	43	1051	35	1078	47	97
040916/3	A_361	1028	164	236	11278	0.23	1.649	0.066	0.1600	0.0053	0.84	0.0748	0.0016	989	40	956	32	1062	44	90
040916/3	A_362	728	108	573	9795	0.79	1.562	0.063	0.1490	0.0050	0.83	0.0760	0.0017	955	38	895	30	1096	44	82
040916/3	A_363	556	99	195	33268	0.35	1.837	0.074	0.1773	0.0059	0.83	0.0752	0.0017	1059	43	1052	35	1073	45	98
040916/3	A_364	71	14	29	502	0.40	2.032	0.120	0.1903	0.0068	0.61	0.0774	0.0036	1126	66	1123	40	1133	93	99
040916/3	A_365	281	40	2048	1960	7.28	1.507	0.069	0.1412	0.0048	0.75	0.0774	0.0023	933	42	851	29	1132	60	75
040916/3	A_366	233	33	662	5725	2.84	1.496	0.062	0.1424	0.0048	0.81	0.0762	0.0019	929	39	858	29	1101	49	78
040916/3	A_367	308	58	198	26385	0.64	2.001	0.081	0.1882	0.0063	0.82	0.0771	0.0018	1116	45	1111	37	1124	46	99
040916/3	A_368	563	101	39	245738	0.07	1.836	0.074	0.1789	0.0060	0.83	0.0744	0.0017	1058	43	1061	35	1053	45	101
040916/3	A_369	541	98	166	51192	0.31	1.885	0.079	0.1817	0.0061	0.80	0.0752	0.0019	1076	45	1076	36	1074	51	100
040916/3	A_370	218	33	105	5946	0.48	1.533	0.064	0.1518	0.0051	0.81	0.0732	0.0018	944	39	911	31	1020	50	89
040916/3	A_371	197	34	68	146423	0.34	1.770	0.074	0.1722	0.0058	0.80	0.0746	0.0019	1034	43	1024	34	1056	50	97
040916/3	A_372	864	147	125	634212	0.14	1.784	0.072	0.1705	0.0057	0.83	0.0759	0.0017	1040	42	1015	34	1092	44	93
040916/3	A_373	784	127	520	10047	0.66	1.647	0.066	0.1620	0.0054	0.83	0.0738	0.0016	988	40	968	32	1035	45	94
040916/3	A_374	362	61	339	261842	0.94	1.756	0.077	0.1682	0.0057	0.77	0.0757	0.0021	1029	45	1002	34	1088	57	92
040916/3	A_375	412	71	88	13478	0.21	1.738	0.071	0.1719	0.0058	0.83	0.0733	0.0017	1023	42	1023	34	1023	46	100
040916/3	A_378	366	65	137	109030	0.38	1.839	0.075	0.1771	0.0059	0.82	0.0753	0.0017	1059	43	1051	35	1077	46	98
040916/3	A_379	256	46	153	99237	0.60	1.897	0.078	0.1808	0.0061	0.81	0.0761	0.0018	1080	45	1071	36	1098	48	98
040916/3	A_380	646	117	370	18114	0.57	1.878	0.076	0.1805	0.0061	0.83	0.0755	0.0017	1074	43	1070	36	1081	45	99
040916/3	A_381	107	20	58	3041	0.54	1.911	0.083	0.1823	0.0062	0.78	0.0760	0.0021	1085	47	1080	37	1095	54	99
040916/3	A_382	206	33	101	141673	0.49	1.630	0.068	0.1601	0.0054	0.80	0.0739	0.0018	982	41	957	32	1038	50	92
040916/3	A_383	209	38	102	162516	0.49	1.904	0.079	0.1813	0.0061	0.81	0.0762	0.0019	1083	45	1074	36	1099	49	98
040916/3	A_384	1400	213	473	7459	0.34	1.584	0.065	0.1522	0.0051	0.82	0.0755	0.0017	964	39	913	31	1082	46	84
040916/3	A_385	299	51	155	220086	0.52	1.741	0.072	0.1713	0.0058	0.82	0.0737	0.0018	1024	42	1019	34	1033	48	99
040916/3	A_386	146	24	105	200451	0.72	1.702	0.073	0.1654	0.0056	0.79	0.0746	0.0019	1009	43	986	33	1059	52	93
040916/3	A_387	702	120	64	34981	0.09	1.741	0.070	0.1713	0.0058	0.83	0.0737	0.0017	1024	41	1019	34	1033	46	99
040916/3	A_388	205	37	97	11401	0.47	1.894	0.079	0.1812	0.0061	0.81	0.0758	0.0019	1079	45	1074	36	1090	49	99
040916/3	A_389	354	67	105	7859	0.30	2.028	0.087	0.1902	0.0064	0.79	0.0773	0.0020	1125	48	1122	38	1129	52	99
040916/3	A_390	147	26	69	21021	0.47	1.836	0.079	0.1775	0.0060	0.79	0.0750	0.0020	1058	46	1053	36	1070	54	98
040916/3	A_391	461	75	278	8393	0.60	1.673	0.068	0.1631	0.0055	0.82	0.0744	0.0017	998	41	974	33	1052	47	93
040916/3	A_392	274	44	133	187098	0.48	1.652	0.069	0.1590	0.0054	0.81	0.0754	0.0018	990	41	951	32	1079	48	88
040916/3	A_395	253	45	145	194220	0.57	1.874	0.078	0.1790	0.0060	0.81	0.0760	0.0018	1072	45	1061	36	1094	48	97
040916/3	A_396	982	161	447	8514	0.45	1.702	0.069	0.1642	0.0055	0.83	0.0752	0.0017	1009	41	980	33	1073	45	91
040916/3	A_397	192	33	168	10882	0.88	1.769	0.075	0.1730	0.0059	0.80	0.0742	0.0019	1034	44	1028	35	1047	51	98
040916/3	A_398	504	86	139	9281	0.27	1.791	0.074	0.1696	0.0057	0.81	0.0766	0.0018	1042	43	1010	34	1111	48	91
040916/3	A_399	481	84	165	99825	0.34	1.772	0.072	0.1740	0.0059	0.83	0.0739	0.0017	1035	42	1034	35	1037	46	100
040916/3	A_400	385	64	93	275536	0.24	1.691	0.069	0.1672	0.0056	0.82	0.0734	0.0017	1005	41	996	34	1024	47	97
040916/3	A_402	161	29	90	122749	0.56	1.834	0.078	0.1786	0.0061	0.80	0.0745	0.0019	1058	45	1060	36	1054	51	101
040916/3	A_403	257	47	107	9105	0.42	1.908	0.080	0.1816	0.0061	0.81	0.0762	0.0019	1084	45	1076	36	1101	49	98
040916/3	A_404	531	95	62	7293	0.12	1.864	0.076	0.1794	0.0061	0.83	0.0754	0.0017	1068	44	1064	36	1078	46	99
040916/3	A_405	190	34	56	14383	0.29	1.896	0.080	0.1816	0.0062	0.80	0.0757	0.0019	1080	46	1076	36	1088	50	99
040916/3	A_406	447	80	327	10117	0.73	1.862	0.077	0.1778	0.0060	0.82	0.0760	0.0018	1068	44	1055	36	1094	47	96
040916/3	A_407	263	46	175	12401	0.67	1.778	0.074	0.1738	0.0059	0.81	0.0742	0.0018	1037	43	1033	35	1046	49	99
040916/3	A_408	981	147	314	8462	0.32	1.606	0.070	0.1504	0.0051	0.79	0.0774	0.0021	972	42	903	31	1132	53	80
040916/3	A_409	192	34	102	146475	0.53	1.835	0.078	0.1787	0.0061	0.80	0.0745	0.0019	1058	45	1060	36	1054	51	101

Appendix B - LA-ICP-MS U-Pb geochronological data for zircons of sample 040916/2

040916/2								RATIOS							AGES [Ma]						Conc.
Sample	Analysis	Analysis	U [ppm]^a	Pb [ppm]^a	Th [ppm]	$^{206}Pb/^{204}Pb$	Th/U meas	$^{207}Pb/^{235}U^b$	2 σ^d	$^{206}Pb/^{238}U^b$	2 σ^d	rho^c	$^{207}Pb/^{206}Pb^e$	2 σ^d	$^{207}Pb/^{235}U$	2 σ	$^{206}Pb/^{238}U$	2 σ	$^{207}Pb/^{206}Pb$	2 σ	%
040916/2	042-1	A_140	677	116	183	2563	0.27	1.842	0.074	0.1715	0.0056	0.80	0.0779	0.0019	1061	43	1021	33	1144	48	89
040916/2	042-2	A_141	424	73	85	9460	0.20	1.743	0.068	0.1721	0.0055	0.83	0.0735	0.0016	1025	40	1023	33	1027	45	100
040916/2	042-3	A_142	222	38	73	19528	0.33	1.765	0.070	0.1728	0.0056	0.81	0.0741	0.0017	1033	41	1027	33	1044	47	98
040916/2	042-4	A_143	403	69	111	40703	0.28	1.709	0.068	0.1703	0.0055	0.82	0.0728	0.0017	1012	40	1014	33	1008	46	101
040916/2	042-5	A_144	164	28	90	3540	0.55	1.762	0.072	0.1721	0.0056	0.80	0.0743	0.0018	1032	42	1024	33	1049	49	98
040916/2	042-6	A_145	511	89	184	21582	0.36	1.791	0.070	0.1743	0.0056	0.83	0.0745	0.0016	1042	41	1035	33	1056	44	98
040916/2	042-7	A_146	548	91	201	3364	0.37	1.782	0.087	0.1655	0.0055	0.68	0.0781	0.0028	1039	51	987	33	1149	71	86
040916/2	042-8	A_147	578	40	44	1755	0.08	0.688	0.031	0.0687	0.0023	0.73	0.0727	0.0022	532	24	428	14	1004	63	43
040916/2	042-9	A_148	386	67	39	300602	0.10	1.788	0.070	0.1736	0.0056	0.82	0.0747	0.0017	1041	41	1032	33	1061	45	97
040916/2	042-10	A_149	206	35	106	84587	0.51	1.730	0.070	0.1713	0.0056	0.80	0.0732	0.0018	1020	41	1019	33	1021	49	100
040916/2	042-11	A_150	85	28	84	127171	0.98	5.278	0.212	0.3332	0.0108	0.81	0.1149	0.0027	1865	75	1854	60	1878	42	99
040916/2	042-12	A_151	353	48	94	1074	0.27	1.421	0.073	0.1369	0.0046	0.66	0.0753	0.0029	898	46	827	28	1076	77	77
040916/2	042-13	A_152	282	49	42	218326	0.15	1.770	0.070	0.1729	0.0056	0.82	0.0742	0.0017	1034	41	1028	33	1048	46	98
040916/2	042-15	A_154	391	39	54	173557	0.14	0.821	0.033	0.0991	0.0032	0.80	0.0601	0.0015	609	25	609	20	608	53	100
040916/2	042-16	A_157	247	44	64	5222	0.26	1.879	0.075	0.1804	0.0059	0.81	0.0755	0.0018	1074	43	1069	35	1082	47	99
040916/2	042-17	A_158	1573	231	618	351	0.39	2.321	0.091	0.1467	0.0048	0.82	0.1148	0.0026	1219	48	882	29	1876	40	47
040916/2	042-18	A_159	440	51	25	229507	0.06	1.021	0.041	0.1165	0.0038	0.81	0.0635	0.0015	714	29	711	23	725	49	98
040916/2	042-20	A_161	569	82	173	2844	0.30	1.500	0.063	0.1439	0.0047	0.78	0.0756	0.0020	931	39	867	28	1084	52	80
040916/2	042-21	A_162	67	12	32	51603	0.48	1.769	0.078	0.1733	0.0057	0.74	0.0741	0.0022	1034	46	1030	34	1043	60	99
040916/2	042-23	A_164	814	139	93	13282	0.11	1.725	0.067	0.1709	0.0055	0.83	0.0732	0.0016	1018	40	1017	33	1020	44	100
040916/2	042-24	A_165	822	150	124	1808	0.15	1.898	0.089	0.1827	0.0061	0.71	0.0753	0.0025	1080	51	1082	36	1078	67	100
040916/2	042-27	A_168	1138	111	113	5737	0.10	0.825	0.044	0.0975	0.0033	0.63	0.0614	0.0025	611	33	600	20	653	89	92
040916/2	042-29	A_170	366	64	119	8148	0.33	1.780	0.070	0.1745	0.0057	0.82	0.0740	0.0017	1038	41	1037	34	1041	45	100
040916/2	042-30	A_171	302	52	26	6020	0.09	1.745	0.069	0.1722	0.0056	0.82	0.0735	0.0017	1025	41	1024	33	1027	46	100
040916/2	042-31	A_174	347	60	126	15061	0.36	1.774	0.070	0.1733	0.0056	0.82	0.0743	0.0017	1036	41	1030	33	1049	46	98
040916/2	042-32	A_175	254	44	71	194553	0.28	1.749	0.070	0.1715	0.0056	0.81	0.0740	0.0017	1027	41	1020	33	1041	47	98
040916/2	042-34	A_177	56	10	38	965	0.69	1.935	0.127	0.1848	0.0066	0.55	0.0760	0.0042	1093	72	1093	39	1094	110	100
040916/2	042-35	A_178	620	111	158	17434	0.26	1.846	0.072	0.1785	0.0058	0.83	0.0750	0.0016	1062	41	1059	34	1069	43	99
040916/2	042-36	A_179	344	38	144	20537	0.42	0.951	0.043	0.1107	0.0037	0.74	0.0623	0.0019	679	31	677	22	685	65	99
040916/2	042-37	A_180	238	43	76	17067	0.32	1.873	0.075	0.1813	0.0059	0.81	0.0749	0.0018	1072	43	1074	35	1067	47	101
040916/2	042-38	A_181	176	30	17	15111	0.10	1.698	0.071	0.1687	0.0055	0.79	0.0730	0.0019	1008	42	1005	33	1014	52	99
040916/2	042-39	A_182	232	40	66	90000	0.29	1.760	0.071	0.1731	0.0056	0.81	0.0737	0.0018	1031	42	1029	34	1034	48	100
040916/2	042-40	A_183	581	97	80	5592	0.14	1.725	0.073	0.1670	0.0055	0.78	0.0749	0.0020	1018	43	996	33	1066	53	93
040916/2	042-41	A_184	102	18	47	1497	0.46	1.795	0.130	0.1740	0.0064	0.51	0.0748	0.0046	1044	75	1034	38	1064	125	97
040916/2	042-42	A_185	163	12	63	332	0.39	0.996	0.057	0.0710	0.0025	0.61	0.1017	0.0046	702	40	442	16	1655	84	27
040916/2	042-43	A_186	315	50	48	10077	0.15	1.614	0.064	0.1600	0.0052	0.82	0.0732	0.0017	976	39	957	31	1018	47	94
040916/2	042-44	A_187	217	37	58	163109	0.27	1.699	0.069	0.1690	0.0055	0.81	0.0729	0.0017	1008	41	1006	33	1012	48	99
040916/2	042-45	A_188	276	47	25	208445	0.09	1.733	0.070	0.1701	0.0056	0.81	0.0739	0.0017	1021	41	1013	33	1038	47	98
040916/2	042-46	A_191	262	46	84	47197	0.32	1.802	0.073	0.1743	0.0057	0.81	0.0750	0.0018	1046	42	1036	34	1068	47	97
040916/2	042-47	A_192	85	16	26	4751	0.31	2.033	0.150	0.1916	0.0072	0.51	0.0770	0.0049	1127	83	1130	42	1120	127	101
040916/2	042-49	A_194	441	69	96	306999	0.22	1.584	0.063	0.1568	0.0051	0.82	0.0733	0.0016	964	38	939	31	1021	45	92
040916/2	042-50	A_195	349	60	30	266590	0.09	1.747	0.071	0.1722	0.0056	0.80	0.0736	0.0018	1026	42	1024	34	1031	49	99
040916/2	042-51	A_196	1122	110	382	1414	0.34	0.994	0.042	0.0983	0.0032	0.77	0.0734	0.0020	701	30	604	20	1024	55	59
040916/2	042-52	A_197	337	62	81	275816	0.24	1.918	0.082	0.1845	0.0061	0.77	0.0754	0.0021	1087	47	1091	36	1079	55	101
040916/2	042-53	A_198	1023	167	1905	3054	1.86	1.738	0.072	0.1632	0.0054	0.80	0.0772	0.0019	1023	42	974	32	1127	50	86
040916/2	042-54	A_199	339	59	27	10792	0.08	1.772	0.071	0.1744	0.0057	0.82	0.0737	0.0017	1035	41	1036	34	1033	46	100
040916/2	042-55	A_200	266	46	24	19074	0.09	1.763	0.078	0.1748	0.0058	0.75	0.0732	0.0022	1032	46	1038	34	1019	60	102
040916/2	042-57	A_202	329	57	65	6865	0.20	1.751	0.070	0.1728	0.0057	0.82	0.0735	0.0017	1028	41	1028	34	1027	46	100
040916/2	042-58	A_203	604	104	134	4941	0.22	1.754	0.069	0.1717	0.0056	0.83	0.0741	0.0016	1029	40	1021	33	1045	44	98
040916/2	042-59	A_204	107	18	39	5643	0.37	1.704	0.074	0.1692	0.0056	0.76	0.0730	0.0020	1010	44	1008	33	1015	57	99
040916/2	042-60	A_205	197	33	29	6411	0.15	1.689	0.069	0.1687	0.0055	0.80	0.0726	0.0018	1004	41	1005	33	1003	50	100
040916/2	042-62	A_214	415	74	81	7313	0.20	1.849	0.074	0.1789	0.0059	0.82	0.0750	0.0017	1063	42	1061	35	1067	46	99
040916/2	042-63	A_215	440	78	130	344294	0.29	1.808	0.072	0.1770	0.0058	0.83	0.0741	0.0017	1048	42	1051	34	1043	45	101
040916/2	042-64	A_216	125	22	42	21889	0.33	1.760	0.075	0.1724	0.0057	0.78	0.0741	0.0020	1031	44	1025	34	1043	53	98
040916/2	042-65	A_217	642	102	244	3352	0.38	1.653	0.074	0.1590	0.0053	0.75	0.0754	0.0022	991	44	951	32	1079	60	88
040916/2	042-66	A_218	382	66	57	7624	0.15	1.774	0.071	0.1728	0.0057	0.82	0.0744	0.0017	1036	41	1028	34	1053	46	98
040916/2	042-67	A_219	327	43	46	8055	0.14	1.247	0.053	0.1328	0.0044	0.78	0.0681	0.0018	822	35	804	27	872	55	92
040916/2	042-68	A_220	141	24	45	107046	0.32	1.805	0.102	0.1723	0.0060	0.61	0.0760	0.0034	1047	59	1025	36	1095	90	94
040916/2	042-69	A_221	426	62	200	273982	0.47	1.535	0.075	0.1456	0.0049	0.69	0.0765	0.0027	944	46	876	30	1107	71	79
040916/2	042-70	A_222	645	107	310	3110	0.48	1.719	0.071	0.1666	0.0055	0.80	0.0748	0.0018	1016	42	993	33	1064	49	93
040916/2	042-71	A_225	611	103	75	453467	0.12	1.688	0.067	0.1683	0.0055	0.82	0.0728	0.0016	1004	40	1002	33	1008	46	99
040916/2	042-72	A_226	148	26	53	113515	0.36	1.823	0.088	0.1743	0.0059	0.70	0.0758	0.0026	1054	51	1036	35	1091	70	95

040916/2								RATIOS							AGES [Ma]						Conc.
Sample	Analysis	Analysis	U [ppm][a]	Pb [ppm][a]	Th [ppm]	^{206}Pb/^{204}Pb	Th/U meas	^{207}Pb/^{235}U[b]	2 σ[d]	^{206}Pb/^{238}U[b]	2 σ[d]	rho[c]	^{207}Pb/^{206}Pb[e]	2 σ[d]	^{207}Pb/^{235}U	2 σ	^{206}Pb/^{238}U	2 σ	^{207}Pb/^{206}Pb	2 σ	%
040916/2	042-73	A_227	89	16	41	7452	0.46	1.889	0.082	0.1802	0.0060	0.77	0.0760	0.0021	1077	47	1068	35	1096	56	97
040916/2	042-75	A_229	412	73	49	322249	0.12	1.830	0.073	0.1773	0.0058	0.82	0.0749	0.0017	1056	42	1052	35	1065	46	99
040916/2	042-76	A_230	297	53	65	4971	0.22	1.865	0.075	0.1796	0.0059	0.82	0.0753	0.0018	1069	43	1065	35	1077	47	99
040916/2	042-77	A_231	337	34	136	151340	0.41	0.852	0.047	0.1020	0.0035	0.62	0.0606	0.0026	626	35	626	21	624	94	100
040916/2	042-78	A_232	332	64	139	1861	0.42	2.166	0.099	0.1941	0.0065	0.73	0.0809	0.0025	1170	54	1144	38	1219	61	94
040916/2	042-79	A_233	1332	99	316	3288	0.24	0.660	0.030	0.0741	0.0025	0.74	0.0646	0.0020	514	23	461	15	760	65	61
040916/2	042-80	A_234	184	35	61	52132	0.33	2.039	0.084	0.1922	0.0063	0.80	0.0770	0.0019	1129	46	1133	37	1120	49	101
040916/2	042-81	A_235	338	59	90	17411	0.27	1.776	0.072	0.1745	0.0057	0.82	0.0738	0.0017	1037	42	1037	34	1037	47	100
040916/2	042-82	A_236	462	85	80	7197	0.17	1.914	0.077	0.1832	0.0060	0.82	0.0758	0.0017	1086	44	1084	36	1089	46	100
040916/2	042-83	A_237	631	98	250	2352	0.40	1.605	0.069	0.1546	0.0051	0.78	0.0753	0.0020	972	42	927	31	1076	54	86
040916/2	042-85	A_239	281	48	54	210112	0.19	1.700	0.070	0.1699	0.0056	0.80	0.0726	0.0018	1009	42	1011	33	1003	50	101
040916/2	042-87	A_243	630	90	27	49457	0.04	1.360	0.055	0.1435	0.0047	0.82	0.0687	0.0016	872	35	864	29	891	48	97
040916/2	042-88	A_244	446	78	163	35734	0.36	1.784	0.071	0.1753	0.0058	0.82	0.0738	0.0017	1040	42	1041	34	1037	46	100
040916/2	042-89	A_245	285	46	99	2490	0.35	1.728	0.079	0.1621	0.0055	0.74	0.0773	0.0024	1019	47	969	33	1128	62	86
040916/2	042-90	A_246	1023	93	264	1297	0.26	0.935	0.040	0.0913	0.0030	0.77	0.0743	0.0020	670	29	563	19	1048	55	54
040916/2	042-92	A_248	610	80	42	5539	0.07	1.349	0.062	0.1313	0.0044	0.73	0.0745	0.0024	867	40	795	27	1056	64	75
040916/2	042-93	A_249	119	22	23	270	0.19	2.940	0.123	0.1860	0.0062	0.80	0.1146	0.0029	1392	58	1100	37	1874	46	59
040916/2	042-94	A_250	273	46	86	5452	0.32	1.702	0.070	0.1697	0.0056	0.81	0.0728	0.0018	1009	41	1010	33	1008	49	100
040916/2	042-95	A_251	66	13	18	1479	0.27	2.092	0.139	0.1941	0.0071	0.55	0.0781	0.0043	1146	76	1144	42	1150	110	99
040916/2	042-96	A_252	139	14	98	62942	0.71	0.869	0.046	0.1033	0.0035	0.65	0.0610	0.0025	635	34	634	22	639	87	99
040916/2	042-97	A_253	413	80	38	3937	0.09	2.182	0.088	0.1939	0.0064	0.82	0.0816	0.0019	1175	47	1142	38	1236	45	92
040916/2	042-98	A_254	1002	89	184	8785	0.18	0.712	0.032	0.0887	0.0030	0.74	0.0582	0.0018	546	25	548	18	538	67	102
040916/2	042-99	A_255	223	38	66	4605	0.30	1.747	0.081	0.1717	0.0058	0.73	0.0738	0.0024	1026	48	1021	35	1036	65	99
040916/2	042-100	A_256	318	54	87	8445	0.27	1.704	0.070	0.1689	0.0056	0.81	0.0732	0.0017	1010	41	1006	33	1018	48	99
040916/2	042-101	A_259	530	85	284	10796	0.54	1.616	0.066	0.1597	0.0053	0.81	0.0734	0.0018	976	40	955	32	1025	49	93
040916/2	042-102	A_260	1120	120	83	1386	0.07	1.069	0.043	0.1070	0.0035	0.83	0.0725	0.0016	738	30	655	22	999	46	66
040916/2	042-103	A_261	163	17	50	72317	0.30	0.855	0.038	0.1012	0.0034	0.75	0.0613	0.0018	627	28	622	21	648	63	96
040916/2	042-104	A_262	471	48	147	37830	0.31	0.855	0.036	0.1022	0.0034	0.79	0.0607	0.0016	627	26	627	21	628	55	100
040916/2	042-105	A_263	423	75	105	326585	0.25	1.823	0.074	0.1764	0.0059	0.81	0.0750	0.0018	1054	43	1047	35	1067	48	98
040916/2	042-106	A_264	224	28	90	124626	0.40	1.184	0.054	0.1272	0.0043	0.73	0.0675	0.0021	793	36	772	26	853	65	90
040916/2	042-108	A_266	483	83	158	5092	0.33	1.790	0.074	0.1713	0.0057	0.81	0.0758	0.0018	1042	43	1019	34	1090	49	94
040916/2	042-109	A_267	572	97	35	11255	0.06	1.709	0.069	0.1700	0.0056	0.82	0.0729	0.0017	1012	41	1012	34	1011	47	100
040916/2	042-110	A_268	312	43	21	7334	0.07	1.267	0.054	0.1373	0.0046	0.78	0.0669	0.0018	831	36	829	28	836	56	99
040916/2	042-111	A_269	1876	148	186	1058	0.10	0.825	0.036	0.0788	0.0026	0.77	0.0760	0.0021	611	27	489	16	1094	55	45
040916/2	042-112	A_270	106	18	24	5366	0.23	1.705	0.075	0.1695	0.0057	0.76	0.0729	0.0021	1010	44	1010	34	1012	58	100
040916/2	042-113	A_271	422	74	77	325164	0.18	1.810	0.074	0.1764	0.0059	0.82	0.0744	0.0017	1049	43	1047	35	1053	47	99
040916/2	042-114	A_272	690	71	254	309468	0.37	0.859	0.036	0.1026	0.0034	0.80	0.0607	0.0015	629	26	630	21	628	55	100
040916/2	042-115	A_273	171	29	64	1678	0.37	1.731	0.108	0.1681	0.0061	0.58	0.0747	0.0038	1020	64	1002	36	1060	103	94

Appendix C - LA-ICP-MS U-Pb geochronological data for zircons of sample 040916/5

040916/5								RATIOS							AGES [Ma]							Conc.
Sample	Analysis	Analysis	U [ppm]^{a}	Pb [ppm]^{a}	Th [ppm]	^{206}Pb/^{204}Pb	Th/U meas	^{207}Pb/^{235}U^{b}	$2\sigma^{d}$	^{206}Pb/^{238}U^{b}	$2\sigma^{d}$	rho^{c}	^{207}Pb/^{206}Pb^{e}	$2\sigma^{d}$	^{207}Pb/^{235}U	2σ	^{206}Pb/^{238}U	2σ	^{207}Pb/^{206}Pb	2σ	%
040916/5	045-1	A_004	189	33	79	224827	0.42	1.778	0.075	0.1729	0.0061	0.83	0.0746	0.0018	1038	44	1028	36	1058	47	97
040916/5	045-2	A_005	359	43	74	15889	0.20	1.068	0.045	0.1206	0.0042	0.84	0.0643	0.0014	738	31	734	26	750	47	98
040916/5	045-3	A_006	110	19	47	130298	0.43	1.743	0.075	0.1721	0.0061	0.82	0.0735	0.0018	1025	44	1023	36	1027	50	100
040916/5	045-5	A_008	1148	153	228	2402	0.20	1.386	0.059	0.1334	0.0047	0.83	0.0754	0.0018	883	37	807	28	1079	47	75
040916/5	045-6	A_009	621	102	713	2531	1.15	1.719	0.081	0.1644	0.0059	0.75	0.0758	0.0024	1016	48	981	35	1091	62	90
040916/5	045-8	A_011	367	64	115	36377	0.31	1.828	0.075	0.1750	0.0061	0.85	0.0758	0.0016	1056	43	1040	36	1089	43	95
040916/5	045-10	A_013	447	77	113	26061	0.25	1.753	0.072	0.1721	0.0060	0.85	0.0739	0.0016	1028	42	1024	36	1038	43	99
040916/5	045-11	A_014	612	85	95	4238	0.15	1.417	0.058	0.1395	0.0049	0.85	0.0737	0.0016	896	37	842	29	1033	43	81
040916/5	045-14	A_017	288	97	180	667731	0.63	5.345	0.217	0.3359	0.0117	0.86	0.1154	0.0024	1876	76	1867	65	1886	37	99
040916/5	045-15	A_018	365	69	34	3609	0.09	2.026	0.095	0.1901	0.0068	0.76	0.0773	0.0024	1124	53	1122	40	1129	61	99
040916/5	045-16	A_021	569	99	150	67568	0.26	1.796	0.073	0.1736	0.0061	0.86	0.0750	0.0016	1044	43	1032	36	1070	42	96
040916/5	045-17	A_022	698	127	56	2826	0.08	1.903	0.081	0.1818	0.0064	0.82	0.0759	0.0018	1082	46	1077	38	1093	49	99
040916/5	045-19	A_024	306	53	101	12715	0.33	1.779	0.073	0.1731	0.0060	0.85	0.0745	0.0016	1038	43	1029	36	1056	44	97
040916/5	045-20	A_025	473	91	146	3181	0.31	2.055	0.092	0.1920	0.0068	0.79	0.0776	0.0021	1134	51	1132	40	1137	55	100
040916/5	045-21	A_026	275	49	75	4389	0.27	1.850	0.076	0.1781	0.0062	0.85	0.0753	0.0016	1063	44	1057	37	1077	44	98
040916/5	045-22	A_027	283	49	19	336500	0.07	1.761	0.073	0.1719	0.0060	0.85	0.0743	0.0016	1031	43	1023	36	1050	44	97
040916/5	045-23	A_028	365	63	103	9096	0.28	1.746	0.071	0.1721	0.0060	0.85	0.0736	0.0016	1026	42	1024	36	1030	43	99
040916/5	045-24	A_029	462	73	128	13129	0.28	1.650	0.073	0.1580	0.0056	0.80	0.0758	0.0020	990	44	945	33	1089	53	87
040916/5	045-25	A_030	68	12	35	1212	0.51	1.872	0.082	0.1804	0.0063	0.80	0.0752	0.0020	1071	47	1069	38	1075	53	100
040916/5	045-27	A_032	325	56	48	6097	0.15	1.711	0.070	0.1708	0.0059	0.84	0.0726	0.0016	1013	42	1017	35	1004	45	101
040916/5	045-28	A_033	1162	205	703	5210	0.61	1.838	0.074	0.1765	0.0061	0.86	0.0755	0.0016	1059	43	1048	36	1082	41	97
040916/5	045-29	A_034	356	64	144	445701	0.40	1.861	0.076	0.1804	0.0063	0.85	0.0748	0.0016	1068	44	1069	37	1064	43	101
040916/5	045-30	A_035	332	57	79	12828	0.24	1.749	0.072	0.1717	0.0060	0.84	0.0739	0.0016	1027	42	1022	36	1038	45	98
040916/5	045-31	A_038	63	12	29	83448	0.46	1.996	0.088	0.1890	0.0066	0.80	0.0766	0.0020	1114	49	1116	39	1111	53	100
040916/5	045-34	A_041	288	46	45	319277	0.16	1.562	0.064	0.1594	0.0055	0.85	0.0711	0.0016	955	39	953	33	960	45	99
040916/5	045-35	A_042	294	52	53	4494	0.18	1.821	0.074	0.1766	0.0061	0.85	0.0748	0.0016	1053	43	1048	36	1062	44	99
040916/5	045-36	A_043	280	48	29	331991	0.10	1.703	0.070	0.1700	0.0059	0.85	0.0727	0.0016	1010	41	1012	35	1004	44	101
040916/5	045-37	A_044	388	71	77	33686	0.20	1.884	0.077	0.1821	0.0063	0.85	0.0750	0.0016	1075	44	1079	37	1069	43	101
040916/5	045-38	A_045	434	75	216	16904	0.50	1.754	0.071	0.1727	0.0060	0.85	0.0737	0.0016	1029	42	1027	36	1033	43	99
040916/5	045-39	A_046	812	140	40	8538	0.05	1.783	0.072	0.1726	0.0060	0.86	0.0749	0.0016	1039	42	1026	36	1067	42	96
040916/5	045-40	A_047	250	44	56	27206	0.22	1.775	0.073	0.1746	0.0061	0.84	0.0737	0.0017	1036	43	1037	36	1034	45	100
040916/5	045-42	A_049	97	19	56	1282	0.58	2.043	0.133	0.1931	0.0073	0.58	0.0768	0.0041	1130	73	1138	43	1115	106	102
040916/5	045-44	A_051	529	80	174	5992	0.33	1.542	0.063	0.1503	0.0052	0.84	0.0744	0.0016	947	39	903	31	1052	44	86
040916/5	045-45	A_052	349	34	94	5524	0.27	0.818	0.044	0.0984	0.0035	0.67	0.0603	0.0024	607	32	605	22	614	86	99
040916/5	045-46	A_055	276	36	130	856	0.47	1.590	0.065	0.1325	0.0046	0.84	0.0870	0.0019	966	40	802	28	1361	43	59
040916/5	045-47	A_056	357	62	155	12963	0.43	1.763	0.072	0.1746	0.0060	0.85	0.0733	0.0016	1032	42	1037	36	1021	44	102
040916/5	045-49	A_058	252	44	41	13436	0.16	1.822	0.075	0.1764	0.0061	0.84	0.0749	0.0017	1054	43	1047	36	1067	45	98
040916/5	045-51	A_060	155	16	46	110529	0.29	0.855	0.037	0.1015	0.0035	0.80	0.0611	0.0016	627	27	623	22	641	56	97
040916/5	045-52	A_061	800	110	409	21623	0.51	1.460	0.064	0.1377	0.0048	0.79	0.0769	0.0021	914	40	831	29	1119	53	74
040916/5	045-53	A_062	204	36	33	249083	0.16	1.769	0.073	0.1743	0.0060	0.84	0.0736	0.0017	1034	43	1036	36	1030	46	101
040916/5	045-54	A_063	414	72	38	3901	0.09	1.813	0.073	0.1733	0.0060	0.85	0.0759	0.0016	1050	43	1030	35	1092	43	94
040916/5	045-56	A_065	630	99	133	4494	0.21	1.661	0.068	0.1572	0.0054	0.84	0.0766	0.0017	994	41	941	32	1112	44	85
040916/5	045-57	A_066	364	50	94	1390	0.26	1.499	0.071	0.1378	0.0048	0.74	0.0789	0.0025	930	44	832	29	1169	62	71
040916/5	045-58	A_067	373	72	80	3746	0.22	1.999	0.091	0.1936	0.0068	0.77	0.0749	0.0022	1115	51	1141	40	1065	58	107
040916/5	045-59	A_068	511	83	66	2101	0.13	1.711	0.074	0.1630	0.0056	0.81	0.0762	0.0019	1013	44	973	34	1099	51	89
040916/5	045-61	A_077	395	46	10	2027	0.03	1.165	0.052	0.1154	0.0040	0.78	0.0732	0.0020	784	35	704	24	1020	56	69
040916/5	045-62	A_078	633	87	149	1771	0.24	1.468	0.070	0.1371	0.0048	0.73	0.0777	0.0025	917	44	828	29	1138	65	73
040916/5	045-63	A_079	998	96	101	2352	0.10	0.873	0.036	0.0963	0.0033	0.84	0.0657	0.0015	637	26	593	20	798	47	74
040916/5	045-64	A_080	317	57	53	69045	0.17	1.868	0.076	0.1803	0.0062	0.84	0.0752	0.0016	1070	43	1068	37	1073	44	100
040916/5	045-65	A_081	791	122	75	1919	0.10	1.584	0.067	0.1537	0.0053	0.81	0.0747	0.0019	964	41	922	32	1062	50	87
040916/5	045-67	A_083	190	26	65	6840	0.34	1.457	0.100	0.1371	0.0052	0.55	0.0771	0.0044	913	62	828	31	1124	114	74
040916/5	045-69	A_085	335	55	75	12343	0.22	1.605	0.067	0.1629	0.0056	0.82	0.0715	0.0017	972	41	973	33	971	49	100
040916/5	045-70	A_086	505	85	39	5777	0.08	1.674	0.068	0.1678	0.0057	0.85	0.0724	0.0016	999	40	1000	34	996	44	100
040916/5	045-71	A_089	330	50	37	4229	0.11	1.590	0.064	0.1508	0.0051	0.84	0.0765	0.0017	966	39	905	31	1108	44	82
040916/5	045-72	A_090	1012	83	303	1209	0.30	0.823	0.037	0.0816	0.0028	0.77	0.0732	0.0021	610	27	505	17	1019	58	50
040916/5	045-75	A_093	545	96	205	4852	0.38	1.876	0.075	0.1764	0.0060	0.85	0.0772	0.0016	1073	43	1047	36	1125	42	93
040916/5	045-76	A_094	298	46	82	1792	0.27	1.650	0.079	0.1556	0.0054	0.73	0.0769	0.0025	990	47	932	32	1120	65	83
040916/5	045-78	A_096	348	55	83	54136	0.24	1.588	0.064	0.1590	0.0054	0.84	0.0724	0.0016	965	39	951	32	998	45	95
040916/5	045-79	A_097	262	45	58	4230	0.22	1.744	0.071	0.1707	0.0058	0.83	0.0741	0.0017	1025	42	1016	35	1044	46	97
040916/5	045-80	A_098	115	21	93	6753	0.81	1.878	0.079	0.1817	0.0062	0.82	0.0750	0.0018	1073	45	1076	37	1068	49	101
040916/5	045-81	A_099	480	71	38	1861	0.08	1.542	0.069	0.1486	0.0051	0.77	0.0753	0.0021	947	42	893	31	1075	57	83
040916/5	045-82	A_100	128	11	191	81354	1.49	0.723	0.040	0.0894	0.0032	0.64	0.0587	0.0025	552	31	552	20	555	94	100

040916/5								RATIOS							AGES [Ma]						Conc.
Sample	Analysis	Analysis	U [ppm]^a	Pb [ppm]^a	Th [ppm]	^{206}Pb/^{204}Pb	Th/U meas	^{207}Pb/^{235}U^b	2 σ^d	^{206}Pb/^{238}U^b	2 σ^d	rho^c	^{207}Pb/^{206}Pb^e	2 σ^d	^{207}Pb/^{235}U	2 σ	^{206}Pb/^{238}U	2 σ	^{207}Pb/^{206}Pb	2 σ	%
040916/5	045-83	A_101	141	27	45	22341	0.32	2.052	0.095	0.1919	0.0066	0.75	0.0775	0.0024	1133	52	1132	39	1135	61	100
040916/5	045-84	A_102	238	44	20	16825	0.08	1.934	0.079	0.1845	0.0063	0.83	0.0760	0.0017	1093	45	1092	37	1095	45	100
040916/5	045-85	A_103	447	44	122	1124	0.27	1.022	0.042	0.0975	0.0033	0.84	0.0760	0.0017	715	29	600	20	1095	45	55
040916/5	045-86	A_106	69	11	14	2416	0.20	1.700	0.074	0.1621	0.0056	0.79	0.0761	0.0020	1009	44	968	33	1097	53	88
040916/5	045-87	A_107	114	19	25	20701	0.22	1.711	0.072	0.1673	0.0057	0.81	0.0742	0.0018	1013	42	997	34	1046	49	95
040916/5	045-88	A_108	982	137	381	2251	0.39	1.523	0.066	0.1399	0.0048	0.79	0.0790	0.0021	940	41	844	29	1171	53	72
040916/5	045-90	A_110	242	39	66	2951	0.27	1.669	0.068	0.1595	0.0054	0.84	0.0759	0.0017	997	41	954	32	1092	45	87
040916/5	045-91	A_111	266	50	62	356377	0.23	1.982	0.080	0.1879	0.0064	0.84	0.0765	0.0017	1109	45	1110	38	1108	44	100
040916/5	045-92	A_112	950	162	22	14051	0.02	1.732	0.069	0.1709	0.0058	0.85	0.0735	0.0016	1020	41	1017	34	1028	43	99
040916/5	045-93	A_113	313	56	58	5862	0.19	1.850	0.075	0.1780	0.0060	0.84	0.0754	0.0017	1063	43	1056	36	1078	44	98
040916/5	045-94	A_114	360	60	29	431382	0.08	1.687	0.068	0.1681	0.0057	0.84	0.0728	0.0016	1003	40	1001	34	1008	45	99
040916/5	045-95	A_115	163	27	13	192913	0.08	1.696	0.070	0.1660	0.0056	0.82	0.0741	0.0017	1007	42	990	34	1044	47	95
040916/5	045-96	A_116	223	43	91	2966	0.41	2.031	0.086	0.1921	0.0065	0.81	0.0767	0.0019	1126	47	1133	39	1113	49	102
040916/5	045-97	A_117	214	35	17	6222	0.08	1.652	0.068	0.1610	0.0055	0.83	0.0745	0.0017	990	41	962	33	1054	46	91
040916/5	045-98	A_118	756	89	34	909	0.04	1.214	0.050	0.1173	0.0040	0.82	0.0751	0.0018	807	33	715	24	1071	48	67
040916/5	045-99	A_119	211	36	21	4810	0.10	1.722	0.070	0.1709	0.0058	0.83	0.0731	0.0017	1017	41	1017	34	1016	46	100
040916/5	045-100	A_120	327	53	20	2838	0.06	1.683	0.068	0.1609	0.0054	0.84	0.0759	0.0017	1002	41	962	33	1091	44	88
040916/5	045-101	A_123	294	49	31	12562	0.10	1.744	0.071	0.1659	0.0056	0.83	0.0763	0.0017	1025	41	989	33	1102	45	90
040916/5	045-102	A_124	269	46	100	21426	0.37	1.791	0.072	0.1702	0.0057	0.83	0.0763	0.0017	1042	42	1013	34	1103	45	92
040916/5	045-103	A_125	187	29	123	5750	0.66	1.653	0.073	0.1564	0.0053	0.77	0.0767	0.0022	991	44	936	32	1113	56	84
040916/5	045-104	A_126	369	59	84	7710	0.23	1.654	0.067	0.1606	0.0054	0.84	0.0747	0.0016	991	40	960	32	1061	44	90
040916/5	045-105	A_127	137	26	221	2995	1.61	2.043	0.104	0.1923	0.0067	0.69	0.0771	0.0028	1130	57	1134	40	1123	73	101
040916/5	045-106	A_128	370	65	99	26677	0.27	1.829	0.074	0.1771	0.0060	0.84	0.0749	0.0017	1056	43	1051	35	1066	45	99
040916/5	045-107	A_129	559	103	95	741014	0.17	1.936	0.077	0.1846	0.0062	0.84	0.0761	0.0016	1094	44	1092	37	1097	43	100
040916/5	045-109	A_131	195	36	48	256810	0.25	1.918	0.082	0.1832	0.0062	0.79	0.0760	0.0020	1087	47	1084	37	1094	53	99
040916/5	045-110	A_132	483	78	225	3213	0.46	1.668	0.069	0.1613	0.0054	0.82	0.0750	0.0018	997	41	964	33	1069	48	90
040916/5	045-112	A_134	613	65	38	2447	0.06	1.079	0.045	0.1058	0.0036	0.81	0.0740	0.0018	743	31	648	22	1041	49	62
040916/5	045-113	A_135	715	85	131	1080	0.18	1.277	0.062	0.1188	0.0041	0.71	0.0779	0.0027	835	41	724	25	1145	68	63
040916/5	045-114	A_136	362	54	74	3109	0.20	1.602	0.064	0.1496	0.0050	0.83	0.0777	0.0017	971	39	899	30	1138	44	79
040916/5	045-115	A_137	405	66	36	2755	0.09	1.693	0.068	0.1631	0.0055	0.84	0.0753	0.0017	1006	40	974	33	1077	44	90

Appendix D - LA-ICP-MS U-Pb geochronological data for zircons of sample 040916/6

040916/6								RATIOS							AGES [Ma]						Conc.
Sample	**Analysis**	**Analysis**	**U [ppm]^a**	**Pb [ppm]^a**	**Th [ppm]**	**$^{206}Pb/^{204}Pb$**	**Th/U meas**	**$^{207}Pb/^{235}U^b$**	**2 σ^d**	**$^{206}Pb/^{238}U^b$**	**2 σ^d**	**rho^c**	**$^{207}Pb/^{206}Pb^e$**	**2 σ^d**	**$^{207}Pb/^{235}U$**	**2 σ**	**$^{206}Pb/^{238}U$**	**2 σ**	**$^{207}Pb/^{206}Pb$**	**2 σ**	%
040916/6	046-1	A_004	283	50	21	257015	0.07	1.796	0.073	0.1763	0.0060	0.83	0.0739	0.0017	1044	42	1047	35	1038	45	101
040916/6	046-2	A_005	334	58	32	33204	0.09	1.765	0.081	0.1730	0.0060	0.75	0.0740	0.0022	1033	47	1029	35	1041	61	99
040916/6	046-4	A_007	142	24	48	1638	0.34	1.716	0.101	0.1659	0.0060	0.61	0.0750	0.0035	1015	60	989	36	1069	94	93
040916/6	046-6	A_009	357	66	304	12834	0.85	1.910	0.087	0.1837	0.0063	0.76	0.0754	0.0022	1085	49	1087	37	1079	60	101
040916/6	046-7	A_010	270	50	164	254678	0.61	1.924	0.079	0.1832	0.0062	0.82	0.0762	0.0018	1089	45	1084	37	1099	47	99
040916/6	046-8	A_011	617	101	69	14625	0.11	1.657	0.066	0.1632	0.0055	0.84	0.0736	0.0016	992	40	975	33	1031	43	95
040916/6	046-10	A_013	162	23	66	6443	0.41	1.389	0.059	0.1404	0.0048	0.81	0.0718	0.0018	884	37	847	29	979	51	87
040916/6	046-11	A_014	468	83	86	424261	0.18	1.812	0.073	0.1764	0.0060	0.84	0.0745	0.0016	1050	42	1047	36	1054	44	99
040916/6	046-12	A_015	49	9	18	47048	0.37	1.960	0.099	0.1867	0.0065	0.69	0.0761	0.0028	1102	56	1103	39	1098	73	100
040916/6	046-14	A_017	420	71	107	365780	0.25	1.711	0.071	0.1699	0.0058	0.82	0.0731	0.0017	1013	42	1011	34	1016	48	100
040916/6	046-15	A_018	497	85	280	2633	0.56	1.806	0.076	0.1720	0.0059	0.81	0.0762	0.0019	1048	44	1023	35	1099	49	93
040916/6	046-16	A_021	301	52	82	9953	0.27	1.771	0.079	0.1717	0.0059	0.77	0.0748	0.0021	1035	46	1022	35	1063	58	96
040916/6	046-17	A_022	502	82	79	2406	0.16	1.786	0.088	0.1643	0.0057	0.71	0.0789	0.0028	1041	51	980	34	1169	69	84
040916/6	046-19	A_024	399	68	62	46660	0.16	1.720	0.070	0.1697	0.0058	0.84	0.0735	0.0016	1016	41	1011	34	1028	45	98
040916/6	046-21	A_026	1294	199	62	347	0.05	2.377	0.095	0.1542	0.0052	0.85	0.1118	0.0024	1236	49	925	31	1828	38	51
040916/6	046-22	A_027	230	26	39	1120	0.17	1.202	0.080	0.1117	0.0042	0.56	0.0781	0.0043	802	53	682	25	1149	109	59
040916/6	046-23	A_028	331	45	80	27350	0.24	1.263	0.052	0.1368	0.0047	0.83	0.0670	0.0015	829	34	827	28	837	48	99
040916/6	046-24	A_029	478	52	70	6605	0.15	0.914	0.039	0.1079	0.0037	0.81	0.0615	0.0015	659	28	661	23	655	53	101
040916/6	046-25	A_030	813	145	241	4402	0.30	1.877	0.078	0.1789	0.0061	0.82	0.0761	0.0018	1073	44	1061	36	1097	47	97
040916/6	046-26	A_031	161	54	101	19805	0.62	5.323	0.215	0.3356	0.0114	0.84	0.1150	0.0025	1873	76	1866	64	1880	39	99
040916/6	046-27	A_032	221	37	44	4790	0.20	1.706	0.073	0.1690	0.0058	0.80	0.0732	0.0019	1011	43	1007	34	1020	51	99
040916/6	046-28	A_033	216	41	77	3287	0.36	1.982	0.084	0.1874	0.0064	0.81	0.0767	0.0019	1109	47	1107	38	1114	50	99
040916/6	046-30	A_035	723	102	175	6741	0.24	1.472	0.066	0.1408	0.0049	0.77	0.0758	0.0021	919	41	849	29	1090	57	78
040916/6	046-31	A_038	471	74	78	4027	0.17	1.617	0.066	0.1576	0.0054	0.84	0.0745	0.0016	977	40	943	32	1054	44	90
040916/6	046-32	A_039	144	27	63	3037	0.44	1.938	0.082	0.1850	0.0063	0.81	0.0760	0.0019	1094	46	1094	37	1095	50	100
040916/6	046-33	A_040	1319	195	249	5070	0.19	1.560	0.067	0.1482	0.0051	0.80	0.0764	0.0020	955	41	891	31	1105	51	81
040916/6	046-34	A_041	242	43	48	15890	0.20	1.826	0.076	0.1770	0.0061	0.82	0.0748	0.0018	1055	44	1051	36	1064	47	99
040916/6	046-35	A_042	287	50	58	60091	0.20	1.781	0.074	0.1744	0.0060	0.82	0.0740	0.0018	1038	43	1037	35	1042	48	99
040916/6	046-36	A_043	394	67	188	340604	0.48	1.724	0.073	0.1694	0.0058	0.81	0.0738	0.0018	1017	43	1009	35	1036	50	97
040916/6	046-37	A_044	549	52	622	266652	1.13	0.778	0.034	0.0952	0.0033	0.78	0.0593	0.0016	584	26	586	20	578	59	101
040916/6	046-38	A_045	408	61	34	4094	0.08	1.541	0.069	0.1504	0.0052	0.78	0.0743	0.0021	947	42	903	31	1050	56	86
040916/6	046-39	A_046	361	59	82	2836	0.23	1.704	0.070	0.1619	0.0055	0.84	0.0763	0.0017	1010	41	968	33	1103	45	88
040916/6	046-40	A_047	451	84	114	426602	0.25	1.950	0.081	0.1855	0.0064	0.82	0.0762	0.0018	1098	46	1097	38	1101	48	100
040916/6	046-41	A_048	1315	222	313	10647	0.24	1.745	0.075	0.1689	0.0058	0.80	0.0749	0.0020	1025	44	1006	35	1067	53	94
040916/6	046-42	A_049	982	87	216	771	0.22	0.933	0.045	0.0886	0.0031	0.73	0.0764	0.0025	669	32	547	19	1105	65	50
040916/6	046-43	A_050	834	123	745	369	0.89	2.305	0.101	0.1475	0.0051	0.79	0.1133	0.0030	1214	53	887	31	1853	48	48
040916/6	046-44	A_051	450	80	21	16039	0.05	1.841	0.075	0.1784	0.0061	0.84	0.0748	0.0017	1060	43	1058	36	1064	45	99
040916/6	046-46	A_055	331	58	60	12683	0.18	1.818	0.075	0.1758	0.0060	0.83	0.0750	0.0017	1052	43	1044	36	1069	46	98
040916/6	046-47	A_056	533	82	125	3069	0.23	1.560	0.068	0.1530	0.0053	0.79	0.0739	0.0020	954	42	918	32	1040	55	88
040916/6	046-48	A_057	509	86	137	385	0.27	2.615	0.107	0.1700	0.0058	0.84	0.1116	0.0025	1305	53	1012	35	1825	40	55
040916/6	046-49	A_058	554	114	67	10197	0.12	2.351	0.103	0.2065	0.0071	0.79	0.0826	0.0022	1228	54	1210	42	1259	53	96
040916/6	046-50	A_059	400	71	35	79997	0.09	1.847	0.080	0.1778	0.0061	0.80	0.0754	0.0020	1062	46	1055	36	1078	52	98
040916/6	046-51	A_060	965	134	141	3217	0.15	1.503	0.064	0.1391	0.0048	0.81	0.0784	0.0020	932	40	840	29	1156	50	73
040916/6	046-53	A_062	472	83	22	14155	0.05	1.795	0.073	0.1762	0.0060	0.84	0.0739	0.0016	1044	42	1046	36	1039	44	101
040916/6	046-54	A_063	418	77	147	3113	0.35	1.980	0.087	0.1848	0.0064	0.79	0.0777	0.0021	1109	49	1093	38	1139	53	96
040916/6	046-55	A_064	411	72	105	8725	0.26	1.825	0.075	0.1763	0.0060	0.84	0.0751	0.0017	1054	43	1047	36	1071	45	98
040916/6	046-56	A_065	579	90	206	2770	0.36	1.633	0.077	0.1561	0.0055	0.74	0.0759	0.0024	983	46	935	33	1092	63	86
040916/6	046-59	A_068	722	63	31	4452	0.04	0.714	0.037	0.0876	0.0031	0.69	0.0592	0.0022	547	28	541	19	574	81	94
040916/6	046-60	A_069	773	117	77	1637	0.10	1.587	0.071	0.1513	0.0053	0.78	0.0761	0.0021	965	43	908	32	1097	56	83
040916/6	046-61	A_077	736	127	220	11443	0.30	1.770	0.072	0.1731	0.0059	0.84	0.0741	0.0016	1034	42	1029	35	1045	44	99
040916/6	046-62	A_078	510	72	35	69374	0.07	1.383	0.057	0.1419	0.0049	0.83	0.0707	0.0016	882	36	855	29	949	47	90
040916/6	046-63	A_079	338	58	141	8959	0.42	1.752	0.073	0.1707	0.0059	0.83	0.0744	0.0017	1028	43	1016	35	1053	47	96
040916/6	046-64	A_080	101	9	24	46387	0.24	0.730	0.060	0.0905	0.0035	0.47	0.0585	0.0043	556	46	558	22	549	160	102
040916/6	046-65	A_081	1217	173	439	358	0.36	2.194	0.089	0.1421	0.0049	0.85	0.1120	0.0024	1179	48	856	29	1832	39	47
040916/6	046-66	A_082	175	15	119	260	0.68	0.919	0.075	0.0859	0.0034	0.49	0.0776	0.0055	662	54	531	21	1138	141	47
040916/6	046-67	A_083	1069	168	288	1680	0.27	1.698	0.072	0.1572	0.0054	0.82	0.0783	0.0019	1008	43	941	33	1155	48	81
040916/6	046-70	A_086	443	78	54	9777	0.12	1.834	0.077	0.1767	0.0061	0.82	0.0753	0.0018	1058	45	1049	36	1077	49	97
040916/6	046-71	A_089	432	79	89	4914	0.21	1.917	0.086	0.1830	0.0064	0.78	0.0760	0.0021	1087	49	1083	38	1095	56	99
040916/6	046-72	A_090	585	65	156	2431	0.27	0.957	0.049	0.1118	0.0040	0.70	0.0621	0.0023	682	35	683	24	676	78	101
040916/6	046-73	A_091	1037	101	10	508524	0.01	0.799	0.036	0.0972	0.0034	0.77	0.0596	0.0017	596	27	598	21	589	63	101
040916/6	046-74	A_092	209	39	71	1754	0.34	1.938	0.084	0.1845	0.0064	0.80	0.0762	0.0020	1094	47	1092	38	1100	51	99

040916/6								**RATIOS**							**AGES [Ma]**						**Conc.**
040916/6	046-75	A_093	1217	176	929	404	0.76	2.215	0.090	0.1445	0.0050	0.85	0.1111	0.0024	1186	48	870	30	1818	39	48
040916/6	046-76	A_094	319	56	51	9897	0.16	1.786	0.074	0.1744	0.0060	0.83	0.0743	0.0017	1041	43	1036	36	1049	47	99
040916/6	046-77	A_095	653	57	136	287742	0.21	0.707	0.034	0.0874	0.0031	0.73	0.0587	0.0019	543	26	540	19	554	71	97
040916/6	046-78	A_096	434	226	238	13717	0.55	13.347	0.546	0.5201	0.0180	0.85	0.1861	0.0041	2705	111	2699	93	2708	36	100
040916/6	046-79	A_097	465	82	132	5727	0.28	1.840	0.084	0.1761	0.0062	0.76	0.0758	0.0022	1060	49	1046	37	1090	59	96
040916/6	046-81	A_099	1032	89	169	1052	0.16	0.884	0.038	0.0866	0.0030	0.80	0.0741	0.0019	643	28	535	19	1043	52	51
040916/6	046-82	A_100	400	71	24	16967	0.06	1.793	0.074	0.1765	0.0061	0.83	0.0737	0.0017	1043	43	1048	36	1033	46	101
040916/6	046-83	A_101	601	87	44	3630	0.07	1.535	0.063	0.1453	0.0050	0.84	0.0767	0.0017	945	39	875	30	1112	45	79
040916/6	046-84	A_102	318	55	32	2718	0.10	1.768	0.083	0.1739	0.0061	0.75	0.0737	0.0023	1034	48	1034	36	1034	62	100
040916/6	046-85	A_103	159	28	80	1917	0.50	1.849	0.100	0.1755	0.0063	0.66	0.0764	0.0031	1063	58	1042	38	1105	81	94
040916/6	046-86	A_106	380	64	148	9212	0.39	1.796	0.092	0.1677	0.0060	0.70	0.0777	0.0028	1044	53	999	36	1139	73	88
040916/6	046-87	A_107	154	30	23	2939	0.15	2.054	0.113	0.1965	0.0071	0.66	0.0758	0.0031	1134	62	1156	42	1091	82	106
040916/6	046-89	A_109	417	74	22	374501	0.05	1.854	0.078	0.1785	0.0062	0.83	0.0754	0.0018	1065	45	1059	37	1078	47	98
040916/6	046-90	A_110	327	59	39	294476	0.12	1.849	0.079	0.1789	0.0062	0.81	0.0750	0.0019	1063	46	1061	37	1067	50	99
040916/6	046-92	A_112	716	57	296	970	0.41	0.824	0.038	0.0797	0.0028	0.77	0.0750	0.0022	610	28	494	17	1069	58	46
040916/6	046-93	A_113	165	30	69	2021	0.42	1.876	0.085	0.1800	0.0063	0.77	0.0756	0.0022	1073	49	1067	37	1084	58	98
040916/6	046-94	A_114	680	103	56	6228	0.08	1.574	0.068	0.1522	0.0053	0.81	0.0750	0.0019	960	41	913	32	1069	50	85
040916/6	046-95	A_115	278	52	72	263014	0.26	2.001	0.087	0.1888	0.0066	0.80	0.0769	0.0020	1116	49	1115	39	1119	52	100
040916/6	046-96	A_116	509	52	77	6482	0.15	0.857	0.036	0.1021	0.0035	0.82	0.0609	0.0015	628	27	626	22	635	53	99
040916/6	046-97	A_117	199	35	37	12116	0.19	1.789	0.080	0.1735	0.0061	0.79	0.0748	0.0021	1041	46	1032	36	1062	55	97
040916/6	046-98	A_118	264	48	145	4494	0.55	1.916	0.107	0.1832	0.0067	0.65	0.0758	0.0032	1087	61	1085	39	1091	85	99
040916/6	046-100	A_120	393	70	41	1454	0.10	1.949	0.111	0.1791	0.0066	0.64	0.0789	0.0035	1098	63	1062	39	1170	87	91
040916/6	046-101	A_123	257	38	126	3315	0.49	1.567	0.068	0.1493	0.0052	0.80	0.0761	0.0020	957	42	897	31	1098	52	82
040916/6	046-106	A_128	267	46	20	230140	0.07	1.756	0.075	0.1720	0.0060	0.82	0.0741	0.0018	1030	44	1023	36	1043	50	98
040916/6	046-107	A_129	216	30	82	1792	0.38	1.452	0.080	0.1391	0.0051	0.66	0.0757	0.0031	911	50	840	31	1088	83	77
040916/6	046-108	A_130	103	19	31	94209	0.30	1.897	0.088	0.1819	0.0064	0.76	0.0756	0.0023	1080	50	1077	38	1086	60	99
040916/6	046-109	A_131	256	33	75	538	0.29	1.388	0.099	0.1270	0.0049	0.54	0.0793	0.0048	884	63	770	30	1180	119	65
040916/6	046-110	A_132	556	87	90	1265	0.16	1.692	0.090	0.1572	0.0057	0.68	0.0780	0.0030	1005	53	941	34	1148	77	82
040916/6	046-111	A_133	456	69	74	3729	0.16	1.563	0.066	0.1523	0.0053	0.83	0.0744	0.0017	956	40	914	32	1053	47	87
040916/6	046-112	A_134	319	51	17	2340	0.05	1.661	0.086	0.1584	0.0057	0.70	0.0760	0.0028	994	51	948	34	1096	74	86
040916/6	046-113	A_135	635	69	211	350	0.33	1.666	0.072	0.1082	0.0038	0.81	0.1117	0.0028	996	43	662	23	1827	45	36
040916/6	046-114	A_136	379	49	99	322	0.26	1.979	0.083	0.1299	0.0045	0.83	0.1105	0.0026	1108	47	787	28	1808	43	44
040916/6	046-115	A_137	386	57	28	282568	0.07	1.533	0.070	0.1464	0.0052	0.77	0.0760	0.0022	944	43	881	31	1094	58	81

Appendix E - LA-ICP-MS U-Pb geochronological data for zircons of sample 050916/1

050916/1								RATIOS							AGES [Ma]						Conc.
Sample	Analysis	Analysis	U [ppm][a]	Pb [ppm][a]	Th [ppm]	^{206}Pb/^{204}Pb	Th/U meas	^{207}Pb/^{235}U[b]	2 σ[d]	^{206}Pb/^{238}U[b]	2 σ[d]	rho[c]	^{207}Pb/^{206}Pb[e]	2 σ[d]	^{207}Pb/^{235}U	2 σ	^{206}Pb/^{238}U	2 σ	^{207}Pb/^{206}Pb	2 σ	%
050916/1	051-1	A_140	612	57	318	281528	0.52	0.752	0.032	0.0924	0.0032	0.82	0.0591	0.0014	570	24	570	20	569	52	100
050916/1	051-2	A_141	282	50	49	247385	0.17	1.803	0.080	0.1764	0.0062	0.79	0.0741	0.0020	1047	47	1047	37	1045	55	100
050916/1	051-3	A_142	278	49	118	3970	0.42	1.826	0.076	0.1775	0.0062	0.84	0.0746	0.0017	1055	44	1053	37	1059	45	99
050916/1	051-4	A_143	209	21	69	1381	0.33	0.814	0.036	0.0981	0.0034	0.80	0.0602	0.0016	605	27	603	21	609	57	99
050916/1	051-5	A_144	85	8	56	3126	0.67	0.830	0.040	0.0997	0.0035	0.73	0.0604	0.0020	614	30	613	22	617	72	99
050916/1	051-6	A_145	374	66	207	18362	0.55	1.830	0.076	0.1762	0.0062	0.84	0.0753	0.0017	1056	44	1046	37	1077	45	97
050916/1	051-7	A_146	427	75	215	16475	0.50	1.807	0.074	0.1761	0.0061	0.85	0.0744	0.0016	1048	43	1046	36	1053	44	99
050916/1	051-8	A_147	863	133	309	3370	0.36	1.598	0.071	0.1537	0.0054	0.79	0.0754	0.0021	969	43	922	33	1079	55	85
050916/1	051-10	A_149	685	71	206	351052	0.30	0.863	0.036	0.1030	0.0036	0.84	0.0608	0.0014	632	26	632	22	632	48	100
050916/1	051-12	A_151	224	39	43	191721	0.19	1.735	0.073	0.1721	0.0060	0.83	0.0731	0.0017	1022	43	1024	36	1018	47	101
050916/1	051-13	A_152	280	48	102	9945	0.36	1.743	0.073	0.1706	0.0060	0.84	0.0741	0.0017	1025	43	1015	35	1045	46	97
050916/1	051-14	A_153	274	48	101	28238	0.37	1.820	0.076	0.1759	0.0061	0.84	0.0751	0.0017	1053	44	1044	36	1070	46	98
050916/1	051-16	A_157	177	32	81	156598	0.46	1.848	0.079	0.1782	0.0062	0.82	0.0752	0.0018	1063	45	1057	37	1075	49	98
050916/1	051-17	A_158	198	20	108	943	0.54	1.006	0.046	0.1017	0.0036	0.77	0.0717	0.0021	707	32	624	22	978	59	64
050916/1	051-18	A_159	280	28	87	57892	0.31	0.841	0.036	0.1010	0.0035	0.82	0.0604	0.0015	620	27	620	22	619	54	100
050916/1	051-20	A_161	510	46	220	4354	0.43	0.725	0.031	0.0896	0.0031	0.82	0.0587	0.0014	554	24	553	19	556	53	99
050916/1	051-21	A_162	54	9	18	1052	0.33	1.728	0.083	0.1705	0.0061	0.74	0.0735	0.0024	1019	49	1015	36	1028	65	99
050916/1	051-22	A_163	1275	125	29	14216	0.02	0.833	0.035	0.0977	0.0034	0.82	0.0618	0.0015	615	26	601	21	668	52	90
050916/1	051-23	A_164	222	22	51	109275	0.23	0.823	0.036	0.0990	0.0035	0.80	0.0603	0.0016	610	27	608	21	614	57	99
050916/1	051-24	A_165	185	17	2	8169	0.01	0.761	0.034	0.0930	0.0033	0.78	0.0594	0.0017	575	26	573	20	580	61	99
050916/1	051-27	A_168	976	92	77	1795	0.08	0.785	0.046	0.0946	0.0035	0.62	0.0602	0.0028	589	35	583	21	610	100	95
050916/1	051-31	A_174	375	37	49	183441	0.13	0.823	0.038	0.0985	0.0035	0.76	0.0606	0.0018	609	28	605	21	624	65	97
050916/1	051-32	A_175	366	38	151	4361	0.41	0.864	0.037	0.1031	0.0036	0.83	0.0608	0.0015	632	27	633	22	630	52	100
050916/1	051-33	A_176	270	51	77	252640	0.28	1.995	0.083	0.1887	0.0066	0.84	0.0767	0.0017	1114	46	1114	39	1113	45	100
050916/1	051-34	A_177	279	49	152	241466	0.55	1.776	0.074	0.1748	0.0061	0.84	0.0737	0.0017	1037	43	1038	36	1033	46	101
050916/1	051-35	A_178	136	14	54	1424	0.40	0.854	0.042	0.1016	0.0036	0.72	0.0609	0.0021	627	31	624	22	636	73	98
050916/1	051-36	A_179	91	18	34	746	0.38	2.078	0.146	0.1944	0.0075	0.55	0.0775	0.0045	1142	80	1145	44	1135	116	101
050916/1	051-37	A_180	429	75	24	9492	0.05	1.755	0.073	0.1736	0.0061	0.85	0.0733	0.0016	1029	43	1032	36	1022	45	101
050916/1	051-39	A_182	65	11	23	3397	0.35	1.710	0.086	0.1694	0.0061	0.72	0.0732	0.0026	1012	51	1009	36	1019	71	99
050916/1	051-40	A_183	183	23	51	3858	0.28	1.090	0.082	0.1231	0.0048	0.52	0.0642	0.0041	749	56	749	29	748	136	100
050916/1	051-42	A_185	351	35	64	1258	0.18	0.930	0.040	0.0987	0.0035	0.82	0.0683	0.0017	667	29	607	21	879	51	69
050916/1	051-43	A_186	147	13	4	66825	0.03	0.740	0.049	0.0915	0.0034	0.57	0.0587	0.0032	562	37	564	21	554	118	102
050916/1	051-44	A_187	1618	186	130	1072	0.08	1.164	0.049	0.1152	0.0040	0.84	0.0733	0.0017	784	33	703	25	1021	46	69
050916/1	051-46	A_191	1926	157	174	970	0.09	0.825	0.037	0.0815	0.0029	0.78	0.0734	0.0021	611	28	505	18	1026	57	49
050916/1	051-48	A_193	283	55	33	4957	0.12	2.055	0.092	0.1931	0.0068	0.79	0.0772	0.0021	1134	51	1138	40	1126	54	101
050916/1	051-49	A_194	955	93	279	1601	0.29	0.937	0.039	0.0973	0.0034	0.85	0.0698	0.0015	671	28	599	21	923	45	65
050916/1	051-52	A_197	147	14	145	67920	0.99	0.767	0.040	0.0934	0.0034	0.69	0.0596	0.0022	578	30	575	21	588	81	98
050916/1	051-53	A_198	313	56	133	6803	0.42	1.879	0.079	0.1800	0.0063	0.84	0.0757	0.0017	1074	45	1067	37	1087	46	98
050916/1	051-54	A_199	177	19	43	91826	0.24	0.884	0.067	0.1050	0.0041	0.51	0.0611	0.0040	643	49	643	25	642	141	100
050916/1	051-56	A_201	1116	196	56	160676	0.05	1.786	0.073	0.1753	0.0061	0.85	0.0739	0.0016	1040	43	1041	36	1039	43	100
050916/1	051-57	A_202	1616	194	485	972	0.30	1.224	0.051	0.1200	0.0042	0.85	0.0740	0.0016	811	34	731	26	1040	44	70
050916/1	051-58	A_203	320	48	146	1484	0.46	1.562	0.080	0.1502	0.0054	0.70	0.0755	0.0027	955	49	902	33	1081	73	83
050916/1	051-59	A_204	349	57	36	7436	0.10	1.673	0.085	0.1634	0.0059	0.71	0.0742	0.0027	998	51	976	35	1047	73	93
050916/1	051-61	A_213	222	24	76	984	0.34	1.110	0.059	0.1087	0.0040	0.68	0.0741	0.0029	758	41	665	24	1043	79	64
050916/1	051-63	A_215	405	43	256	683	0.63	1.085	0.062	0.1067	0.0039	0.64	0.0738	0.0033	746	43	654	24	1035	89	63
050916/1	051-64	A_216	194	21	136	1036	0.70	1.113	0.050	0.1093	0.0039	0.79	0.0739	0.0021	760	34	669	24	1038	56	64
050916/1	051-66	A_218	162	17	75	81724	0.46	0.857	0.039	0.1024	0.0036	0.78	0.0607	0.0017	629	28	629	22	629	60	100
050916/1	051-67	A_219	72	13	31	2063	0.43	1.810	0.083	0.1751	0.0062	0.77	0.0750	0.0022	1049	48	1040	37	1069	58	97
050916/1	051-71	A_225	168	31	102	10396	0.61	1.915	0.084	0.1823	0.0065	0.81	0.0762	0.0020	1086	48	1080	38	1100	52	98
050916/1	051-72	A_226	273	28	75	7666	0.27	0.864	0.038	0.1034	0.0037	0.81	0.0606	0.0015	632	28	634	22	625	55	102
050916/1	051-75	A_229	165	30	37	2206	0.22	1.866	0.109	0.1797	0.0067	0.64	0.0753	0.0034	1069	62	1065	40	1077	90	99
050916/1	051-76	A_230	79	12	27	1416	0.34	1.539	0.071	0.1523	0.0054	0.78	0.0733	0.0021	946	43	914	33	1022	59	89
050916/1	051-77	A_231	24	4	11	313	0.44	1.924	0.270	0.1826	0.0096	0.38	0.0764	0.0099	1089	153	1081	57	1106	260	98
050916/1	051-78	A_232	380	37	274	12105	0.72	0.823	0.035	0.0987	0.0035	0.82	0.0605	0.0015	610	26	607	21	620	54	98
050916/1	051-80	A_234	519	54	65	1730	0.12	1.001	0.043	0.1035	0.0037	0.83	0.0701	0.0017	704	30	635	22	932	49	68
050916/1	051-81	A_235	826	77	93	195359	0.11	0.760	0.040	0.0930	0.0034	0.69	0.0593	0.0022	574	30	573	21	578	81	99
050916/1	051-82	A_236	54	6	21	428	0.39	0.873	0.054	0.1032	0.0038	0.60	0.0613	0.0030	637	39	633	24	650	106	97
050916/1	051-85	A_239	416	72	126	22979	0.30	1.825	0.083	0.1719	0.0061	0.78	0.0770	0.0022	1054	48	1023	36	1121	56	91
050916/1	051-86	A_242	450	45	10	3535	0.02	0.843	0.046	0.1003	0.0036	0.67	0.0610	0.0025	621	34	616	22	638	87	97
050916/1	051-89	A_245	220	40	118	6373	0.54	1.878	0.084	0.1813	0.0064	0.79	0.0752	0.0020	1073	48	1074	38	1073	55	100
050916/1	051-90	A_246	405	41	63	202850	0.16	0.861	0.050	0.1017	0.0037	0.63	0.0614	0.0028	631	37	624	23	653	97	96

050916/1								RATIOS							AGES [Ma]						Conc.
Sample	Analysis	Analysis	U [ppm][a]	Pb [ppm][a]	Th [ppm]	^{206}Pb/^{204}Pb	Th/U meas	^{207}Pb/^{235}U[b]	2 σ[d]	^{206}Pb/^{238}U[b]	2 σ[d]	rho[c]	^{207}Pb/^{206}Pb[e]	2 σ[d]	^{207}Pb/^{235}U	2 σ	^{206}Pb/^{238}U	2 σ	^{207}Pb/^{206}Pb	2 σ	%
050916/1	051-92	A_248	947	147	215	12088	0.23	1.579	0.066	0.1557	0.0055	0.85	0.0735	0.0016	962	40	933	33	1029	45	91
050916/1	051-93	A_249	571	61	55	3257	0.10	0.892	0.046	0.1060	0.0038	0.70	0.0610	0.0023	647	34	649	24	641	80	101
050916/1	051-96	A_252	537	55	186	7177	0.35	0.847	0.038	0.1019	0.0036	0.79	0.0603	0.0016	623	28	625	22	615	59	102
050916/1	051-97	A_253	516	51	77	10055	0.15	0.831	0.035	0.0990	0.0035	0.83	0.0609	0.0015	614	26	609	22	634	52	96
050916/1	051-98	A_254	225	20	156	98725	0.69	0.730	0.033	0.0891	0.0032	0.79	0.0594	0.0016	557	25	550	20	583	60	94
050916/1	051-99	A_255	437	75	181	11648	0.42	1.752	0.074	0.1729	0.0061	0.84	0.0735	0.0017	1028	43	1028	36	1027	47	100
050916/1	051-100	A_256	692	127	264	6206	0.38	1.915	0.081	0.1839	0.0065	0.84	0.0755	0.0017	1086	46	1088	38	1082	46	101
050916/1	051-101	A_259	284	51	121	13381	0.42	1.869	0.080	0.1798	0.0064	0.82	0.0754	0.0018	1070	46	1066	38	1079	49	99
050916/1	051-103	A_261	122	23	59	115032	0.48	2.053	0.102	0.1915	0.0069	0.73	0.0777	0.0026	1133	56	1130	41	1140	68	99
050916/1	051-104	A_262	426	41	98	203415	0.23	0.801	0.035	0.0971	0.0034	0.81	0.0599	0.0015	598	26	598	21	598	55	100
050916/1	051-105	A_263	352	43	143	209636	0.41	1.096	0.047	0.1213	0.0043	0.82	0.0656	0.0016	751	32	738	26	792	51	93
050916/1	051-106	A_264	266	27	91	8234	0.34	0.856	0.038	0.1023	0.0036	0.81	0.0607	0.0016	628	28	628	22	628	56	100
050916/1	051-107	A_265	99	10	37	1005	0.37	0.887	0.055	0.1056	0.0039	0.60	0.0609	0.0031	645	40	647	24	637	108	102
050916/1	051-108	A_266	262	44	59	1050	0.22	1.825	0.107	0.1683	0.0063	0.64	0.0786	0.0036	1055	62	1003	38	1163	90	86
050916/1	051-109	A_267	501	57	174	1145	0.35	1.157	0.052	0.1138	0.0041	0.80	0.0737	0.0020	780	35	695	25	1034	55	67
050916/1	051-110	A_268	207	38	69	6506	0.33	1.993	0.094	0.1852	0.0067	0.76	0.0781	0.0024	1113	53	1095	39	1149	61	95
050916/1	051-111	A_269	248	42	110	2378	0.44	1.732	0.077	0.1707	0.0061	0.80	0.0736	0.0019	1020	45	1016	36	1030	53	99
050916/1	051-112	A_270	392	70	88	4187	0.22	1.836	0.079	0.1787	0.0063	0.83	0.0745	0.0018	1058	45	1060	38	1055	48	101
050916/1	051-113	A_271	453	74	149	1688	0.33	1.742	0.085	0.1639	0.0059	0.74	0.0771	0.0025	1024	50	978	35	1123	65	87

Appendix F - LA-ICP-MS U-Pb geochronological data for zircons of sample 050916/2B

050916/2B								RATIOS							AGES [Ma]						Conc.
Sample	Analysis	Analysis	U [ppm]^{a}	Pb [ppm]^{a}	Th [ppm]	^{206}Pb/^{204}Pb	Th/U meas	^{207}Pb/^{235}U^{b}	2 σ^{d}	^{206}Pb/^{238}U^{b}	2 σ^{d}	rho^{c}	^{207}Pb/^{206}Pb^{e}	2 σ^{d}	^{207}Pb/^{235}U	2 σ	^{206}Pb/^{238}U	2 σ	^{207}Pb/^{206}Pb	2 σ	%
050916/2B	052-1	A_276	741	76	32	366578	0.04	0.873	0.036	0.1019	0.0036	0.85	0.0621	0.0014	637	27	626	22	678	47	92
050916/2B	052-2	A_277	474	88	175	5671	0.37	1.949	0.084	0.1855	0.0066	0.82	0.0762	0.0019	1098	47	1097	39	1101	49	100
050916/2B	052-3	A_278	260	26	138	5311	0.53	0.849	0.039	0.1002	0.0036	0.78	0.0615	0.0018	624	29	616	22	655	62	94
050916/2B	052-4	A_279	237	23	106	4100	0.45	0.819	0.036	0.0987	0.0035	0.81	0.0602	0.0015	607	27	607	22	609	55	100
050916/2B	052-5	A_280	234	42	134	202611	0.57	1.838	0.078	0.1784	0.0063	0.84	0.0747	0.0017	1059	45	1058	37	1061	47	100
050916/2B	052-6	A_281	329	59	205	6997	0.62	1.839	0.077	0.1795	0.0063	0.85	0.0743	0.0017	1059	44	1064	38	1050	45	101
050916/2B	052-7	A_282	55	6	77	562	1.40	0.848	0.088	0.1008	0.0044	0.42	0.0610	0.0058	623	65	619	27	640	204	97
050916/2B	052-8	A_283	114	19	43	6073	0.38	1.678	0.074	0.1639	0.0058	0.81	0.0742	0.0019	1000	44	979	35	1048	52	93
050916/2B	052-9	A_284	560	58	98	17977	0.17	0.868	0.038	0.1031	0.0037	0.82	0.0610	0.0015	634	28	633	22	640	54	99
050916/2B	052-10	A_285	174	33	57	8419	0.33	2.004	0.097	0.1882	0.0068	0.74	0.0773	0.0025	1117	54	1112	40	1128	64	99
050916/2B	052-11	A_286	644	112	134	29402	0.21	1.790	0.074	0.1743	0.0062	0.85	0.0745	0.0016	1042	43	1036	37	1055	43	98
050916/2B	052-12	A_287	313	30	33	4623	0.10	0.797	0.034	0.0962	0.0034	0.82	0.0601	0.0015	595	26	592	21	606	53	98
050916/2B	052-13	A_288	848	85	191	3227	0.23	0.863	0.043	0.1003	0.0036	0.73	0.0624	0.0021	632	31	616	22	689	73	89
050916/2B	052-14	A_289	355	30	486	986	1.37	0.868	0.039	0.0845	0.0030	0.79	0.0746	0.0021	635	29	523	19	1056	56	49
050916/2B	052-15	A_290	1016	89	85	2598	0.08	0.754	0.035	0.0873	0.0031	0.78	0.0627	0.0018	571	26	539	19	698	62	77
050916/2B	052-16	A_293	207	21	91	1212	0.44	0.860	0.049	0.1016	0.0037	0.64	0.0614	0.0027	630	36	624	23	653	94	96
050916/2B	052-17	A_294	376	64	89	5944	0.24	1.721	0.072	0.1702	0.0060	0.85	0.0734	0.0016	1016	43	1013	36	1024	45	99
050916/2B	052-18	A_295	1003	102	171	616	0.17	1.084	0.051	0.1017	0.0037	0.76	0.0773	0.0024	746	35	624	22	1130	61	55
050916/2B	052-19	A_296	376	35	176	5009	0.47	0.772	0.045	0.0939	0.0035	0.63	0.0596	0.0027	581	34	579	21	589	99	98
050916/2B	052-20	A_297	238	22	19	7963	0.08	0.754	0.034	0.0926	0.0033	0.79	0.0591	0.0016	570	26	571	20	569	60	100
050916/2B	052-21	A_298	697	70	38	4246	0.05	0.837	0.035	0.1000	0.0035	0.84	0.0607	0.0014	618	26	614	22	630	49	98
050916/2B	052-22	A_299	808	136	337	6974	0.42	1.727	0.076	0.1685	0.0060	0.81	0.0743	0.0019	1019	45	1004	36	1050	52	96
050916/2B	052-23	A_300	652	112	43	50450	0.07	1.739	0.072	0.1717	0.0061	0.85	0.0735	0.0016	1023	42	1021	36	1027	43	99
050916/2B	052-24	A_301	1059	109	124	6483	0.12	0.861	0.036	0.1026	0.0036	0.85	0.0608	0.0013	630	26	630	22	633	47	99
050916/2B	052-25	A_302	615	105	30	128837	0.05	1.724	0.072	0.1709	0.0061	0.85	0.0731	0.0016	1017	42	1017	36	1018	44	100
050916/2B	052-26	A_303	683	68	170	331444	0.25	0.835	0.035	0.1001	0.0035	0.84	0.0605	0.0014	616	26	615	22	620	49	99
050916/2B	052-27	A_304	49	8	8	1170	0.16	1.750	0.084	0.1722	0.0062	0.75	0.0737	0.0023	1027	49	1024	37	1034	64	99
050916/2B	052-28	A_305	83	14	27	4788	0.33	1.745	0.079	0.1722	0.0062	0.79	0.0735	0.0021	1025	47	1024	37	1027	57	100
050916/2B	052-29	A_306	39	4	24	1051	0.62	0.881	0.060	0.1036	0.0039	0.55	0.0617	0.0035	642	44	635	24	663	122	96
050916/2B	052-30	A_307	779	80	21	7940	0.03	0.864	0.036	0.1027	0.0036	0.85	0.0610	0.0013	632	26	630	22	640	47	98
050916/2B	052-31	A_310	657	73	9	351230	0.01	0.949	0.040	0.1105	0.0039	0.85	0.0623	0.0014	678	28	675	24	685	47	99
050916/2B	052-32	A_311	172	30	87	145765	0.51	1.775	0.077	0.1748	0.0062	0.82	0.0737	0.0018	1036	45	1038	37	1032	50	101
050916/2B	052-33	A_312	276	46	20	7276	0.07	1.642	0.073	0.1651	0.0059	0.81	0.0721	0.0019	986	44	985	35	989	53	100
050916/2B	052-34	A_313	644	114	166	7924	0.26	1.814	0.075	0.1771	0.0063	0.85	0.0743	0.0016	1051	44	1051	37	1049	43	100
050916/2B	052-35	A_314	295	29	220	106500	0.74	0.824	0.036	0.0994	0.0035	0.82	0.0601	0.0015	610	27	611	22	607	55	101
050916/2B	052-36	A_315	219	33	47	161917	0.21	1.527	0.066	0.1529	0.0054	0.82	0.0725	0.0018	941	41	917	33	999	50	92
050916/2B	052-37	A_316	119	20	30	96590	0.25	1.714	0.077	0.1685	0.0060	0.80	0.0738	0.0020	1014	45	1004	36	1036	54	97
050916/2B	052-39	A_318	162	27	39	2129	0.24	1.668	0.073	0.1673	0.0060	0.81	0.0723	0.0018	997	44	997	36	996	52	100
050916/2B	052-41	A_320	111	18	24	88963	0.21	1.622	0.101	0.1652	0.0062	0.61	0.0712	0.0035	979	61	986	37	963	100	102
050916/2B	052-42	A_321	97	16	35	75826	0.36	1.624	0.076	0.1609	0.0058	0.77	0.0732	0.0022	980	46	962	35	1019	60	94
050916/2B	052-43	A_322	128	23	70	109169	0.55	1.806	0.081	0.1767	0.0063	0.80	0.0741	0.0020	1047	47	1049	38	1044	54	100
050916/2B	052-44	A_323	310	46	76	2149	0.24	1.505	0.065	0.1486	0.0053	0.83	0.0734	0.0018	932	40	893	32	1026	49	87
050916/2B	052-45	A_324	644	73	158	1764	0.25	0.972	0.050	0.1132	0.0041	0.71	0.0623	0.0023	689	35	691	25	684	77	101
050916/2B	052-46	A_327	335	43	162	3026	0.48	1.295	0.055	0.1296	0.0046	0.84	0.0725	0.0017	843	36	786	28	999	47	79
050916/2B	052-47	A_328	182	32	62	14167	0.34	1.824	0.078	0.1775	0.0063	0.83	0.0745	0.0018	1054	45	1053	38	1056	48	100
050916/2B	052-48	A_329	266	27	140	129237	0.53	0.840	0.037	0.1007	0.0036	0.81	0.0605	0.0016	619	27	619	22	621	56	100
050916/2B	052-49	A_330	171	17	93	3522	0.55	0.833	0.044	0.0992	0.0036	0.70	0.0609	0.0023	615	32	610	22	635	81	96
050916/2B	052-50	A_331	665	72	110	14892	0.17	0.924	0.039	0.1088	0.0039	0.84	0.0616	0.0014	665	28	666	24	660	49	101
050916/2B	052-51	A_332	329	62	93	298133	0.28	1.972	0.087	0.1877	0.0067	0.81	0.0762	0.0020	1106	49	1109	40	1101	52	101
050916/2B	052-52	A_333	526	59	35	165636	0.07	0.971	0.042	0.1130	0.0040	0.83	0.0624	0.0015	689	30	690	25	686	51	101
050916/2B	052-53	A_334	98	9	32	42960	0.32	0.731	0.046	0.0904	0.0034	0.60	0.0587	0.0029	557	35	558	21	556	109	100
050916/2B	052-54	A_335	391	38	97	9817	0.25	0.814	0.039	0.0983	0.0035	0.75	0.0600	0.0019	605	29	604	22	605	68	100
050916/2B	052-55	A_336	274	27	115	2685	0.42	0.837	0.041	0.0994	0.0036	0.73	0.0611	0.0021	618	31	611	22	643	72	95
050916/2B	052-56	A_337	169	22	34	3036	0.20	1.197	0.053	0.1322	0.0047	0.81	0.0657	0.0017	799	35	800	29	797	54	100
050916/2B	052-57	A_338	636	107	147	35715	0.23	1.672	0.070	0.1675	0.0059	0.85	0.0724	0.0016	998	42	998	35	997	44	100
050916/2B	052-58	A_339	313	32	65	694	0.21	0.871	0.059	0.1030	0.0039	0.56	0.0613	0.0035	636	43	632	24	650	121	97
050916/2B	052-60	A_341	349	34	140	162832	0.40	0.798	0.034	0.0968	0.0034	0.82	0.0598	0.0015	596	26	595	21	596	53	100
050916/2B	052-62	A_350	388	72	132	3563	0.34	1.938	0.082	0.1853	0.0066	0.84	0.0759	0.0017	1094	46	1096	39	1091	46	100
050916/2B	052-63	A_351	800	79	346	12858	0.43	0.817	0.034	0.0984	0.0035	0.84	0.0602	0.0014	606	26	605	22	611	49	99
050916/2B	052-64	A_352	157	18	105	2299	0.67	1.033	0.054	0.1163	0.0042	0.70	0.0644	0.0024	720	37	709	26	754	78	94
050916/2B	052-65	A_353	319	38	124	8096	0.39	1.199	0.051	0.1203	0.0043	0.83	0.0723	0.0017	800	34	732	26	994	48	74

050916/2B								RATIOS							AGES [Ma]						Conc.
Sample	**Analysis**	**Analysis**	**U [ppm]^{a}**	**Pb [ppm]^{a}**	**Th [ppm]**	**^{206}Pb/^{204}Pb**	**Th/U meas**	**^{207}Pb/^{235}U^{b}**	**2 σ^{d}**	**^{206}Pb/^{238}U^{b}**	**2 σ^{d}**	**rho^{c}**	**^{207}Pb/^{206}Pb^{e}**	**2 σ^{d}**	**^{207}Pb/^{235}U**	**2 σ**	**^{206}Pb/^{238}U**	**2 σ**	**^{207}Pb/^{206}Pb**	**2 σ**	%
050916/2B	052-66	A_354	630	108	51	7583	0.08	1.719	0.072	0.1708	0.0061	0.85	0.0730	0.0016	1016	43	1017	36	1013	45	100
050916/2B	052-67	A_355	1860	188	455	5315	0.24	0.840	0.038	0.1010	0.0036	0.80	0.0603	0.0016	619	28	620	22	614	58	101
050916/2B	052-68	A_356	392	70	91	5284	0.23	1.848	0.084	0.1794	0.0065	0.79	0.0747	0.0021	1063	48	1064	38	1060	56	100
050916/2B	052-69	A_357	205	36	78	8580	0.38	1.798	0.077	0.1763	0.0063	0.83	0.0740	0.0018	1045	45	1047	37	1040	48	101
050916/2B	052-72	A_362	162	27	28	5143	0.17	1.667	0.073	0.1667	0.0060	0.82	0.0725	0.0018	996	44	994	36	1000	51	99
050916/2B	052-73	A_363	78	12	27	11270	0.35	1.547	0.077	0.1501	0.0055	0.73	0.0748	0.0025	949	47	902	33	1062	68	85
050916/2B	052-74	A_364	24	4	19	605	0.77	1.643	0.158	0.1581	0.0069	0.45	0.0754	0.0065	987	95	946	41	1078	173	88
050916/2B	052-75	A_365	522	59	120	2385	0.23	1.112	0.049	0.1129	0.0040	0.81	0.0715	0.0019	759	34	689	25	971	53	71
050916/2B	052-76	A_366	256	45	100	6129	0.39	1.779	0.076	0.1742	0.0062	0.84	0.0741	0.0017	1038	44	1035	37	1044	47	99
050916/2B	052-77	A_367	415	76	111	9928	0.27	1.929	0.082	0.1844	0.0066	0.84	0.0759	0.0017	1091	46	1091	39	1092	45	100
050916/2B	052-78	A_368	869	102	106	4955	0.12	1.034	0.046	0.1174	0.0042	0.80	0.0639	0.0017	721	32	716	26	738	56	97
050916/2B	052-79	A_369	996	94	109	450010	0.11	0.777	0.033	0.0938	0.0033	0.84	0.0601	0.0014	584	25	578	21	606	49	95
050916/2B	052-80	A_370	407	68	223	328618	0.55	1.682	0.071	0.1676	0.0060	0.84	0.0728	0.0017	1002	42	999	36	1008	46	99
050916/2B	052-81	A_371	810	77	192	369895	0.24	0.806	0.043	0.0949	0.0035	0.69	0.0616	0.0024	600	32	584	21	659	83	89
050916/2B	052-82	A_372	347	60	105	23303	0.30	1.783	0.076	0.1736	0.0062	0.84	0.0745	0.0017	1039	44	1032	37	1054	46	98
050916/2B	052-83	A_373	342	46	84	26932	0.25	1.224	0.053	0.1344	0.0048	0.82	0.0661	0.0016	812	35	813	29	808	52	101
050916/2B	052-84	A_374	254	33	154	2489	0.61	1.167	0.062	0.1283	0.0047	0.69	0.0660	0.0026	785	42	778	29	806	81	97
050916/2B	052-85	A_375	182	33	52	158413	0.29	1.872	0.081	0.1807	0.0065	0.83	0.0751	0.0018	1071	46	1071	38	1072	49	100
050916/2B	052-86	A_378	484	215	118	27609	0.24	9.641	0.422	0.4445	0.0160	0.82	0.1573	0.0039	2401	105	2371	86	2427	42	98
050916/2B	052-87	A_379	652	64	11	308597	0.02	0.817	0.035	0.0984	0.0035	0.84	0.0602	0.0014	606	26	605	22	610	50	99
050916/2B	052-88	A_380	90	15	36	25897	0.39	1.753	0.083	0.1704	0.0062	0.76	0.0746	0.0023	1028	49	1014	37	1058	62	96
050916/2B	052-89	A_381	650	81	43	9166	0.07	1.203	0.051	0.1250	0.0045	0.84	0.0698	0.0016	802	34	759	27	922	47	82
050916/2B	052-90	A_382	252	28	76	1203	0.30	1.122	0.049	0.1108	0.0040	0.82	0.0735	0.0018	764	33	677	24	1027	51	66
050916/2B	052-91	A_383	1212	138	455	1600	0.38	1.157	0.049	0.1142	0.0041	0.85	0.0735	0.0016	781	33	697	25	1028	45	68
050916/2B	052-92	A_384	339	63	127	301166	0.37	1.937	0.082	0.1850	0.0066	0.84	0.0759	0.0017	1094	46	1094	39	1093	46	100
050916/2B	052-93	A_385	148	27	83	3811	0.56	1.843	0.081	0.1795	0.0064	0.82	0.0745	0.0019	1061	46	1064	38	1054	50	101
050916/2B	052-94	A_386	483	84	24	15098	0.05	1.758	0.075	0.1737	0.0062	0.84	0.0734	0.0017	1030	44	1033	37	1024	46	101
050916/2B	052-95	A_387	467	82	112	15085	0.24	1.779	0.076	0.1750	0.0063	0.84	0.0737	0.0017	1038	44	1039	37	1034	47	101
050916/2B	052-97	A_389	805	97	141	464643	0.17	1.065	0.046	0.1202	0.0043	0.83	0.0643	0.0015	736	32	731	26	751	50	97
050916/2B	052-98	A_390	320	69	71	13623	0.22	2.449	0.104	0.2145	0.0077	0.84	0.0828	0.0019	1257	53	1253	45	1265	45	99
050916/2B	052-99	A_391	106	11	1	53048	0.01	0.879	0.042	0.1045	0.0038	0.75	0.0610	0.0019	641	31	641	23	641	68	100
050916/2B	052-101	A_395	221	28	142	9072	0.64	1.219	0.063	0.1259	0.0046	0.71	0.0703	0.0026	809	42	764	28	936	75	82
050916/2B	052-102	A_396	439	76	72	364448	0.16	1.768	0.076	0.1731	0.0062	0.83	0.0741	0.0018	1034	44	1029	37	1044	48	99
050916/2B	052-103	A_397	25	2	12	11745	0.50	0.824	0.058	0.0995	0.0038	0.54	0.0600	0.0036	610	43	611	23	605	128	101
050916/2B	052-104	A_398	287	48	51	228389	0.18	1.648	0.071	0.1659	0.0059	0.83	0.0720	0.0017	989	43	990	35	987	49	100
050916/2B	052-105	A_399	962	101	8	29043	0.01	0.885	0.038	0.1050	0.0038	0.84	0.0612	0.0014	644	27	643	23	646	50	100
050916/2B	052-106	A_400	1361	139	281	153462	0.21	0.847	0.036	0.1019	0.0036	0.85	0.0603	0.0014	623	26	625	22	615	49	102
050916/2B	052-107	A_401	641	62	361	298204	0.56	0.798	0.034	0.0970	0.0035	0.83	0.0597	0.0014	596	26	597	21	592	52	101
050916/2B	052-108	A_402	156	27	71	127815	0.46	1.726	0.076	0.1712	0.0062	0.81	0.0731	0.0019	1018	45	1019	37	1017	52	100
050916/2B	052-109	A_403	86	14	36	69115	0.42	1.698	0.078	0.1684	0.0061	0.79	0.0732	0.0021	1008	46	1003	36	1018	58	99
050916/2B	052-110	A_404	528	92	26	74957	0.05	1.784	0.076	0.1746	0.0062	0.84	0.0741	0.0017	1040	44	1037	37	1045	46	99
050916/2B	052-111	A_405	550	71	135	61688	0.25	1.154	0.049	0.1290	0.0046	0.84	0.0649	0.0015	779	33	782	28	771	49	101
050916/2B	052-112	A_406	211	37	36	4831	0.17	1.835	0.080	0.1771	0.0064	0.82	0.0751	0.0019	1058	46	1051	38	1072	50	98
050916/2B	052-113	A_407	102	10	27	49493	0.26	0.854	0.048	0.1012	0.0038	0.66	0.0612	0.0026	627	35	621	23	647	91	96
050916/2B	052-114	A_408	441	67	74	8793	0.17	1.523	0.065	0.1516	0.0054	0.84	0.0729	0.0017	940	40	910	33	1010	48	90
050916/2B	052-115	A_409	528	92	218	3802	0.41	1.776	0.093	0.1741	0.0064	0.70	0.0740	0.0028	1037	54	1034	38	1041	75	99